

# **NUMERICAL MODELING OF JET GROUTING CELLS TO REDUCE LIQUEFACTION**

**A Thesis Submitted to  
the Graduate School of Engineering and Sciences of  
İzmir Institute of Technology  
in Partial Fulfillment of the Requirements for the Degree of**

**MASTER OF SCIENCE  
in Civil Engineering**

**by  
Çağdaş GÜRBÜZ**

**July 2019**

**İZMİR**

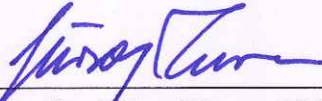
We approve the thesis of Çağdaş GÜRBÜZ

**Examining Committee Members:**



**Assoc. Prof. Dr. Nurhan ECEMIŞ ZEREN**

Department of Civil Engineering, İzmir Institute of Technology



**Assoc. Prof. Dr. Gürsoy TURAN** Department of Civil Engineering, İzmir Institute of Technology



**Assoc. Prof. Dr. Alper SEZER**

Department of Civil Engineering, Ege University

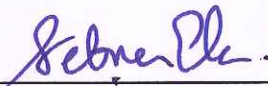
16 July 2019



**Assoc. Prof. Dr. Nurhan ECEMIŞ ZEREN**

Supervisor,

Department of Civil Engineering



**Prof. Dr. Şebnem ELÇİ**

Head of the Department of  
Civil Engineering

**Prof. Dr. Aysun SOFUOĞLU**

Dean of the Graduate School of  
Engineering and Science

## **ACKNOWLEDGMENTS**

I would like to express my deep appreciation to my supervisor Assoc. Prof. Dr. Nurhan Ecemiş for her invaluable supervision, guidance and care throughout this thesis, as well as for her scientific support, encouragement and patient during this study.

I would like to thank the members of my dissertation committee; Assoc. Prof. Dr. Gürsoy TURAN and Assoc. Prof. Dr. Alper SEZER for their attendance at my thesis defence seminar and for providing useful suggestions for my thesis.

I am grateful to my family and my friends for their understanding and support.

Finally, thanks to my family and my wife for their endless patient and love. Especially my wife who made me to overcome all the difficulties with their encouragement, support, and love. I could not come to this point without her. This thesis dedicated to them.

## **ABSTRACT**

### **NUMERICAL MODELING OF JET GROUTING CELLS TO REDUCE LIQUEFACTION**

The importance of the preservation of historical and culturally important buildings is essential nowadays. While improving the performance of the buildings under dynamic loadings, it is essential to evaluate and improve the subsoil conditions. It is evident, that strengthening of the building will not provide the desired performance, if serious ground problems such as liquefaction are not eliminated during earthquake loading.

In this study, liquefaction evaluation of the foundation soil of a historical building (Vali Konagi), which is in the Konak district of İzmir province, has been carried out. The simplified liquefaction assessment results based on the standard penetration tests showed that under 0.45g loading, the liquefaction problem could be observed. Therefore, soil improvement is necessary for the upper profile beneath this historical building.

The jet grout cells, which is a new method were suggested as a soil improvement technique against the liquefaction of the soil below the building. The parameters related to the jet grout cells were determined, and the improved soil status was analyzed. The numerical analyses of the liquefaction investigation at unimproved and improved soil were compared by finite difference program FLAC-2D. The constitutive model (UBCSand), which can simulate liquefaction was used in the program. As a result, it is observed that; by using jet grout cells liquefaction was not triggered and deformations were kept under control.

# ÖZET

## JET GROUT HÜCRELERİNİN SIVILAŞMAYI ÖNLEMELİK İÇİN KULLANILMASININ SAYISAL MODELLENMESİ

Günümüzde tarihi yada kültürel olarak önemi olan yapıların korunmasına oldukça önem verilmektedir. Bu yapıların deprem yükleri karşısında performansları iyileştirilken, üzerinde buldukları zemin koşullarının da değerlendirilmesi çok önemlidir. Zemin koşullarının gerekli durumlarda iyileştirilmesi önem kazanmaktadır. Yapı üzerinde yapılan güçlendirme çalışmaları, zeminde sıvılaşma gibi ciddi zemin sorunları giderilmediği takdirde istenen performansı sağlamayacağı aşikardır.

Bu çalışmada İzmir ili Konak ilçesinde bulunan bir yapının temel zeminin sıvılaşma değerlendirmesi yapılmıştır. SPT deneylerini baz alan sıvılaşma değerlendirmesi sonucunda 0.45g ivmeli deprem yükü altında sıvılaşma probleminin gerçekleşebileceği görülmüştür. Bu nedenle tarihi öneme sahip binanın zeminin iyileştirilmesi gerekmektedir.

Yeni bir yöntem olan jet grout hücreleri ile zeminin sıvılaşmaya karşı iyileştirme yöntemi önerilmektedir. Jet grout tasarımı parametreleri ve iyileştirilmiş zemin parametreleri hesaplanmıştır. İyileştirilmiş zemin koşullarının sıvılaşma direnci ile ilgili nümerik analizler 2-B sonlu farklar programı olan FLAC-2D ile yapılmıştır. Bu analizlerde sıvılaşma için özel olarak oluşturulmuş UBCSand modeli kullanılmıştır. Sonuç olarak yapılan analizlerde zeminde iyileştirme olmadığı durumda sıvılaşmanın tetiklendiği analizlerde gözlemlenmektedir. Tasarlanan jet grout hücreleri ile ilgili parametreler belirlenmiş ve iyileştirilmiş durum analiz edilmiştir. İyileştirilmiş durumda sıvılaşmanın tetiklenmediği ve deformasyonların kontrol altında tutulduğu analizler sonucunda ortaya çıkarılmıştır.

# TABLE OF CONTENTS

CHAPTER 1 INTRODUCTION .....	1
1.1. General .....	1
1.2. Problem Statement and Scope of the Study .....	2
1.3. Organization of the Thesis.....	2
CHAPTER 2 REVIEW OF SOIL LIQUEFACTION .....	4
2.1. Introduction .....	4
2.2. Liquefaction Phenomena .....	4
2.3. Liquefaction Triggering Assessments .....	13
2.4. Effects of Liquefaction .....	23
CHAPTER 3 REVIEW OF JET-GROUT METHOD .....	28
3.1. Introduction .....	28
3.2. Jet-Grouting Procedure.....	29
3.3. Operating and Treatment Parameters of Jet Grouting .....	34
3.4 Jet Grout Column Mechanical Properties.....	40
3.5 Jet Grout Structures .....	46
3.6 Application Control and Monitoring .....	52
3.7 Use of Jet Grout Against Liquefaction .....	56
CHAPTER 4 DESIGN OF JET GROUTING CELLS TO MITIGATE SOIL LIQUEFACTION UNDER A HISTORICAL BUILDING .....	59
4.1. Introduction .....	59
4.2. Site Investigation and Sub Soil Condition.....	60
4.3. Calculation of Liquefaction Potential.....	62
4.4. Mitigation of Liquefaction Under An Existing Building .....	65
CHAPTER 5 NUMERICAL ANALYSIS OF LIQUEFACTION MITIGATION .....	76
5.1. Introduction .....	76
5.2. Background of Method.....	78
5.3. Model Geometry and Boundary Conditions.....	79
5.4. Materials Used in Model .....	83
5.5. Dynamic Analysis .....	88
5.6. Analysis Results .....	90

CHAPTER 6 CONCLUSION .....	96
6.1. Summary of Findings .....	96
6.2. Suggestions for Future Research .....	97
REFERENCES .....	99

APPENDICES

APPENDIX A SITE INVESTIGATION DATA and EXAMPLE CALCULATIONS.....	110
APPENDIX B JET-GROUT PLANS and ELEVATIONS.....	113

# LIST OF FIGURES

<b><u>Figure</u></b>	<b><u>Page</u></b>
Figure 2.1. Liquefaction phenomenon (a) situation of soil particles in steady state condition, (b) the connection forces between grains, (c) the effect of excess pore pressure on connection forces. (Source: Washington University).....	5
Figure 2.2. (a) Flow liquefaction mechanisms in terms of shear stress versus shear strain and (b) in terms of shear stress versus effective stress for both monotonic and cycling loading (Source: Kramer, 1996).....	7
Figure 2.3. The behavior of granular soil under undrained loading (Source: Erginağ, 2015). ....	8
Figure 2.4. Cyclic liquefaction. (Source: Kramer,1996) .....	10
Figure 2.5. Ranges of Grain Size Distribution for Liquefaction Susceptible Soils (Source: Tsuchida, 1970) .....	11
Figure 2.6. Liquefaction potential for plastic soils (Seed et al., 2003).....	13
Figure 2.7. Cyclic stresses on a soil element beneath level ground during horizontal shaking (Idriss and Boulanger, 2008). ....	14
Figure 2.8. Setup and Equipment for the Standard Penetration Test (SPT) (Source: Kovacs et al., 1981). ....	17
Figure 2.9. Overview of the Cone Penetration Test (CPT) Per ASTM D 5778 Procedures (Source: NCHRP Project 20-05 Final Report, 2007).....	22
Figure 2.10. Curve for calculation of CRR based on CPT (Source:Robertson and Wride,1998). ....	23
Figure 2.11. Acceleration – time graphics (EW: east-west direction, NS: north-souht direction) (Source:CEEN, 2017).....	24
Figure 2.12. Sand boils on the field (Source: USGS).....	25
Figure 2.13. Major tilting of the buildings due to subsoil liquefaction (Source:Ada Pazarı 1999). ....	26
Figure 2.14. Loss of bearing capacity of buildings caused by liquefaction (Source: Niigata Nippo Newspaper, 1964). ....	26
Figure 2.15. Lateral spreading (Source: wikipedia). ....	27
Figure 3.1. Different applications of jet grouting: (a) foundation support, (b) water sealing bottom plug and excavation support, (c) provisional tunnelling support and (d) water cutoff (Source:Croce et al. 2014). ....	29
Figure 3.2. Jet grouting method (Source: Croce et al. 2014).....	31
Figure 3.3. General jetting methods: (a) single fluid, (b) double fluid and (c) triple fluid (Source: Croce et al. 2014). ....	31
Figure 3.4. The Equipments of jet grouting application(Source:Croce et al. 2014).....	32
Figure 3.5. Jet grouting elements (Source:Croce et al. 2014).....	32
Figure 3.6. Schematic drawings of nozzle groups in jet grouting a)single fluid method, b)double fluid method, c)triple fluid method(Source:Croce et al. 2014). ...	34



<b><u>Figure</u></b>	<b><u>Page</u></b>
Figure 3.7. Photograph (a) and sketch (b) of a highspeed submerged jet (Source: Bergschneider 2002).....	38
Figure 3.8. Lifting methods of drilling rods (Source: Croce et al. 2014).....	39
Figure 3.9. Effect of angular velocity on soilcrete diameter (Source: Shibasaki 1996). 40	40
Figure 3.10. Dependency of $\Lambda^*$ on grout composition ( $\Omega$ is the cement–water ratio by weight, $\mu_g$ is the viscosity of a cement grout.) (Source: Croce et al. 2014 ).41	41
Figure 3.11. Typical strength increment provided by single-fluid jet grouting.....	44
Figure 3.12. The expression of the Mohr Coulomb failure criteria. ....	45
Figure 3.13. The ranges of uniaxial compressive strength for different soil types and variable injected amounts of cement. (Source: Fiorotto, 2000.).....	46
Figure 3.14. The comparison of methods in point of uniaxial compressive strength versus depth. ( Source: Van der Stoel, 2001.).....	47
Figure 3.15. Elasticity for large strains modulus $E_{50\%}$ valuaes change small strain Elasticity for small strains modulus $E_0$ of jet grout (Croce et al. 2014 ). ....	47
Figure 3.16. Different methods of jet grout application (a): Discrete columns, (b): Cellular (Lattice) Columns, (c): Block Type of Columns. ....	49
Figure 3.17. Discrete jetgrout columns.....	50
Figure 3.18. Jet grouted mass gravity wall: (a) plan view and (b) elevation (Vincent et al. 2014) .....	51
Figure 3.19. An example of jet grout block (Source: zakladani.cz) .....	51
Figure 3.20. Cellular design of jet grout columns (a): plan dimension of cell, (b): an example application near the sea(Source Bolunger., 2012).....	52
Figure 3.21. Test columns (Source: Kellerindia.).....	54
Figure 3.22. Investigation excavation and diameter control of jet grout column (Source: Gökalp and Düzceer 2000). ....	55
Figure 3.23. Sonic integrity test over the jet grout column (Gökalp and Düzceer 2000). .....	55
Figure 3.24. Measurement of the quality of jet grouting with sonic logging (Croce et al. 2014 ). ....	56
Figure 3.25 Axial loading tests on jet grouting columns (a) experimental setup; (b) picture taken during a compression loading test; (c) results of compression test; (d) results of pullout test. (Source: Bzówka, 2009.).....	56
Figure 4.1. The front view of the building.....	61
Figure 4.2. Plan of the blocks and the locations of the three boreholes. ....	61
Figure 4.3. B-B elevation and D-D elevation drawings. ....	62
Figure 4.4. Drilling machine.....	63
Figure 4.5. SPT sampler (a) and testing (b). ....	64
Figure 4.6. External forces applied to jet grout cells during an earthquake.(Source: Jeremic, 2010).....	67
Figure 4.7. Application plan drawings of jet grout cells of I block. ....	69
Figure 4.8. Application plan drawings of jet grout cells of I block. ....	69

<b><u>Figure</u></b>	<b><u>Page</u></b>
Figure 4.9. Elevation drawings of jet grout cells (a): the section of H block, (b): the section of I block. ....	70
Figure 5.1. Elements of a FLAC model(Source: Flac, 2008). ....	77
Figure 5.2. Basic explicit calculation cycle. ....	79
Figure 5.3. Foundation geometry and the soil profile.....	80
Figure 5.4. The rigid base type of dynamic loading boundary conditions available in Flac (Source: Flac, 2008). ....	81
Figure 5.5. Mesh convergence results according to the relation between mesh size .....	82
Figure 5.11. The unbalanced force of static stage. ....	90
Figure 5.12. Total, effective stress and pore pressure versus time; before the foundation soil improvement. ....	92
Figure 5.13. Excess pore pressure ratio ( $r_u$ ) before the foundation soil improvement. ..	92
Figure 5.14. Horizontal displacement vectors before the foundation soil improvement and maximum horizontal displacement is 106.2 cm.....	93
Figure 5.15. Horizontal and vertical displacement under the foundation, before the foundation soil improvement. ....	93
Figure 5.16. Total, effective stress and pore pressure versus time; after the foundation soil improvement. ....	94
Figure 5.17. Pore pressure ratio ( $r_u$ ) versus time, after the foundation soil improvement. ....	95
Figure 5.18. Horizontal and vertical displacement under the foundation, after the foundation soil improvement. ....	95

## LIST OF TABLES

<b><u>Table</u></b>	<b><u>Page</u></b>
Table 2.1. Chinese criteria .....	12
Table 2.2. Modified Chinese criteria (Andrews and Martin, 2000) .....	12
Table 2.3. Comparison of various field tests for assessment of liquefaction potential (Youd, 2001). .....	17
Table 2.4. SPT Correction Factors.....	18
Table 2.5. Magnitude correction factors .....	20
Table 3.1. List of fundamental treatment parameters (Croce et al. 2014 ). .....	35
Table 3.2. List of derived treatment parameters (Croce et al. 2014 ). .....	35
Table 3.3. Typical values of treatment parameters (Croce et al. 2014 ). .....	36
Table 3.4. Values of the parameters to be adopted for the prediction of mean diameter of columns (Croce et al. 2014).....	42
Table 3.5. Friction and cohesion parameters according to soil type from case studies(Croce et al. 2014 ). .....	45
Table 3.6. The variety of values of the coefficient $\beta_E$ depends on soil types and young modulus for different strain conditions in the literature. (Croce et al. 2014). .....	48
Table 4.1. Soil profile of the site from boreholes. ....	66
Table 4.2. Factor of safety values according to depth for all boreholes. ....	66
Table 4.3. Recommended application parameters intervals (according to Croce et al. 2014) for single fluid system and values to be used in this study.....	68
Table 4.4. Calculated jet grout column diameter parameters for the borehole-1. ....	71
Table 4.5. Calculated jet grout column diameter parameters for the borehole-2. ....	71
Table 4.6. Calculated jet grout column diameter parameters for the borehole-3. ....	71
Table 4.7. Calculated jet grout column mechanical parameters for the borehole-1. ....	71
Table 4.8. Calculated jet grout column mechanical parameters for the borehole-2. ....	71
Table 4.9. Calculated jet grout column mechanical parameters for the borehole-3. ....	71
Table 4.10. Calculated jet grout column liquefaction potential parameters for the borehole-1. ....	71
Table 4.11. Calculated jet grout column liquefaction potential parameters for the borehole-2. ....	71
Table 4.12. Calculated jet grout column liquefaction potential parameters for the borehole-3. ....	71
Table 4.13. Calculated jet grout - soil composite parameters.....	71
Table 5.1. Mesh convergence parameters.....	82
Table 5.2. Material Models and their short description. ....	84
Table 5.3. Mohr-Coulomb material properties. ....	85
Table 5.4. Main input parameters of UBCSAND Constitutive Model version 904aR. .	87

<b><u>Table</u></b>	<b><u>Page</u></b>
Table 5.5. Liquefiable material properties.....	87
Table 5.6. Beam elements properties in the model.....	88
Table 5.7. The excess pore pressure ratio and deformation, and their times under the foundation before and after improvement.....	94

## LIST OF SYMBOLS

$a_{\max}$  = Maximum acceleration amplitude of the applied ground acceleration  
 $d$  = Diameter of the nozzle  
 $D_a$  = Average column diameter  
 $D_m$  = Mean diameter  
 $E'_n$  = specific energy (per unit length of column) at the nozzle  
 $E'_p$  = specific energy (per unit length of column) at the pump  
 $E$  = Young modulus  
 $E_n$  = energy at the nozzle  
 $E_p$  = energy at the pump  
 $FC$  = Fines Content  
 $FS$  = Factor of safety  
 $g$  = Acceleration due to gravity  
 $G_s$  = Specific gravity  
 $k$  = Permeability  
 $LL$  = Liquid limit  
 $PL$  = Plastic limit  
 $PI$  = Plasticity Index  
 $PP$  = Pore water pressure  
 $q_c$  = Cone tip resistance  
 $Q_c$  = Total force acting on the cone  
 $r_u$  = Pore pressure ratio  
 $u$  = Pore water pressure  
 $w$  = Water content  
 $W$  = Weight  
 $\Delta u$  = Excess pore pressure  
 $\gamma_{\text{sat}}$  = Saturated unit weight  
 $\sigma_{\text{vo}'}$  = Effective vertical stress  
 $CRR$  = cyclic resistance ratio  
 $CSR$  = cyclic stress ratio  
 $\tau_{\text{av}}$  = the average horizontal shear stress  
 $N$  = measured standart penetration resistance  
 $(N_1)_{60}$  = normalized standart penetration resistance  
 $C_E$  = correction for donut hammer energy ratio of 60%  
 $C_B$  = correction factor for borehole diameter  
 $C_R$  = correction factor for rod length  
 $C_S$  = correction for standard samplers  
 $C_Q$  = correction factor for cone penetration resistance  
 $q_{c1}$  = corrected cone penetration resistance  
 $q_{c1N}$  = normalized cone penetration resistance  
 $m$  = factor based on soil density

$I_c$  = soil behavior index  
 $(q_{c1N})_{cs}$  = normalized dimensionless tip resistance equivalent to clean sand  
 $K_c$  = correction factor based on grain size characteristics.  
 $k$  = permeability coefficient  
 $M$  = number of nozzles  
 $\gamma_{cyc}$  = cyclic shear strainis calculated by  $a_{max}$   
 $G_{(\gamma_{cyc})}$  = shear modulus of the soil at shear strain level  
 $r_d$  = stress reduction factor  
 $\Delta u$  = change in the excess pore pressure  
 $u_i$  = measured pore pressure at the depth  
 $u_0$  = equilibrium in situ pore pressure at the depth  
 $\Delta u_t$  = excess pore pressure at any time  $t$   
 $u_t$  = total pore pressure at any time  $t$   
 $t_{50}$  = the time value for 50% dissipation of excess pore water pressure  
 $c_h$  = coefficient of consolidation  
 $G_s$  = specific gravity of soil  
 $W_s$  = weight of dry soil sample  
 $k$  = Darcy's coefficient for water  
 $\rho_{dmin}$  = minimum index density  
 $\rho_{dmax}$  = maximum index density  
 $\rho_w$  = density of water (1 g/cm<sup>3</sup>)  
 $m_v$  = compressibility of the soil  
 $q_u$  = unconfned compressive strength of the jet-grouted material  
 $v_r$  = average lifting speed of the monitor  
 $\alpha_E$  = parameter accounting the influence of air shrouding on  $\Lambda$   
 $\beta_E$  = coeffcient relating the stiffness and the uniaxial compressive strength of jet-grouted material  
 $\Delta s$  = lifting step  
 $\Delta t$  = time interval per lifting step  
 $\Lambda$  = parameter defning the profile of velocity outside the nozzle  
 $\Lambda^*$ ,  $\Lambda^*_w$ ,  $\Lambda^*_g$  = parameter  $\Lambda$  for single fluid, and values computed for water and grout

# CHAPTER 1

## INTRODUCTION

### 1.1. General

Liquefaction is one of the major problems in which the strength and stiffness of a soil are reduced by earthquake shaking or other rapid loading. Liquefaction is first observed after 1964 Niigata and same year Prince William Sound Alaska earthquakes, because of dramatical damages. Following devastating effects of liquefaction, researches and efforts are focused on finding methods to improve liquefaction by soil mitigation techniques such as jet grout columns. In this study, a series of numerical studies were carried out to investigate the effectiveness of jet grout columns in liquefaction mitigation. A historical building in Izmir, Konak was chosen for this purpose.

In this study simplified procedure (Seed and Idriss, 1971) and numerical analysis methods were both practiced. The liquefaction triggering conditions was evaluated by using the field test results. Changes of effective stress, pore pressures, and deformations of subsoil were obtained by using the constitutive model, UBCSand.

After determining liquefaction potential a soil improvement method was suggested, which was jet grouting cells (in ground shear wall method). Jet grout parameters such as the diameter of columns, the pressure of grouting, average lifting speed, and W-C ratio were decided according to site investigation performed in the study area after the soil mitigation composite soil conditions were analyzed by FLAC-2D under dynamic loading conditions.

## **1.2. Problem Statement and Scope of the Study**

In the past decades engineers tried to overcome hazardous effect of liquefaction. Studies and researches are focused on finding methods to mitigate liquefaction by soil improvement techniques. Moreover nowadays, cement injection, stone columns and jet-grout columns are some examples of the improvement methods that are widely used to reduce liquefaction induced hazards in geotechnical engineering practice. The aims of the soil mitigation are improving the stiffness of soil and to avoid excess pore water pressure exceed effective stress during the earthquake. The previous studies and experiments showed us that, jet grout columns can be used for soil treating against liquefaction. Although the improvement mechanism is too far a complex to be, the optimization and control problem is staying still. The optimization of the design of the improvement is gaining more value than ever; due to increasing demands for infrastructure in urbanized areas. A rising number of constructions are built on or in soft ground with poor soil properties in terms of stiffness and strength. In order to facilitate construction and to prevent structures from excessive deformations, jet grouting columns have become an essential method for soil improvement.

This study aims to investigate the jet grout design to reduce liquefaction in a circumstance, which the bearing capacity is not a problem under vertical loads to avoid. Thus conventional grid methods are put aside and focusing on the efficacy of larger cell dimensions in order to reduce project costs and necessary construction time. Within this scope, an existing building(Vali Konagi) is chosen, which is in İZMİR under restoration construction and suitable for our study.

## **1.3. Organization of the Thesis**

The thesis consists of seven chapters. Then the current chapter represents a summary of this study. According to this, the contents of the study are put in order below:



Chapter 2 presents a literature review of liquefaction. In this chapter, the liquefaction phenomena, triggering assessment and its effects were mentioned.

Chapter 3 presents a literature review of Jet Grouting. In this chapter, the jet grouting procedure, operating and treatment parameters, mechanical properties, jet grout structures, application control and monitoring, jet grout using against liquefaction are mentioned.

Chapter 4 presents the design approach of jet grouting cells to reduce liquefaction. In this chapter site investigation and subsoil condition, calculation of liquefaction potential, and mitigation of liquefaction under an existing building were mentioned.

Chapter 5 presents a numerical analysis of liquefaction mitigation. In this chapter, background of finite difference method (FDM), model geometry, boundary conditions, constitutive materials used in model (UBCSand), dynamic analysis results were mentioned.

Chapter 6: presents the conclusion of the study. In this chapter summary of findings and suggestions for future research were given.

At the end of these six chapters, the list of references was given. Design drawings of the jet grouting cells and site investigation test results were given in Appendix A at the end of this thesis.

## CHAPTER 2

### REVIEW OF SOIL LIQUEFACTION

#### 2.1. Introduction

The liquefaction phenomena is a contradictive and complicated geotechnical earthquake engineering problem which attracted attention of many researchers from all over the world. Soil liquefaction should come apart from the other effects of the earthquake. This phenomenon could be observed during the earthquakes or instantly after that. However, when an earthquake occurs, liquefaction phenomena may or may not occur depending on the soil conditions. For example, the Niigata Earthquake (1964), Loma Prieta Earthquake (1989), Kobe Earthquake (1995), in our geography Kocaeli Earthquake (1999) caused liquefaction of the soil.

In this section, a literature review of soil liquefaction phenomena is glanced over. The definition of liquefaction, as well as its mechanisms and the resulting types of damages are described. The mechanisms of liquefaction are given detailed in part of flow liquefaction and cyclic softening.

#### 2.2. Liquefaction Phenomena

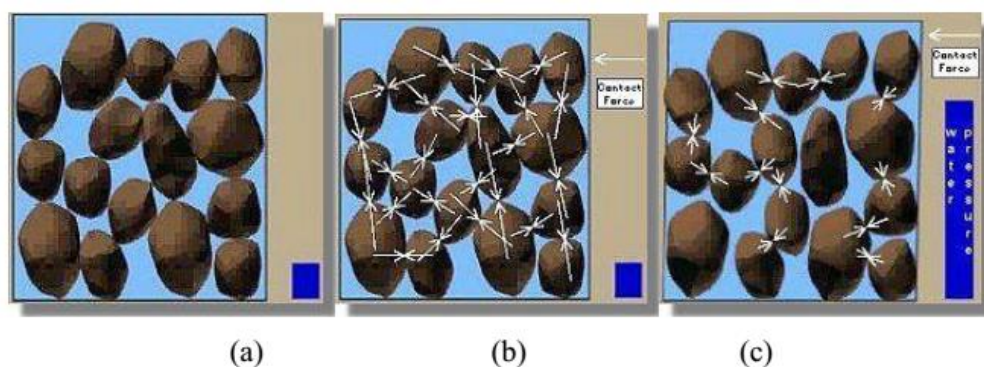
Since Terzaghi and Pack (1948), the term “liquefaction” used to express soil behaviour imitating that of a viscous fluid causing suddenly strength loss of saturated sands.

The key features of the liquefaction phenomenon are the generation of excess pore water pressure, and drainage conditions of cohesionless soils. If there is no saturation, there is neither pore water pressure increase nor liquefaction susceptibility. Liquefaction can occur under undrained conditions saturated cohesionless soils. The

dynamic loadings (earthquake) which is simply ground shaking of high frequency, create impacts; that impacts affect that soils due to the tendency for densification. The densification means increasing of the effective stress between soil grains. Increased pressure is not transferred between the soil grains, due to the existence of pore water, therefore excess pore water pressure is generated.

One of the newest definition has presented by Idriss and Boulanger (2008):

“Loose cohesionless soils tend to contract during cyclic loading, which can transfer normal stress from the soil skeleton to pore water, if the soil is saturated and largely unable to drain during shaking. The result is a reduction in effective confining stress within the soil and an associated loss of strength and stiffness that contributes to deformations of the soil deposit. This loss of strength and stiffness due to increasing pore pressures is called liquefaction.”



*Note : Blue column represents the level of pore water pressure in the soil. The arrows represent the contact force between soil particles.*

Figure 2.1. Liquefaction phenomenon (a) situation of soil particles in steady state condition, (b) the connection forces between grains, (c) the effect of excess pore pressure on connection forces. (Source: Washington University)

In the extreme case, the excess pore water pressure extensively increase, thus the effective stress becomes zero ( $\sigma_{v0}'=0$ ). Since the effective stress stands for the contact force at grain-to-grain contacts in soil, the zero effective stress causes that there is no effective contact between grains as shown in Figure 2.1. Hence, grains are actually floating in pore water without constraint from surrounding sand particles. When ground shaking due to seismic action is initiated, pore water pressure suddenly increases. The

contact points and forces are decreased with time and soil deposits behave like a liquid than a solid. This phenomenon is called ‘liquefaction’.

Robertson and Wride (1997) explained the liquefaction mechanism with two interrelated different responses of soil during earthquake shaking, (a) flow liquefaction and (b) cyclic softening. In terms of evaluation of liquefaction-related hazards, these two terms are crucial due to the difference between levels of the hazard they can cause (Kramer, 1996). That is, flow liquefaction can result in much severe hazard as compared to cyclic mobility. Whereas, the rate of occurrence of cyclic mobility is high. Although cyclic mobility could occur in a wide range of site conditions comprising a broad range of soil type, insignificant damage can occur as well as severe damage can be observed. Due to this variability of effects, it is difficult to distinguish from each other. However, characteristics of these two terms should be known in order to understand the mechanism behind the liquefaction.

### **2.2.1 Flow Liquefaction**

Flow liquefaction was defined as the state of soil having very low residual shear strength where force equilibrium is lost due to exposure to either monotonic loading such as the construction of new a structure and filling of the dam with water or dynamic loading, including pile driving process and earthquake. A soil sample attains its own residual strength after undergoing very large strains. Figure 2.2 shows us flow liquefaction triggering behaviour under monotonic and cyclic loading conditions in terms of shear stress versus shear strain (a) and in terms of terms of shear stress versus effective stress. As it seen that under cyclic loading conditions flow liquefaction occurs under lower shear stresses in comparison with those generated by monotonic loading conditions.

Whether loading type is monotonic or dynamic, both of them exert additional forces by affecting internal force equilibrium. Also, if the soil does not resist those additional forces, flow liquefaction occurs due to loss in shear strength. In the case of flow liquefaction, a rapid and extensive amount of displacements known as “flow failure” may occur.

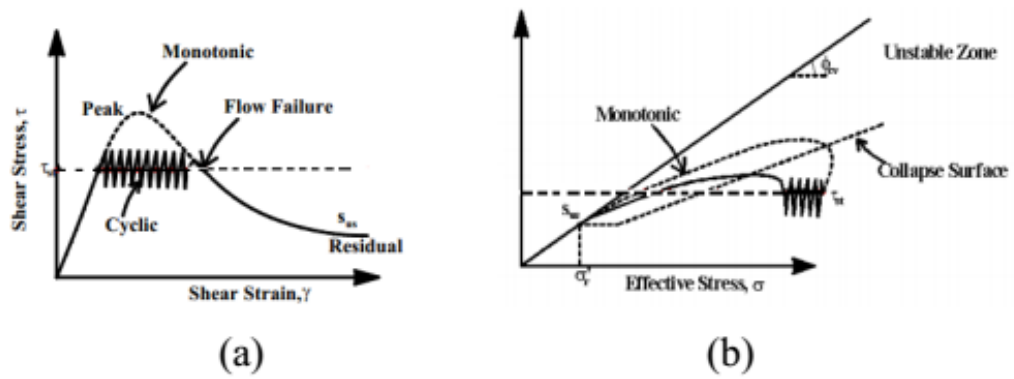


Figure 2.2. (a) Flow liquefaction mechanisms in terms of shear stress versus shear strain and (b) in terms of shear stress versus effective stress for both monotonic and cycling loading (Source: Kramer, 1996).

In the past, there exist several examples of flow liquefaction, namely; Fort Peck Dam (Casagrande, 1965), Aberfan flowslide (Bishop, 1973) and Stava tailings dam. Also, in flow liquefaction, the fact that early signings do not usually emerge increase the severity of the hazard.

Both Robertson & Catherine (1997) and 1997 Northwestern Center of Engineering Education Research (NCEER) Workshop mentioned required characteristics or properties that there exists a possibility of occurrence of flow liquefaction:

- Strain softening response of soil against undrained loading is needed. Furthermore, unchanged shear and effective stress should occur under such kind of loading Ultimate undrained shear strength should be lower than the in-situ shear stresses.
- Flow liquefaction may occur under either monotonic loading or cyclic loading.
- In order to attain failure, a large amount of volume should be strain soften. Flow type failure could occur while the failure type could be slide, as well. The main cause of failure is because of internal stresses.
- Sensitive clays, very loose deposits and silt deposits are more prone to expose flow liquefaction under undrained loading.

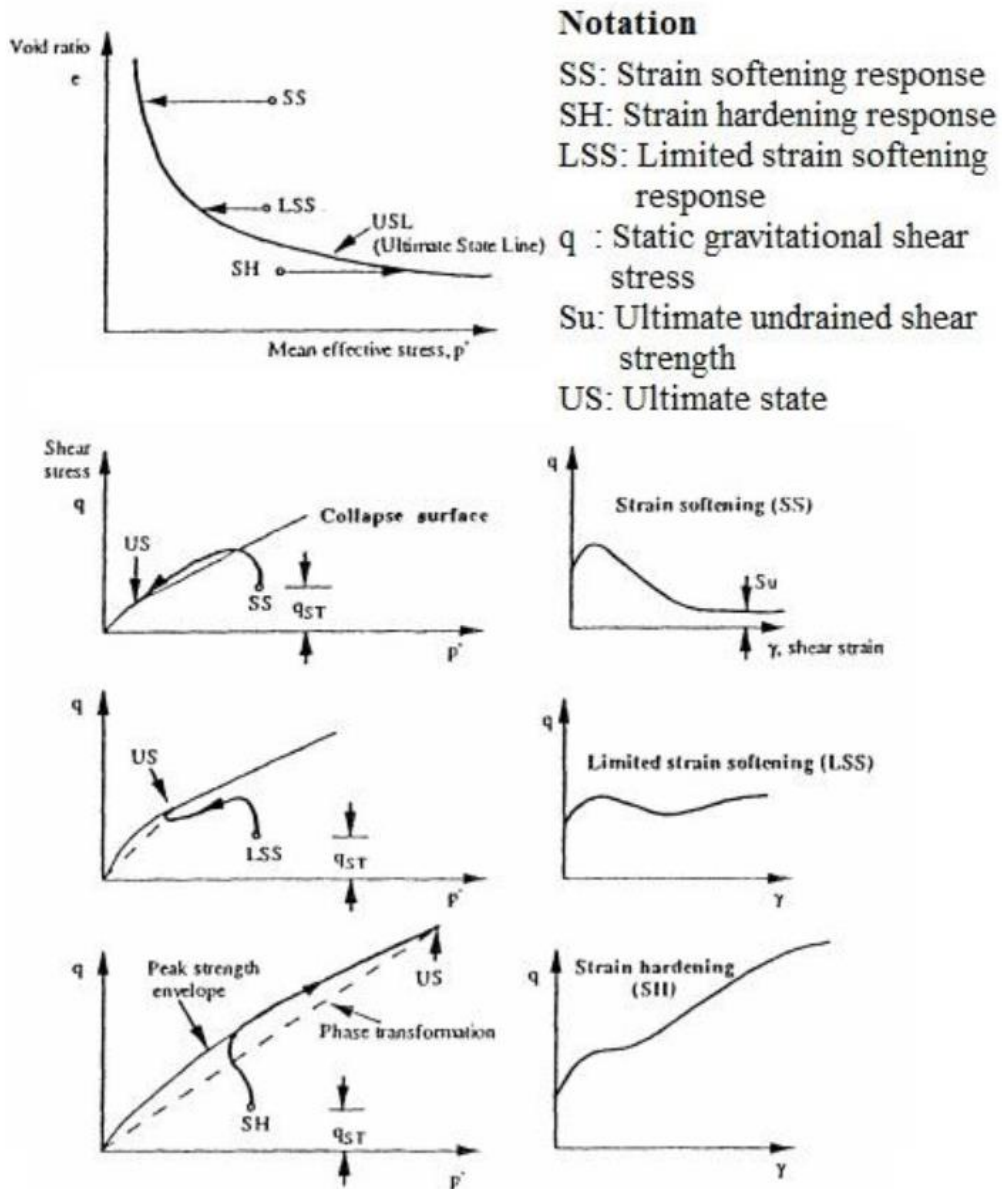


Figure 2.3. The behavior of granular soil under undrained loading (Source: Erginağ, 2015).

### 2.2.2 Cyclic Softening

Robertson and Catherine (1997) and 1997 NCEER Workshop described cyclic softening as a phenomenon comprising two sub-phenomena, (a) cyclic mobility, (b) cyclic liquefaction where it occurs that soil deposits are exposed to relatively low shear stresses as compared to its own ultimate shear strength. In this type liquefaction, incrementally increasing deformations take place triggered by either static or dynamic

stresses. Unlike flow liquefaction, cyclic softening may occur for both strain softening and strain hardening.

### **2.2.2.1 Cyclic Mobility**

Cyclic mobility can result in undesired very large deformations known as “lateral spreading” under dynamic load (Kramer, 1996). Unlike flow liquefaction, the combination of static and cyclic shear stresses are driving forces and they cause such kind of liquefaction. In order to attain cyclic mobility, the conditions to be introduced should be fulfilled:

- There exist no shear stress reversals. That is, shear stresses should be different than zero.
- Effective stresses should be different than zero. In other words, zero effective stress is not necessarily required.
- External causes result in final deformations of soil except that very loose soils and flow liquefaction take place.

### **2.2.2.2 Cyclic Liquefaction**

Cyclic liquefaction occurs if following conditions are present;

- It occurs under in-situ shear stresses lower than shear stresses caused by cyclic loading. That is, due to the occurrence of shear stress reversal, zero shear stresses could develop provided that cyclic loading can leads to mentioned phenomena (Figure 2.4).
- Effective stress should decrease to zero under cyclic loading.
- Whenever effective stress converges to zero, shear stresses also decreases to zero. If additional shear stresses are applied, the soil has a tendency of becoming dilated as pore water pressure decreases. However, even if soft initial strain occurs under initial stresses, it may cause large deformations.

- Generally, deformations become levelled as cyclic loading stops. Unlike flow liquefaction, external factors are the cause of final deformations rather than internal forces.
- For a given cyclic loading having sufficient magnitude and duration, independent of type sand, almost all types of sand undergo cyclic liquefaction.
- Apart from sandy soil, cyclic liquefaction can occur in clayey soils although resulting deformations are small as compared to sandy soils due to presence of cohesion. Besides, time effect is governing case for deformations of clayey soils.

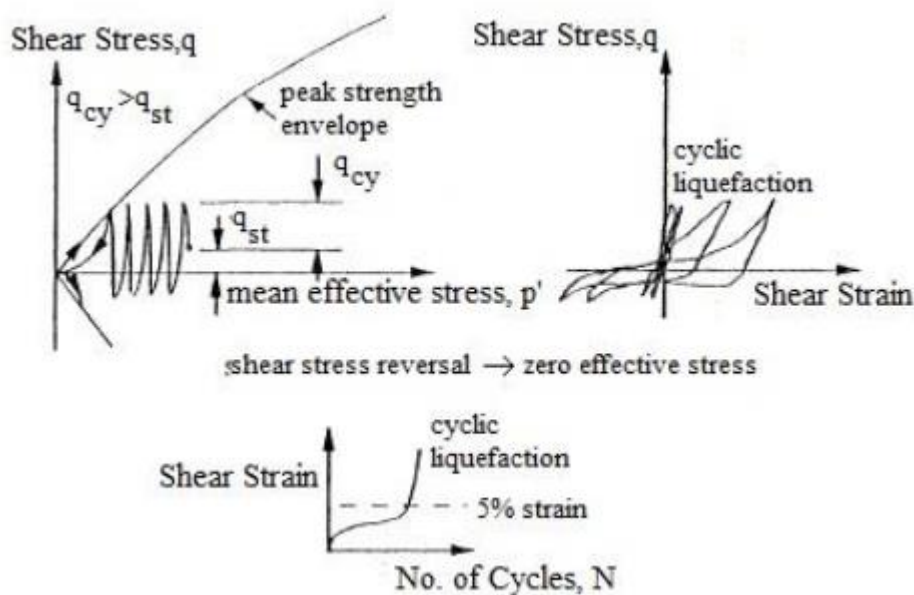


Figure 2.4. Cyclic liquefaction. (Source: Kramer,1996)

### 2.2.3. Identification of Liquefiable Soil

Generally, fully saturated cohesionless soil deposits are the most critical soil type which are highly prone to liquefaction. Also, risk of liquefaction of a soil deposit boosts if it is loose enough to contract under dynamic loading provided that sufficient drainage cannot occur resulting in induced pore water pressure is not likely to dissipate (Terzaghi, Peck & Mesri, 1996). With respect to the geological aspect, most common liquefiable sediments are alluvial, beach, terrace deposits including uncontrolled



manmade fill (Kramer, 1996). Whether a soil deposit can liquefy or not is determined with respect to compositional, state and historical record criteria. This composition can be observed in grain size analysis. Ranges of the grain size distribution for liquefaction susceptible soils, as defined by Tsuchida (1970), are given in Figure 2.5.

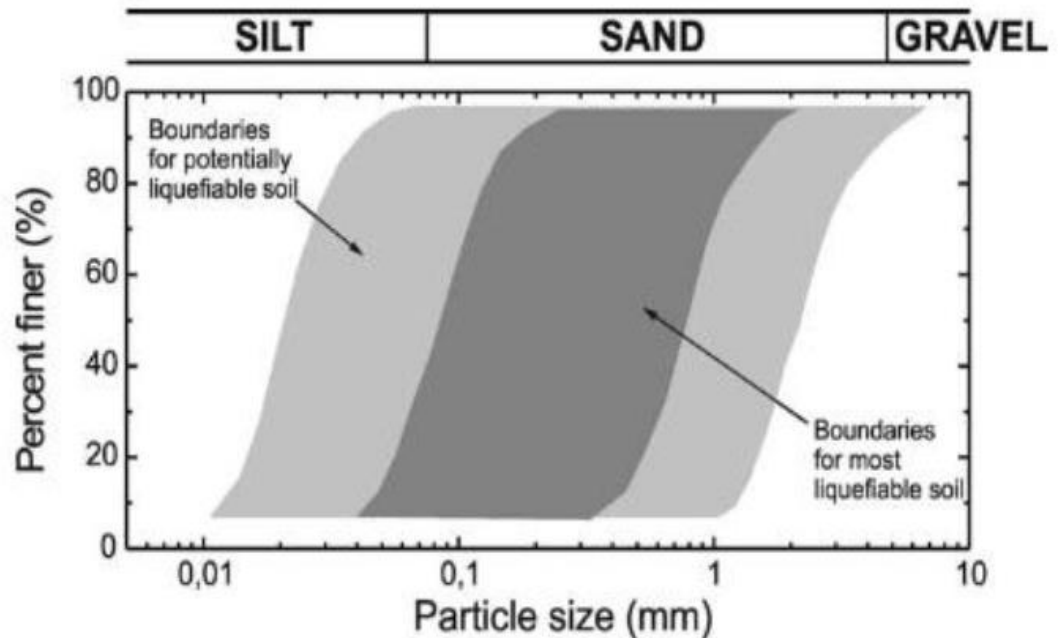


Figure 2.5. Ranges of Grain Size Distribution for Liquefaction Susceptible Soils (Source: Tsuchida, 1970)

As it is seen in Figure 2.5.; not just sandy soil types, non-plastic silts fulfilling specific criteria can also liquefy under undrained conditions (Ishihara, 1985). The mentioned criteria indicated that plasticity characteristics instead of grain size only have impact on liquefaction potential of fine-grained soil. Furthermore, non-plastic cohesionless coarser silts particle shape of whom is bulky are prone to liquefaction (Ishihara, 1993). Besides, finer silts having platelike or platy shape (as clay grains) which are not in danger of liquefaction because they have enough cohesion to prevent it. This type of silty soils behave like clayey soils. Although consensus on whether all type of clays do not have liquefaction potential, due to strain softening behavior, highly sensitive clays can liquefy. Based on findings gathered from 1964 Niigata and 1964 Alaska Earthquakes, “Chinese Criteria” was established so as to assess liquefaction potential of fine grained soils (Seed & Idriss, 1982). That is, if a fine grained soil satisfy three criteria according to the Chinese Criteria, it is likely to liquefy (Table 2.1).

Table 2.1. Chinese criteria

<b>Fine Grained Soils Having Liquefaction Potential</b>		
<b>Liquid Limit (LL)</b>	<b>Water Content (<math>w_c</math>)</b>	<b>Finest Content (&lt;0.005 mm)</b>
$\leq 35 \%$	$\geq 0.9*LL \%$	$\leq 15 \%$

Although Chinese Criteria has been robust and it predicted several liquefaction cases, its validity has become under question after the 1989 Loma Prieta Earthquake (NCEER, 1997). Due to the effect of the presence of non-plastic fines and the influence of plasticity index on liquefaction potential which were not included in the criteria. It was understood that Chinese Criteria needs to be improved. Therefore, Andrews and Martin (2000) modified the Chinese Criteria (Table 2.2).

Table 2.2. Modified Chinese criteria (Andrews and Martin, 2000)

	<b>Clay Content (&lt; 10 %) (&lt; 0.002 mm)</b>	<b>Clay Content (<math>\geq 10 \%</math>) (<math>\geq 0.002</math> mm)</b>
<b>Liquid Limit &lt; 32 %</b>	High Potential	Laboratory Test Needed
<b>Liquid Limit <math>\geq 32 \%</math></b>	Laboratory Test Needed	Non-liquefiable

Apart from mentioned studies on plastic fine-grained soils, based on performed tests on samples gathered from Adapazari-Turkey and Chi Chi-Taiwan Earthquakes, Seed et al. (2003) provided similar results on Atterberg limit chart with Bray et al. (2001) that amount of clayey minerals have more importance than the amount of clay-size fraction (Figure 2.6). That is, if the liquid limit is less than 37 percent and plasticity index is lower than 12 percent, high potential of liquefaction emerges provided that natural water content is higher than 0.8 times its own liquid limit. The only difference between the mentioned one and the preceding approach is the ratio of natural content to liquid limit. The chart corresponding lastly mentioned study divided Atterberg Chart into three parts bounded both plasticity index and liquid limit. Zone A is referred as “classic cyclically induced liquefaction” that closely detects the liquefaction in Adapazari case while Zone B describes the region as potential liquefaction risk.

However, it is still not possible to determine what types of silts and clays are susceptible to liquefaction with the help of this chart (Boulanger & Idriss, 2006).

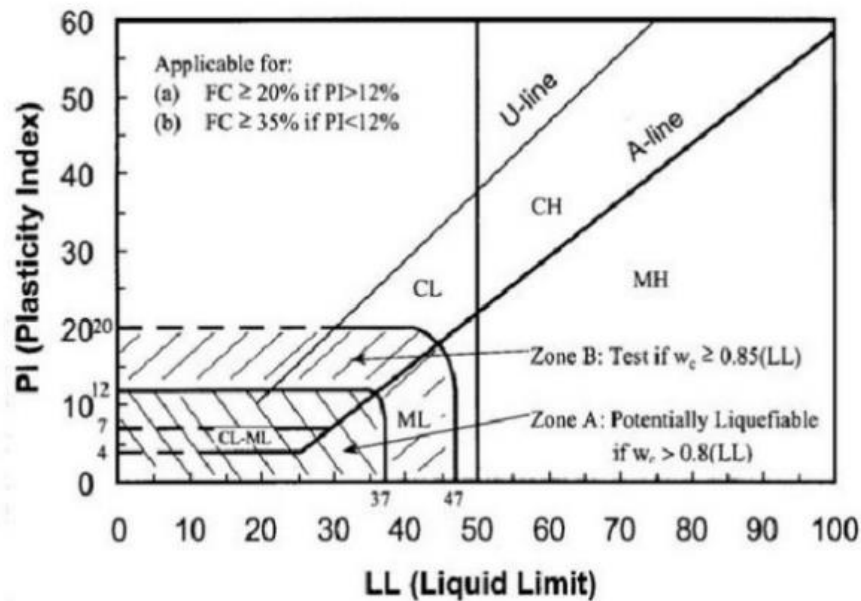


Figure 2.6. Liquefaction potential for plastic soils (Seed et al., 2003)

### 2.3. Liquefaction Triggering Assessments

If the soil is decided to be potentially liquefiable, the next step involves the assessment of liquefaction triggering potential under seismic or cyclic loading. Semi-empirical field-based procedures are widely used for evaluating liquefaction potential during earthquakes, which have two essential components: compiling case histories to develop an analytical framework, and the development of a suitable in-situ index to represent soil liquefaction characteristics. There has been a number of SPT-based semi-empirical method such as: Seed et al. (1984); Ishihara (1985), Liao et al. (1988); Japanese Code of Bridge Design (1990), Youd and Noble (1997); Idriss and Boulanger (2004) and Cetin et al. (2004). The original simplified procedure of Seed and Idriss (1971) for calculating earthquake-induced cyclic shear stresses is still the essential component of liquefaction triggering framework.

In the following chapters, SPT based assessment of seismic soil liquefaction by Seed and Idriss (1971) method will be used for the calibration of the new effectivestress

based constitutive model discussed at this study, so a brief discussion about this method is given in this section.

A liquefiable soil element is subjected to cyclic horizontal acceleration effect which is like the earthquake, as a result the effect turn into the additional shear stresses, besides the pore pressure is pressurized to apart from geostatic state. In Figure 2.7. the soil conditions are compared at geostatic state (there is just vertical and horizontal stresses such as  $\sigma_{vc}$  and  $\sigma_{hc}$ ) and at cyclic loading state (there is stresses added such as  $\tau_{cyc}$ ,  $\Delta\sigma_h$  and  $\Delta u$ ).

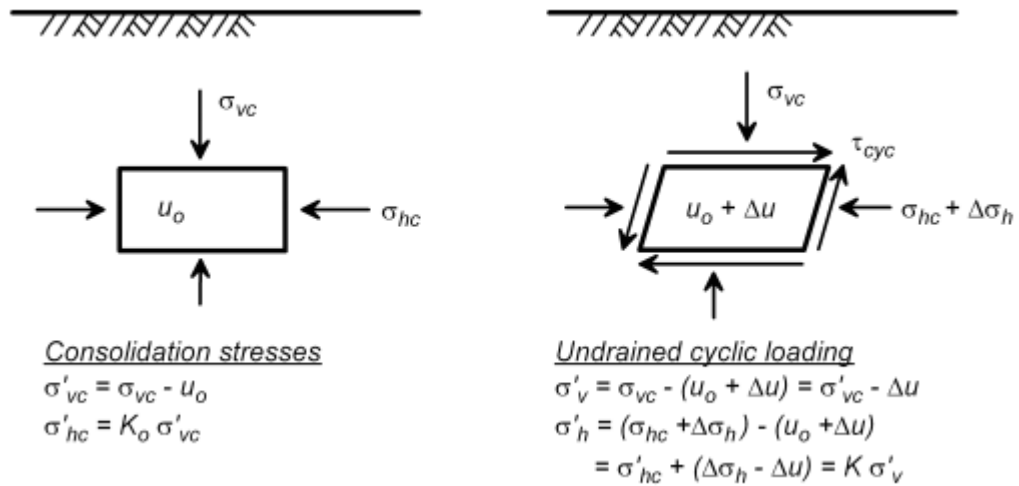


Figure 2.7. Cyclic stresses on a soil element beneath level ground during horizontal shaking (Idriss and Boulanger, 2008).

### 2.3.1 Cyclic Stress Approach

In the evaluation of liquefaction potential, it is crucial to obtain how much load is needed in order to initiate (trigger) liquefaction. Therefore, the cyclic loading term which renders liquefaction potential to just amplitude and number of cycles has started to be used in accordance with cyclic shear stresses. In this approach, there are two main terms, namely; cyclic shear stress caused by seismically generated loading and another cyclic shear stress related to liquefaction resistance (Seed & Idriss, 1971). Slightly modified form of these terms are used in this approach. In other words, “cyclic stress

ratio” (CSR) is representative for loading term while “cyclic resistance ratio” (CRR) is an indicator of the resistance term. It is accepted as an onset of liquefaction if resistance is exceeded by loading.

### 2.3.1 Cyclic Stress Ratio (CSR)

Vertically propagating shear waves in horizontal direction induces shear stresses varying with respect to depth within the soil body during an earthquake. Actually, such kind of stresses could be calculated in an accurate way based on the equation of motion if sufficient amount of data comprising soil profile information and dynamic motion input exist. However, for most cases, information that enables dynamically induced shear stresses to be obtained is not available. Moreover, in general, depth of borings is not extended to the depth where liquefaction potential is present in site investigation works. Therefore, the approach proposed by Seed and Idriss (1971) has become widely accepted practice to take effect of induced shear stresses into account.

Seismically induced shear stresses which are a function of time for a soil body can be calculated with the assumption of soil being perfectly rigid by using the simplified procedure proposed by Seed and Idriss (1971):

The concept of the simplified procedure is dependent on demand (CSR) and capacity (CRR) ratios. The demand is the shear stress generation due to the earthquake. The capacity is the resistance of soil against liquefaction. The concept is estimated to be safe for liquefaction, if the resistance capacity exceeds the demand. Moreover the factor of safety is obtained as the capacity divide by the demand (According to Eurocode 8-98.  $FS > 1.25$ ).

$$\frac{Capacity}{Demand} = \frac{CRR}{CSR} = Factor\ of\ Safety \quad (2.1)$$

Where CRR= cyclic resistance ratio, CSR= cyclic stress ratio. Every earthquake is a unique phenomenon, and its effect is also unique. If a general correlation wants to be obtained, the effect should be normalized. Therefore mean equivalent shear stress is

used for  $M_w$  magnitude of 7.5. Seed et al. (1983) proposed the following formula to calculate the CSR due to earthquake shaking. The earthquake-induced CSR, at a given depth,  $z$ , within the soil profile, is usually expressed as a representative value (or equivalent uniform value) equal to 65% of the maximum cyclic shear stress ratio, i.e.(Boulanger and Idriss 2014):

$$CSR = 0.65 \frac{\tau_{max}}{\sigma'_{v0}} \quad (2.2)$$

In the equation given above;  $\tau_{max}$  is the mean horizontal shear stress in the soil generated by the earthquake,  $\sigma'_{v0}$  is initial effective overburden stresses.

### **2.3.2 Cyclic Resistance Ratio (CRR) and Its In-Situ Determination**

The cyclic resistance ratio, which represents the liquefaction resistance of soil, can be obtained by using laboratory experiments or field tests. The field tests include the standard penetration test (SPT), cone penetration test (CPT), Becker penetration test (BPT), large penetrometer test (LPT), and shear wave velocity ( $V_s$ ) test. The SPT was used first in developing liquefaction correlations and was the most common in practice up through the 1990s. The CPT is also a second common method for assessment of liquefaction potential, that has several advantages; however, that has made it the primary site characterization tool under certain geologic settings. The primary advantages and disadvantages of field tests are summarized by Youd (2001) as given in Table 2.3.

#### **2.3.2.1. Evaluation Cyclic Resistance Ratio (CRR) by Using SPT**

The standard penetration (SPT) test is the most commonly used test due to provide practically an indication of the shear strength of soils, and at the same time, it provides disturbed samples. SPT test is used mainly for granular soils such as sands and gravels, cause it is not able to obtain an undisturbed sample.

The CRR could be derived depend on the standard penetration test. However, SPT results (Nm) needs the various procedural corrections for obtaining at a

standardized value, energy-corrected N60 value is summarized by Idris and Boulanger (2010).

Table 2.3. Comparison of various field tests for assessment of liquefaction potential (Youd, 2001).

Feature	SPT	CPT	Vs
Past measurements at liq. sites	Abundant	Abundant	Limited
Type of stress-strain behavior influencing test	Partially drained, large strain	Drained, large strain	Small strain
Quality control and repeatability	Poor to good	Very good	Good
Detection of variability of soil deposit	Good for closely spaced tests	Very good	Fair
Soil types in which test is recommend	Non gravel	Non gravel	All
Soil sample retrieved	Yes	No	No
Test measures index/Eng. Prop.	Index	Index	Engineering

$$(N_1)_{60} = N_m C_N C_E C_B C_R C_S \quad (2.3)$$

Where  $(N_1)_{60}$  is the corrected SPT number, in which  $N_m$  is the measured standard penetration resistance and  $C_N, C_E, C_B, C_R, C_S$  are correction factors based on former researches. Table 2.3 shows the SPT correction factors for different depth and setup-equipment for the SPT because of dissipation of energy during penetration into the soil.

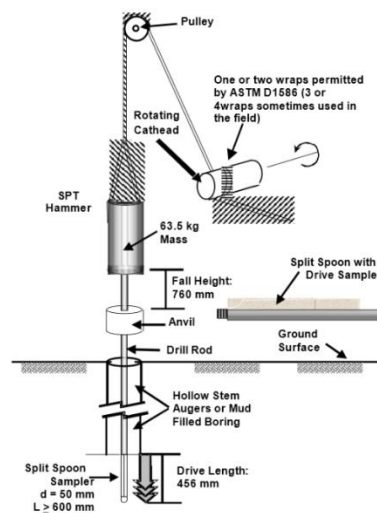


Figure 2.8. Setup and Equipment for the Standard Penetration Test (SPT) (Source: Kovacs et al., 1981).

Table 2.4. SPT Correction Factors

Correction Factor	Variable	Value
$C_R$	3-4m Depth	0.75
	4-6m Depth	0.85
	6-10m Depth	0.95
	>10m Depth	1.00
$C_S$	Standard Sampler	1.00
	Without inner Tube Sampler	1.10-1.3
$C_B$	Diameter 65-115 mm	1.00
	Diameter 150 mm	1.05
	Diameter 200 mm	1.15
$C_E$	Safety Hammer	0. -1.17
	Donat Hammer	0.45-1.00
	Automatic Hammer	0.9-1.60

Where;

$$0.40 \leq C_N = \sqrt{\frac{1}{\sigma_v'}} \leq 1.70 \quad (2.4)$$

$C_N$  is specified by Seed and Idriss (1982).  $\sigma_v'$  = effective overburden pressure.

After SPT results corrected according to sieve analysis, one more correction should be used which is fines content correction.

$$(N_1)_{60,f} = \alpha + \beta(N_1)_{60} \quad (2.5)$$

In the equation,  $\alpha$  and  $\beta$  is change according to fine content of soil.

$$\alpha = 0, \beta = 1 \rightarrow \text{Fine Content} < \%5$$

$$\alpha = e^{1.76 - \left(\frac{190}{FC^2}\right)}, \beta = 0.99 + \left(\frac{FC^{1.5}}{1000}\right) \rightarrow \%5 < \text{Fine Content (FC)} < \%35$$



$$\alpha = 5, \beta = 1.2 \rightarrow \%35 < \text{Fine Content}$$

The actual CRR value of soil can be obtained by using the following equations:

$$CRR = CRR_{7.5} MSF K_{\sigma} K_{\alpha} \quad (2.6)$$

$$MSF = \frac{CRR_M}{CRR_{M=7.5}} \quad (2.7)$$

$$MSF \leq 1.8 \quad (2.8)$$

Required cyclic stress ratio to initiate liquefaction diminishes with the rising of the magnitude of an earthquake due to the fact that both strong motion duration and its corresponding equivalent number of uniform cycles increases with magnitude, during an earthquake. Because the cyclic resistance ratio is a function of both number of cycles (N) and moment magnitudes (M). These two terms are interrelated and they could be adjusted by using Equation 2.6 provided that Equation 2.7 is fulfilled to represent an earthquake magnitude of which is different from 7.5 (Idriss, 1999).

$$CRR_{M=7.5} = \frac{0.048 - 0.048(N_1)_{60,f} + 0.0006136(N_1)_{60,f}^2 - 1.673 \times 10^{-5}(N_1)_{60,f}^3}{1 - 0.1248(N_1)_{60,f} + 0.009578(N_1)_{60,f}^2 - 0.0003285(N_1)_{60,f}^3 + 3.714 \times 10^{-6}(N_1)_{60,f}^4} \quad (2.9)$$

As seen above, CRR value derived for specific moment magnitude of an earthquake because magnitude correction is applied to CRR value according to potential earthquake risk.

Table 2.5. Magnitude correction factors

Magnitude	$CRR_M/CRR_{M=7.5}$
5.25	1.50
6.00	1.32
6.75	1.13
6.75	1.00
8.5	0.89

Cyclic stress was calculated by using the equation below, according to TBDY-2018:

$$\tau_{earthquake} = 0.65\sigma_v(0.4S_{DS})r_d \quad (2.10)$$

Where  $\tau_{earthquake}$  is an amplitude of 65% of the peak cyclic shear stress (i.e.,  $\tau_{cyc} = 0.65 \tau_{max}$ ),  $r_d$  represents the value of a stress reduction factor at a depth of interest,  $S_{DS}$  is spatial design short period spectral acceleration coefficient (non-dimensional) and  $\sigma_v$  is total vertical stress (at a depth of interest). If the original equation (2.2) is considered,  $\tau_{max}$  is transformed into  $S_{DS}$  in equation (2.13), which is a function of earthquake input.  $S_{DS}$  value can be obtained by using <https://tdth.afad.gov.tr> link after login and registration.

In 1997 National Center for Earthquake Engineering Research (NCEER) workshop, it was prescribed that the  $r_d$  values could be determined by using the approach of Liao and Whitman (1986) based on only depth ( $z$ ) for regular works.  $r_d$  values can be calculated by using the following equations:

$$r_d = 1.0 - 0.00765z \quad z \leq 9.15m \quad (2.11)$$

$$r_d = 1.174 - 0.0267z \quad 9.15m \leq z \leq 23m \quad (2.12)$$

$$r_d = 0.744 - 0.008z \quad 23m \leq z \leq 30m \quad (2.13)$$

$$r_d = 0.50 \quad z \leq 30m \quad (2.14)$$

### 2.3.2.2. Evaluation of Cyclic Resistance Ratio (CRR) by Using CPT

The CPT has proved to be a valuable tool for obtaining shear strength parameters. In addition, the different special type of cones can be used to obtain different parameters. It employs various sensors, embedded into a mechanical cone, that collects data related to in-situ soil properties and the pore fluid, as the probe is advanced into the subsurface. The early applications of CPT mainly determined the soil geotechnical property of bearing capacity; nowadays it is complicated data collector about soil layers such as the Piezocone (CPTu) is used to obtain pore water pressures additionally.

A typical CPT (figure 2.9.) involves pushing a 35.7-mm-diameter conical penetrometer into the ground at a standard rate of 2 cm/sec. While electronic transducers record (typically at 2-cm or 5-cm intervals) the force on the conical tip, the drag force on a short sleeve section behind the tip, the pore water pressure behind the tip (or sometimes at other locations), and other quantities (e.g., inclination and temperature). The tip force is divided by the cross-sectional area of the penetrometer to determine the tip resistance,  $q_c$ , and the sleeve drag force is divided by the sleeve surface area to determine the sleeve friction,  $f_s$ . The main advantages of the CPT are that it provides a continuous record of the penetration resistance and the operator error is less than the SPT test. The main disadvantages of the CPT are the difficulty in penetrating layers that have larger particles (e.g., gravels) or very high penetration resistance (e.g., strongly cemented soils) and the need to perform extra borings or soundings to obtain actual soil samples.

In CPT based evaluation of liquefaction potential, the tip resistance ( $q_c$ ) is usually normalized to  $P_a$  (1 atm) to obtain a dimensionless quantity:

$$q_{cN} = \frac{q_c}{P_a} \quad (2.13)$$

After adjusting  $q_c$  as a dimensionless value  $q_{c1N}$ , further management is usually applied to normalize  $q_{cN}$  to standard effective overburden pressure of 1 ton/ft<sup>2</sup>.

$$q_{c1N} = C_N \cdot q_{cN} \quad (2.14)$$

Where  $C_N$  is a normalizing factor, which has different expressions and notations in literature. The purpose of the overburden normalization is to obtain quantities that are more uniquely relate to the sand's relative density ( $D_r$ ) (Youd et. al. (2001)).

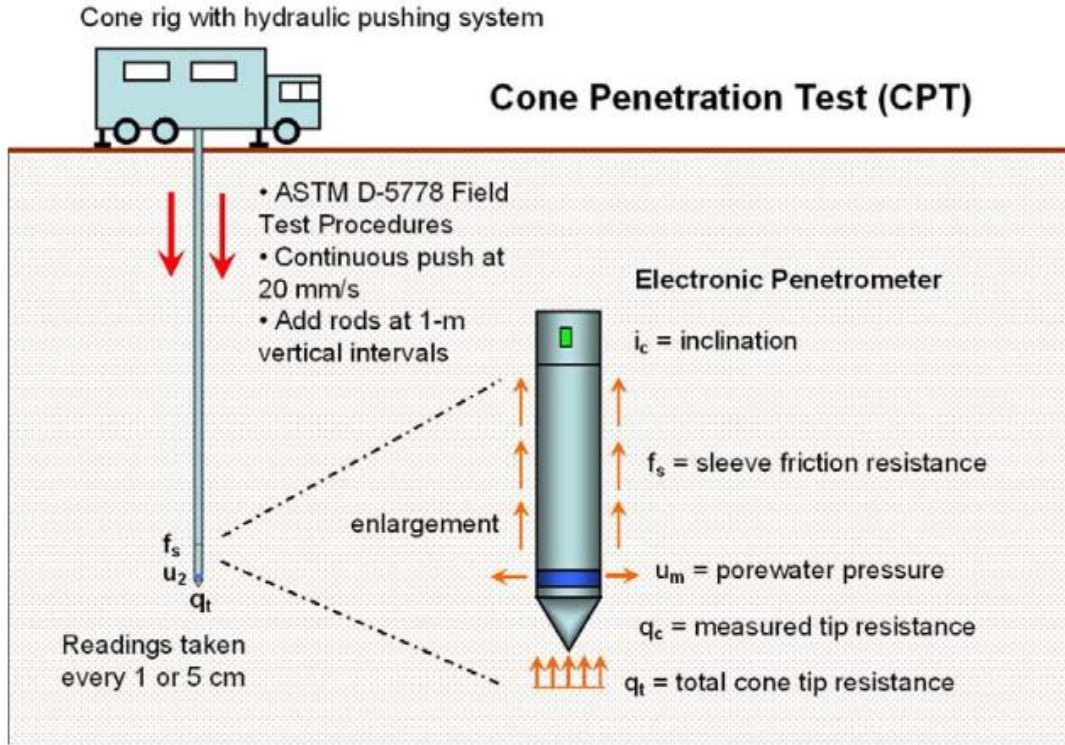


Figure 2.9. Overview of the Cone Penetration Test (CPT) Per ASTM D 5778 Procedures (Source: NCHRP Project 20-05 Final Report, 2007)

In general, the procedure, which was developed by Robertson and Wride (1998), is accepted. Researchers reported that the soil behavior index ( $I_c$ ) obtained from the  $CPT_U$  results for fine-grained soils was an important determinant of the liquefaction, but they could not draw a definite limit on the liquefiable fine-grained soils. The soil behavior index ( $I_c$ ) method depends on grain size characteristic and also obtained from the following equation as suggested by Robertson and Wride (1998);

$$I_c = \sqrt{(3.47 - \log Q)^2 + (1.22 + \log F)^2} \quad (2.15)$$

$$Q = \frac{q_c - \sigma_{v0}}{P_a} \left( \frac{P_a}{\sigma_{v0}} \right)^m \quad (2.16)$$

$$F = \frac{F_s}{q_c - \sigma_{v0}} 100 \quad (2.17)$$

Where;  $Q$  is normalized and modified cone resistance,  $F$  is normalized friction ratio in percent,  $f_s$  is CPT sleeve friction resistance measured in-situ.

According to these deterministic studies and using data from different sites, Robertson and Wride proposed a useful chart for the direct determination of CRR for clean sands ( $FC < 5\%$ ) from CPT data. This figure was developed from CPT case history data compiled from several investigations, including those by Stark and Olson (1995) and Suzuki et al. (1995). Figure 2.10, valid for magnitude 7.5 earthquakes only, shows the calculated cyclic resistance ratio plotted as a function dimensionless vary against, corrected, and normalized CPT resistance  $q_{c1N}$ .

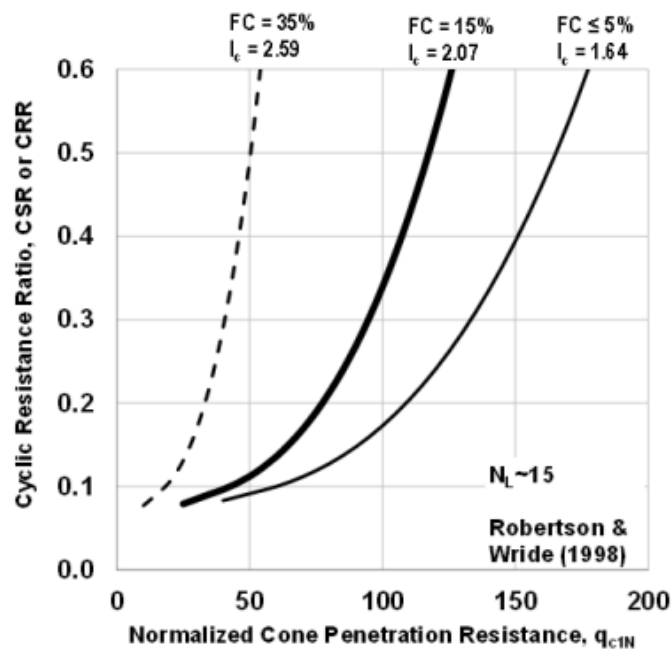


Figure 2.10. Curve for calculation of CRR based on CPT (Source:Robertson and Wride,1998).

## 2.4. Effects of Liquefaction

Liquefaction phenomena is a temporary loss of strength of saturated sandy and silty deposits under transient and cyclic loading due to excess pore water pressure, which was defined in this chapter widely. If the effects of that phenomena would be categorized, the main groups are listed below:

- 1) Alteration of ground motion,

- 2) Sand boils,
- 3) Instability,
- 4) Lateral Spreading

### 2.4.1 Alteration of Ground Motion

During the liquefaction, excess pore pressure is positive and relatively higher effective stress. As a result of this soil stiffness is decreasing from beginning of motion. Amplitude and frequency of the ground motion depend on the stiffness of the medium. If the stiffness of medium decrease due to liquefaction, the amplitude increase. Liquefaction tends to amplify high period ground motions as seen in Figure 2.11 after 5 seconds it happens.

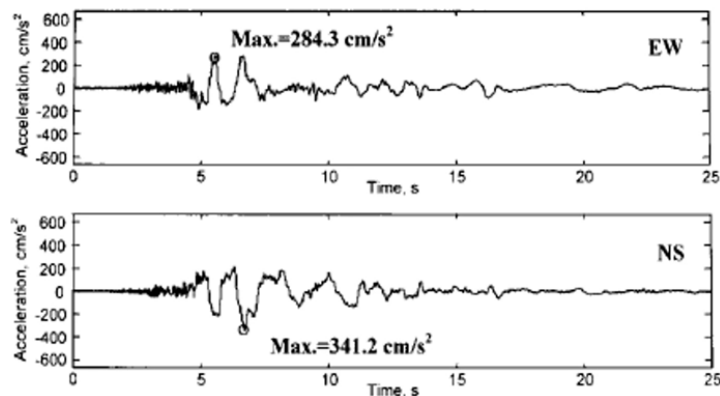


Figure 2.11. Acceleration – time graphics (EW: east-west direction, NS: north-south direction) (Source: CEEN, 2017).

### 2.4.2 Sand Boils

As a result of liquefaction, the sand boils have occurred especially at shallow depth. The liquefaction event is generally considered with sand boiling. The pore pressures are increased due to liquefaction. The need for damping the pore water pressure during the earthquake, causes the water to move upwards. That is observed

as sand boils at the surface. Sand boils could cause floating of embedded structures in the settlement area.



Figure 2.12. Sand boils on the field (Source: USGS).

### **2.4.3 Instability**

In the case of shear stress exceed the shear resistance of soil during liquefaction, instability problems occurs. Soils start to deform and behave like liquid due to shear capacity loss. This may cause lateral deformations, tilting, uplifting of substructures and flow failures. Since shear strength disappears in the sandy ground after liquefaction, bearing capacity disappears as well and significant subsidence occurs in the foundation of surface structures. Figure 2.13 shows a result of instability that the building was tilting due to liquefaction.

Bearing capacity problems are may occurred during liquefaction, depends on shear capacity decline. When effective stress decrease in the sandy ground after liquefaction, bearing capacity decrease as well and significant deformations ( as settlements, tilting and sliding) occurs in the foundation of surface structures.

## 2.4.4 Lateral Spreading

Lateral spreading depends on liquefaction is an instability problem. The lateral spreading is observed mostly in slopes between 0.3 and 3 degrees. This instability problem is effected large horizontal displacement (as seen in figure 2.15).



Figure 2.13. Major tilting of the buildings due to subsoil liquefaction (Source:Ada Pazarı 1999).



Figure 2.14. Loss of bearing capacity of buildings caused by liquefaction (Source: Niigata Nippo Newspaper, 1964).





Figure 2.15. Lateral spreading (Source: wikipedia).

## CHAPTER 3

### REVIEW OF JET-GROUT METHOD

#### 3.1. Introduction

The need for residential areas are growing rapidly and continuously. The suitable areas for settlement and construction not enough after all. Because of that the demand of risky areas and need for geotechnical engineering consultation leveraged. Besides geotechnical engineering and ground improvement methods are improving to solve these problems. Investigations carried out to find out new applications.

A common belief is the first application of jet grouting technique was in Japan (Nakanishi 1974). Jet Grout term was used for different treatment technique, which was eroded soil with high-speed jets. After the eroding process, the soil was filled with cement grout. This methodology was conceived by Yahiro and Yoshida (1973). In the beginning, this method was provided vertical panels of grouted material due to lifting unless rotation of the nozzles.

The jet grouting technology is provided the soil volume filled by grout. This volume is a mixture of soil and grout and it is stiffer than the previous soil. The volume of grouted soil is provided by injection of grout with high velocity and pressure into the soil. The fluids are injected through small-diameter nozzles placed on a pipe that, in its usual application, is first drilled into the soil and is then raised towards the ground surface during jetting.

Jet grouting technique is the use of high-velocity jet streams to erode, replace and then mix the native soil with a cementing agent. The new formation of the jet grouted soil is called as “soilcrete”. The major advantage of jet grouting for soil improvement is that the method can be applied over a wide range of soils, in addition to this fact can be in brief explained by considering the unique outcomes that can be achieved by jet grouting. These include the following:

- Creating mixture soil and grout (cemented) by drilling small holes into the ground, with limited disturbance of the surrounding subsoil,
- Assembling such columns to form continuous elements of various shapes and sizes, provided with good mechanical properties and very low permeability.

Some application of jet grouting is quite new such as water cut off structures in the bottom of excavations. However these new applications are brought on a new point of view for geotechnical problems and influenced the developments of construction. Some different applications of jet grouting are represented in figure 3.1.

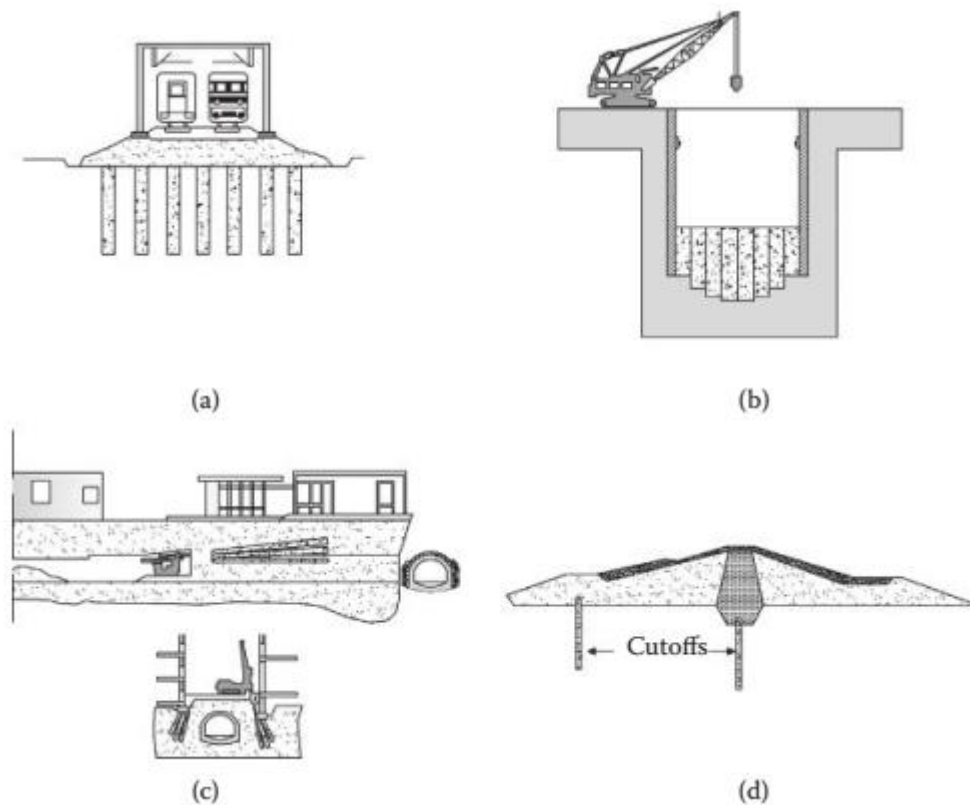


Figure 3.1. Different applications of jet grouting: (a) foundation support, (b) water sealing bottom plug and excavation support, (c) provisional tunnelling support and (d) water cutoff (Source: Croce et al. 2014).

### 3.2. Jet-Grouting Procedure

To construct a jet grouted column, a small diameter bore is drilled with the jet rods and drill bit down to the design depth. For the different diameter of boreholes,

different drilling equipment could be used corresponding to diameter of borehole. In general, this diameter ranges between 100 and 150 mm. Also if it is necessary it can be wider. Drilling can be performed with air, water, grouts or foams as flushing media. Drilling gear and drill fluid are chosen to be appropriate for the soil type. To change the diameter of the jet grouted column and to optimise usage of cement and efficiency in dense, cohesive or very compact soils, pre-cutting with high-pressure water may be employed during initial drilling. Usually, the drilling fluid support side wall of the borehole and prevent collapse. It is pumped throughout the borehole.

When the design depth has been reached, drill bit are slowly withdrawn from the soil. During the withdrawal, grout is injected (jetting) at high pressure (approx. 400 bar) into the soil from jet nozzles which are situated horizontally just above the bottom of the drill bit. Jetting is then performed through one or more nozzles. The speed of particles in the jet is approx. 200m/s. Because the drill rods and drill bit are kept rotating during withdrawal and jetting, a homogenous cylindrical body is produced consisting of a mix of injected grout and displaced soil (Croce et al. 2014). Form and size of the jet grout body can be influenced by varying jet pressure, withdrawal rate and rotation of the jetting gear. Some of the soil-grout mixtures overflow through the drill hole over the ground surface. This spoil is collected and removed. All materials used in the jet grouting process water, cement, occasionally bentonite and the soil are natural inert materials which have no negative impact on groundwater and environment.

In the jet grouting process, cement used for grout is stored in cement bins placed at the site and its freshness should be preserved well. Grout is prepared at batching plant according to intended mixture ratio. After mixing of cement and mixture, grout is conveyed to high pressure pumps and then it is transmitted as high-pressure grout to drill rig machine. Finally, this high-pressure fluid is poured into soil and jet grout column is obtained (Lunardi, 1997).

In figure 3.2. jet grouting procedure is shown schematically. Jet grouted columns can be executed as vertical columns or in any inclination.

Depending on the way how soil is eroded and grouted process, there are the three main process of jet grouting. These processes are single fluid system (grout), double fluid system (air and grout) and triple fluid system (air, water, and grout) as presented in figure 3.3. . Although required equipment does not depend on type of

method, the way how equipment is used, especially in eroding part of the production of a soilcrete, is only the difference between these methods (Figure 3.4).

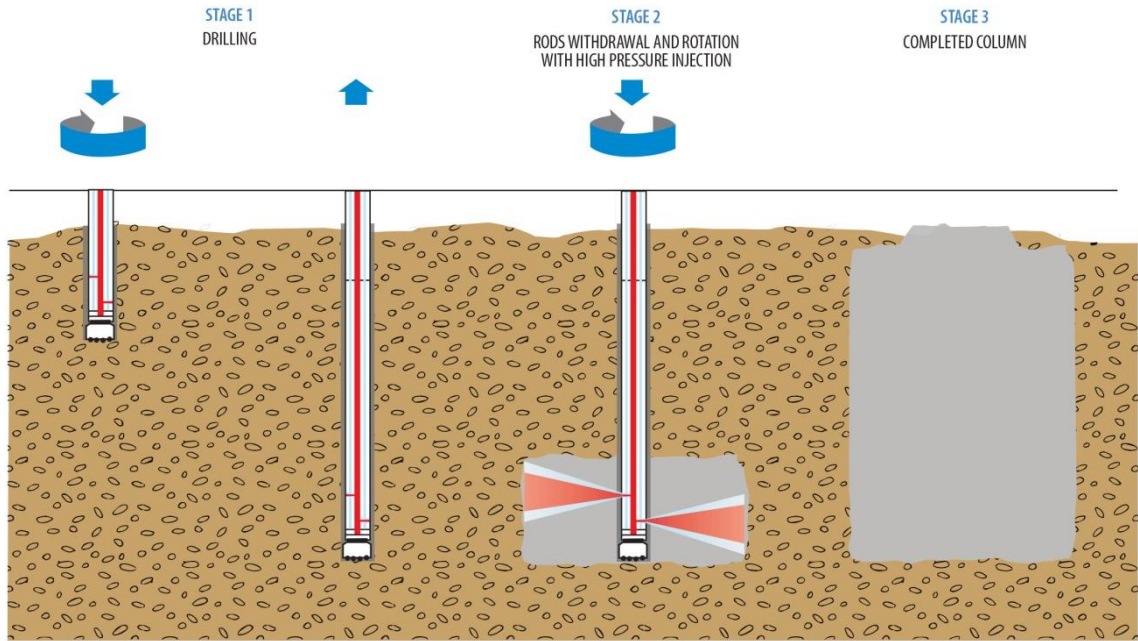


Figure 3.2. Jet grouting method (Source: Croce et al. 2014).

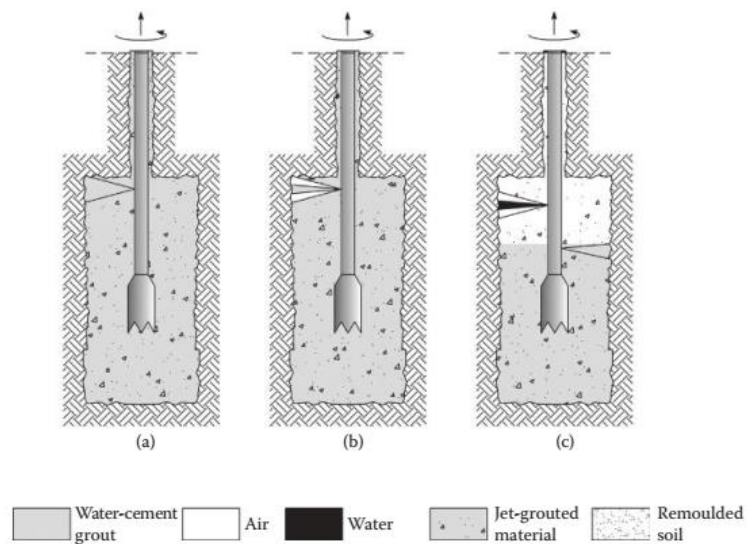


Figure 3.3. General jetting methods: (a) single fluid, (b) double fluid and (c) triple fluid (Source: Croce et al. 2014).

The soilcrete elements are the main feature of this technique. The different arrangements and forms of soilcrete structures are used for different solutions. The partially overlapping of soilcrete columns create some of that complex structures. These structures are used to support the soil in different conditions (figure 3.5.).

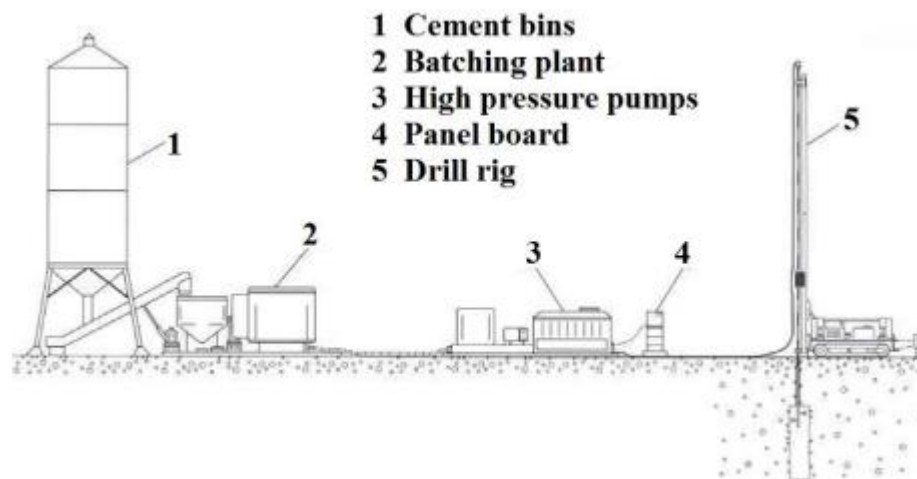


Figure 3.4. The Equipments of jet grouting application(Source:Croce et al. 2014).

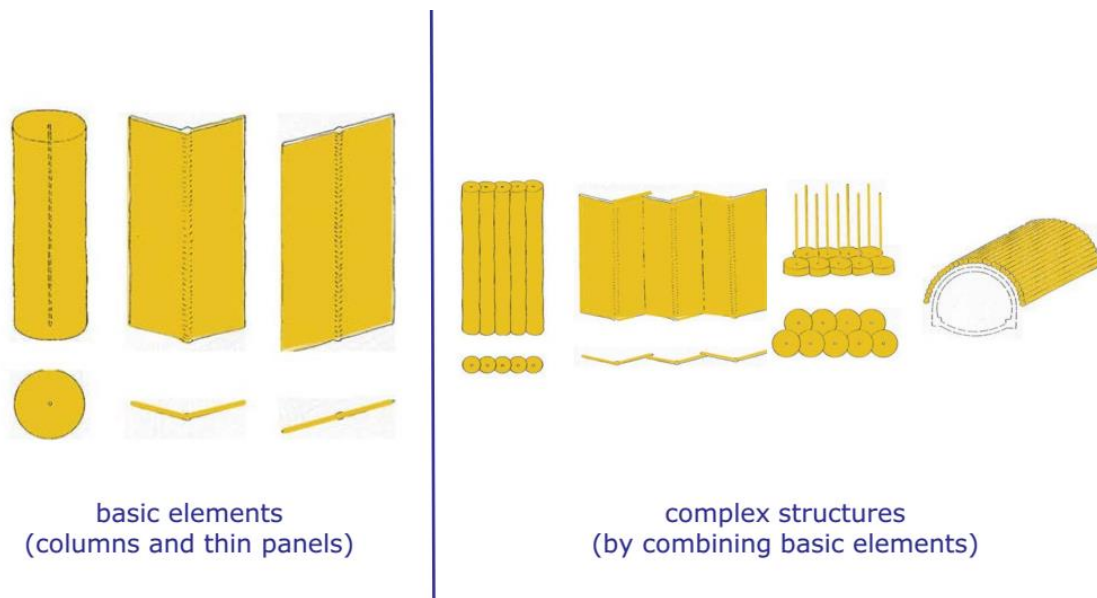


Figure 3.5. Jet grouting elements (Source:Croce et al. 2014).

### **3.2.1 Single Fluid Method**

Single fluid method is the simplest form among three techniques which utilizes cement based fluid to erode and mix the soil (Lunardi, 1997). That means, cementation and subsequent soil remoulding are both caused by the same fluid. Besides, due to only the grout (fluid) is material for eroding, the diameter may not be attained under high level stresses. On the other hand, it should not be forgotten, especially below ground water level, heaving may occur.

### **3.2.2 Double Fluid Method**

By adding compressed air into the single fluid method as auxiliary material, range of sphere of erosion can be increased especially for places under groundwater level. The function of air in this method is to create a buffer zone between groundwater and grout resulting in deeper penetration of grout and to prevent falling of eroded soil into grout which controls energy loss. However, there exists a possibility of grout loss to the surface due to the rise of air content of grout. In the case of encountering such a problem, ground improvement quality may decrease. In comparison to single fluid method, larger column diameter could be obtained (Lunardi, 1997).

### **3.2.3 Triple Fluid Method**

In the triple fluid method, two nozzle groups at different levels which are employed for distinct purposes, one group is responsible for eroding and other group is liable to grouting process. As compared to mentioned two methods, compressed air and jetting water are auxiliary fluid in erosion process. Location of grouting nozzles are at approximately half meter below water-air jetting nozzle so as to make excavated soil particles transmitted to the surface which limits grout ejecting (Xanthakos, Abramson & Bruce, 1994). Although more erosion of soil than double fluid method can be achieved,

triple fluid method promises both erosion and grout injection independent from each other which enables optimization of jetting parameters by providing more control in quality point of view (Lunardi, 1997).

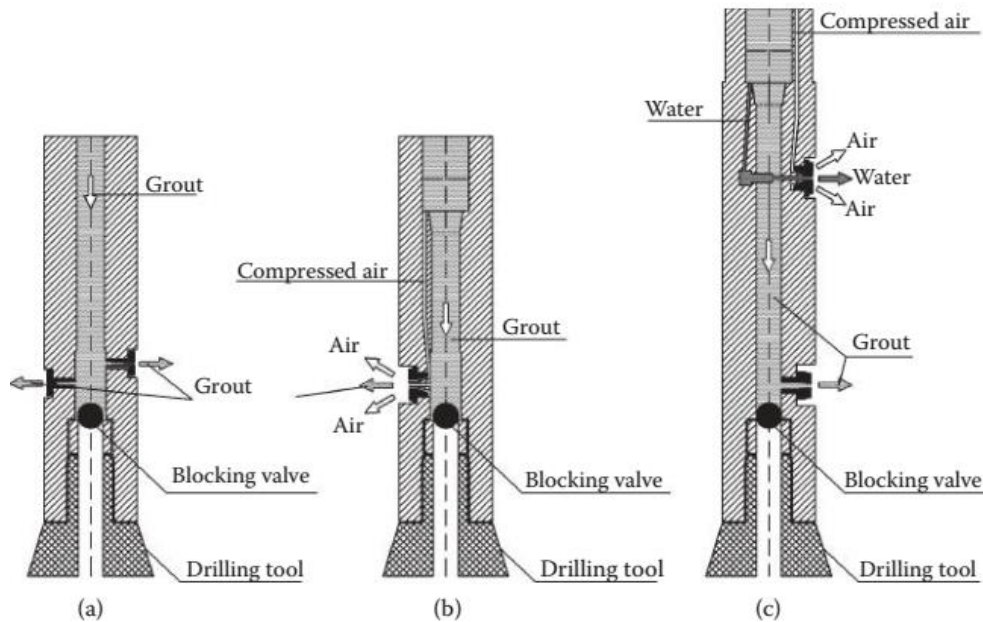


Figure 3.6. Schematic drawings of nozzle groups in jet grouting a) single fluid method, b) double fluid method, c) triple fluid method (Source: Croce et al. 2014).

### 3.3. Operating and Treatment Parameters of Jet Grouting

Every jetting method is tuned by controlling a set of parameters that can be called ‘basic treatment parameters’ and can be grouped as follows (Table 3.1):

- Geometrical characteristics of the mechanical device,
- Kinematic variables defining the movement of the jet grouting string,
- Composition, pressure and flow rate of the injected fluids.

The jet grouting systems have different set of parameters depends on the methods used for grouting, which are single, double and triple fluid mentioned before. Some of them are depend on the fluid method, which are nozzle diameter, fluid pressures and flow rates. These parameters are correlated with each other.



In practice, reference is often made to treatment parameters derived from the basic ones listed in Table 3.2. The derived parameters are as follows:

- Average lifting speed of the monitor,
- Monitor rotations for each lifting step,
- Injected grout volume per treatment unit length,
- Mass of injected cement per treatment unit length.

Table 3.1. List of fundamental treatment parameters (Croce et al. 2014 ).

Parameter	Definition	Symbol	Unit	
			S.I. unit	Practical unit
Geometrical	Number of nozzles	M	–	–
	Nozzle diameter	d	m	mm
	Lifting step	$\Delta s$	m	cm
Kinematic	Time interval per step	$\Delta t$	s	s
	Rotational velocity	$\omega$	rad/s	round/min
	W-C ratio by weight	W/C	–	–
Injected fluids	Fluid pressure <sup>a</sup>	$p_g, p_w, p_a$	MPa	bar
	Fluid flow rate <sup>a</sup>	$Q_g, Q_w, Q_a$	m <sup>3</sup> /s	L/min

<sup>a</sup> The pedex indicates, respectively, grout (g), water (w) and air (a).

Table 3.2. List of derived treatment parameters (Croce et al. 2014 ).

Derived parameter	Relation with the parameters defined in Table 2.1	Unit
Average lifting speed of the monitor	$v_r = \frac{\Delta s}{\Delta t}$	mm/s
Monitor rotations for each lifting step <sup>a</sup>	$n_g = \omega \cdot \Delta t$	–
Injected grout volume per treatment unit length	$V_g = \frac{Q_g}{v_r}$	m <sup>3</sup> /m
Mass of injected cement per treatment unit length <sup>b</sup>	$W_c = \frac{\rho_g \cdot V_g}{1 + W/C}$	kg/m

<sup>a</sup>  $\omega$  expressed in RPM, <sup>b</sup>  $\rho_g$  is the grout density.

In table 3.2 the equations according to derived parameters are given. Those parameters are used for basically diameter estimation and comparison of improving methods.

Considering the results of previous studies the ranges of jet grout parameters are given in table 3.3 (Croce et al. 2014 ). It should be noted, that values are just feedback of typical applications. Different values could be chosen on different conditions. The new jet grouting types of equipment are developed due to technologic development. Because of that, the values given below will change by the time.

Considering the information placed above if the parameters are summerized, four subheads:

- Fluid Pressure
- Nozzle Effect
- Grout Mix (w/c ratio)
- Pull Out Rate and Angular Velocity of Rig

Table 3.3. Typical values of treatment parameters (Croce et al. 2014 ).

<i>Treatment parameter</i>	<i>Symbol</i>	<i>Unit</i>	<i>System</i>		
			<i>Single fluid</i>	<i>Double fluid</i>	<i>Triple fluid</i>
Lifting step	$\Delta s$	mm	40–50	40–80	40–100
Average lifting speed	$v_r$	mm/s	4–10	1–8	0.5–5
Rotational velocity	$\omega$	rpm	5–40	3–30	1–40
Nozzle diameter	$d$	mm	2–8.0	2–8	2–8
Number of nozzles	$M$	–	1–2	1–2	1–2
Grout pressure	$p_g$	MPa	30–55	20–40	2–10
Air pressure	$p_a$	MPa	–	0.5–2.0	0.5–2.0
Water pressure	$p_w$	MPa	–	–	20–55
Grout flow rate	$Q_g$	L/s	2–10	2–10	2.0–5
Air flow rate	$Q_a$	L/s	–	200–300	200–300
Water flow rate	$Q_w$	L/s	–	–	0.5–2.5
W-C ratio by weight	W/C	–	0.60–1.25	0.60–1.25	0.40–1.0

### 3.3.1 Fluid Pressure

In order to erode soil, high pressure is required to obtain soilcrete column for a predetermined diameter. That is, if eroding fluid pressure is greater than the unconfined compressive strength of soil, large diameter jet grout columns are obtained

(Spagnoli, 2008). Instead of using high pressure, same soilcrete diameter can be obtained by using low pressure eroding fluid with longer application time. However, such an application results in extension of construction time of jet grout columns which is an undesired situation with respect to loss of time and money. Operational pressure can be as high as up to 600 bar depending on pumping power.

For a given hydraulic head (pressure at nozzle)  $h$  at the nozzle, the outlet velocity  $v_0$  can be calculated with the following expression:

$$V_n = C\sqrt{2gh} \quad (3.1)$$

in which  $g$  is the gravity acceleration, and  $C$  is a coefficient describing the energetic efficiency of the outflow, that, in turn, depends on the shape and dimensions of the nozzle.

### 3.3.2 Nozzle Effect

Considering the turbulent character of high-velocity jets (figure 3.7.), their characterization will be carried out taking into account only the velocity component parallel to the jet axis. The influence of the shape of the nozzle, of the surrounding fluid pressure and of the shrouding effect of the coaxial annular jet of air will be discussed in the following (Croce et al. 2014 ).

Both number and diameter of nozzles influence jet grouting process with respect to soilcrete diameter. Amount of grout injected to ground, as a result of that, rate of treatment strictly depends on them. However, in order to maintain high pressure, high power pumps are needed to attain high flow rates. Enlarging nozzle diameter provides better efficiency as compared to increasing of the number of nozzles while delivered grout volume is kept constant (Lunardi, 1997).

As the number of nozzles increases, efficiency starts to drop because of high head loss. In case of low power injection pump, limiting number of nozzles by increasing size of nozzle diameter is a common practice in jet grouting. Besides, shape

of nozzle is an important factor from efficiency point of view. That is, high pressure can be obtained by using narrower angles according to Shibazaki (2003).

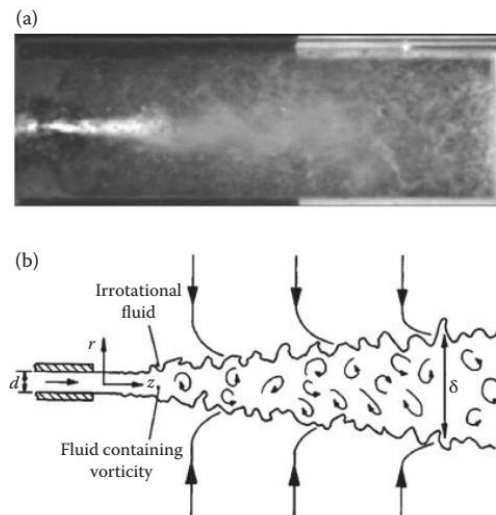


Figure 3.7. Photograph (a) and sketch (b) of a highspeed submerged jet (Source:Bergschneider 2002).

### 3.3.3 Pull-out Rate and Angular Velocity of Drill Rod

In jet grouting, there exist two methods for the way the drill rod is lifted (Figure 3.8). Although intermittent lift method in which drill rod is lifted with constant time interval enables how much rotation of drill rod is necessary to compute by means of integration of unit flow rate over the lifting thickness at that time step, required rotation cannot be obtained in an exact way in steady lift method. Therefore, it is possible to obtain the required diameter for each step. Although soil properties and as a result of that computed thickness varies, as engineering practice, optimum lifting thickness is obtained by means of many trial and error method. That is, 5 cm lifting interval is accepted as optimum for those columns diameter of whom is less than 2 m. As intended diameter rises up, lifting interval becomes larger. Nonetheless, in case of very low extraction speed, the desired diameter may not be obtained due to the accumulation of grout along the outer surface of drill rod.

Angular velocity of drill rod is another factor affecting soilcrete diameter. Due to the fact that angular velocity and pull-out rate is interrelated parameters, optimization of these parameters (Moseley & Kirsch, 2004) is computed according to equation given below:

$$D = KP^\alpha Q^\beta N^\lambda V_n^\delta \quad (3.2)$$

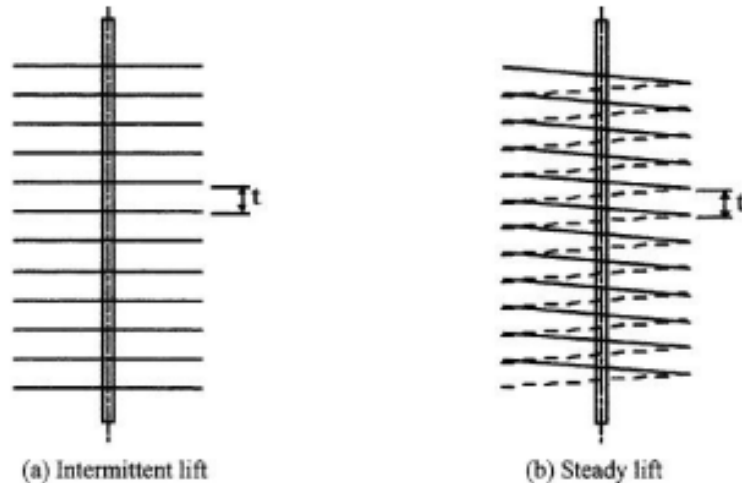


Figure 3.8. Lifting methods of drilling rods (Source: Croce et al. 2014)

Where  $D$  is soilcrete diameter,  $P$  is the pressure of fluid,  $Q$  is flow rate,  $N$  is angular speed,  $V_n$  is pull-out rate, and remaining exponential terms are constants. Likewise pull-out rate, there exists a lower limit for angular velocity in order to prevent reflection of grout from disturbed soil. Also, according to Shibazaki (1996), an increase in angular velocity rises up soilcrete diameter (figure 3.9).

### 3.3.4 Grout Mix (W/C Ratio )

The water and cement are the contains of grout, water/cement ratio is crucial with respect to mechanical properties of soilcrete. That is, uniaxial compressive strength of soilcrete is a function of soil-grout mixture. Besides, in order to attain proper workability of grout, w/c ratio should not be high. In other words, according to

Littlejohn (1982), by using low water/cement ratio, negative effects of bleeding and viscosity decreases. In engineering practice, this ratio is ranging between 0.6 and 1.3. The w/c ratio is decided according to stiffness of soilcrete for each specific improvement. Also w/c ratio is affected on diameter of column.

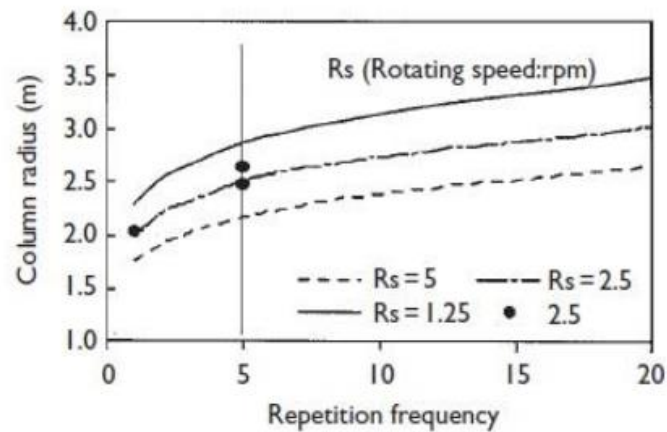


Figure 3.9. Effect of angular velocity on soilcrete diameter (Source:Shibazaki 1996).

### 3.4 Jet Grout Column Mechanical Properties

Mechanical properties of the jet grout columns are an essential part of the proper soil improvement design. These parameters are related to soil type, soil conditions, and grouting process.

#### 3.4.1 Diameter of Column

The estimation of diameter one of the most important thing for jet grout application. Design of jet grout is started to prediction of diameter. Geometry and volume of jet grout structure are decisive in treatment of soil. As an example, columns have to be partially overlapping each other to produce a waterproof structure.

The diameter of jet grout columns depends on erosive fluid parameters and duration of application. However soil conditions have influence reverse due to resistance of erosion.

The designing of the diameter of columns start to decide the jetting method, besides soil conditions should be considering. According to jetting method, basic parameters are assigned, which are lifting speed, grouting pressure and diameter of nozzles. Hence, the experience of applications in variable soil is important to assign these parameters by using correlations. The correlation is given below, can be used to determining mean diameter;

$$D_m = D_{ref} \left( \frac{\alpha_E \Lambda^* E'_n}{75} \right)^\beta \left( \frac{N_{SPT}}{10} \right)^\delta \quad (3.3)$$

where the values of  $\Lambda^*$  are assigned from figure 3.10 depending on the cement– water ratio by weight of the cutting fluid.

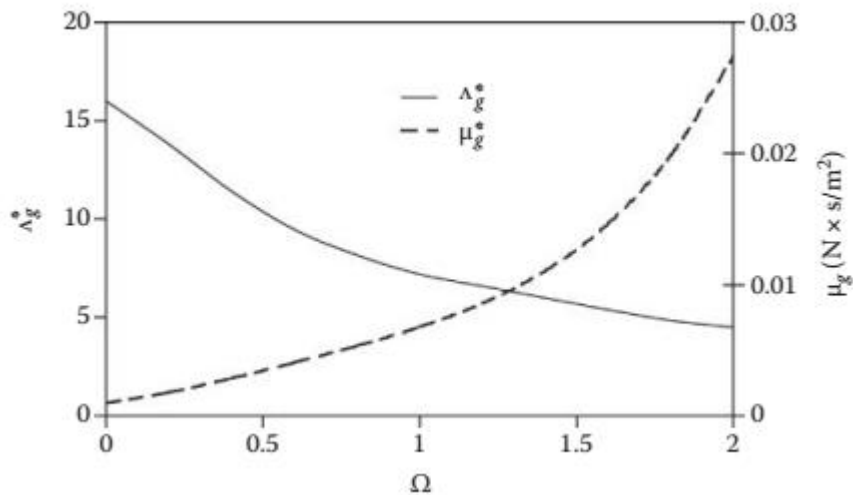


Figure 3.10. Dependency of  $\Lambda^*$  on grout composition ( $\Omega$  is the cement–water ratio by weight,  $\mu_g$  is the viscosity of a cement grout.) (Source: Croce et al. 2014 ).

Because of variety of soil and grouting conditions, the parameters, which are used for determining of mean diameter; must be standardized. Thus reference values are decided for SPT ( $N_{ref}=10$ ), diameter ( $D_{ref}$ ), energy of grouting ( $E'_{ref}= 10$  MJ/m) and cementation dosage ( $\Lambda^*_{ref}\approx 7.5$ ). These parameters are corresponded each other.

As will be shown in the following,  $D_{ref}$  can be calibrated on the results of field trials. Based on the relationship soils between fluid (single, double and triple) of grouting, the mean diameter  $D_m$  expressed as a function of the soil properties ( $N$  and  $q_c$ ) and of the kinetic energy ( $E'_n$ ) at the nozzle per unit length of the column.

$$E'_p = \frac{p_g \times Q_g}{v_r} \quad (3.4)$$

### 3.4.2 Material Properties of Jet Grout Column

Soil grout mixture is decisive in the mechanical properties of the jet grouted material (Croce et al. 2014). In general portland cement is used as the binder material. According to site and soil conditions other type of cements or additives could be used for improving cementation.

During the jet grouting application injection of grout penetrate into soil. That mechanism is an interaction between soil and grout. Soil resists against grouting as it mentioned before, it cause a uprising and damage on the soil. Some waste products uprises. Jet grout column is formed in this process. And material properties of the product depends on interaction between soil and grout.

$$E'_n = 0.9 \times E'_p \quad (3.5)$$

Table 3.4. Values of the parameters to be adopted for the prediction of mean diameter of columns (Croce et al. 2014).

Soil type		ASTM D2487 classification	$D_{ref}$ (m)	$\beta$	$\delta$	$\alpha_E$ (single fluid)	$\alpha_E$ (double and triple fluid)
Coarse grained	Without fine	Gravels and sands with <5% fines (GW-GP-SW-SP)	1.00				
	With fine	Gravels and sands with >5% fines (GM-GC-SM-SC)	0.80	0.2	-0.25	1	6
Fine grained		Silts, clay and organic soils (CL-ML-OL-CH-MH-OH-Pt)	0.50				



The unit weight of the jet-grouted material is of paramount importance for those applications where the self-weight of the jet-grouted structures plays a relevant role. In addition, the unit weight of the jet-grouted material can be seen as an index of treatment effectiveness. In principle, the unit weight depends on the following factors:

- Specific weight of the soil grains
- Specific weight of the hardened grout
- Relative amount of soil and grout
- Amount of voids (i.e., porosity)

The graphic of stress – strain relationship is shown in figure 3.11. And the column is produced in sandy soil. As it seen in figure; behaviour of soilcrete column is significantly stiffer and stronger than natural soil, although soil has a advantage of confinement. Because of the cementation, the jet-grouted material behaves as a soft rock.

The shear strength of the jet grouted material may be expressed considering the effective stress state by the Mohr–Coulomb failure criterion, expressed as:

$$\tau = c_{MC} + \sigma^1 \tan(\varphi_{MC}) \quad (3.4)$$

In the equation  $c_{MC}$  and  $\varphi_{MC}$  are the two parameters of shear strength, which are the friction angle and cohesion. In case of the shear strength would be expressed as a function of cohesion, compressive stress should be neglected. Because Tresca criterion considers that yield occurs under the maximum shear stress. Moreover if the Tresca criterion may be adopted, the equation could be written:

$$\tau = c_T \quad (3.6)$$

The two criteria are obviously related. Since the Tresca parameter  $c_T$  is usually calculated from uniaxial compression tests, the parameters of the two models are linked by the relationship:

$$c_T = c_{MC} \tan\left(\frac{\pi}{4} + \frac{\varphi_{MC}}{2}\right) \quad (3.7)$$

As it known, most common method is Mohr Coulomb used to determine failure criteria in geotechnical engineering. Because, the method is simple and suitable for relatively brittle materials.

However, it is required only when the frictional term is comparable to the cohesive one. This may happen for low values of the cohesion and/or particularly high confining stresses (i.e., very deep or highly confined treatments).

The strength of jet grout column changes with soil type as mentioned before. The study of Fiorotto showed us  $q_u$  values variation for different soils and weight of injected cement in Figure 3.13 (Fiorotto 2000). It is understood that, soilcrete uniaxial compressive strength value getting better in sand and gravel. It is clear, the values of  $q_u$  are the lowest in clay. There are several fundamental reason for this variation. Soil grout interaction is better in coarse-grained soils due to the easy grout penetration. Cementation process is weak for clayey soils because of uncemented parts can exist. When the values are paid attention, soilcrete strength is lower than the concrete. The reason is aggregate is decisive on strength of grout. Xanthakos et al. (1994) give similar indications on the  $q_u$  of jet-grouted materials, suggesting values of the uniaxial compressive strength between 1.5 and 10 MPa for fine-grained soils and between 10 MPa and 30 MPa for coarse-grained soils.

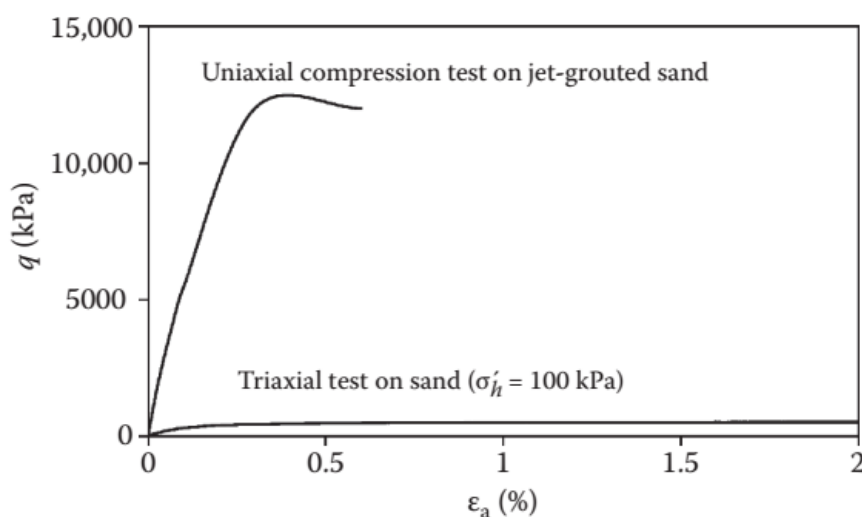


Figure 3.11. Typical strength increment provided by single-fluid jet grouting.

Jetting method is a decisive property on the uniaxial compressive strength ( $q_u$ ). For double fluid method grout is injected with air, as mentioned before. The result of this, dosage of cement is lower than the single fluid method and according to dosage strength is also lower.

This is confirmed by the experimental results reported in Figure 3.14 (van der Stoel 2001). Moreover, the two correlations were proposed by Stoel in 2001 between core uniaxial compressive strength ( $q_u$ ) and w/c ratio for sandy and clayey soils at equation 3.8 and 3.9.

$$\text{For sandy soils: } q_u = 7 + [8.1(w/c)^2] \quad (3.8)$$

$$\text{For clayey soils: } q_u = 2 + [3.6(w/c)^2] \quad (3.9)$$

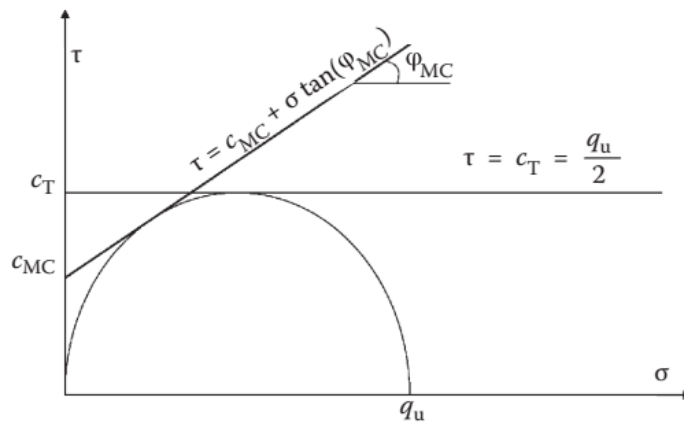


Figure 3.12. The expression of the Mohr Coulomb failure criteria.

Table 3.5. Friction and cohesion parameters according to soil type from case studies (Croce et al. 2014).

Reference	Soil type	$\varphi_T$ (°)	$c_T$ (MPa)
Bzówka (2009)	Sandy	58.2	2.3
Croce and Flora (1998)	Silty sand	26.1	3.2
Mongioli et al. (1991)	Gravel	52.0	2.1
Mongioli et al. (1991)	Gravel	42.0	0.3
Mitchell and Katti (1981)	Clay	39.5	0.58
Yahiro et al. (1982)	Sand and clay	28.5	0.4–1.0
Miki (1982)	Various	20–30	0.7–1.0
Yu (1994)	Clay–silty sand	40.6	1.1
Fang et al. (1994a)	Silty sand	35	4.2
Fang et al. (1994b)	Clay–silty sand	40–44	4.2
Fang and Chung (1997)	Clay and silty sand	38.6	0.8
Fang et al. (2004)	Silt and sand	38.7	0.7
Nikbakhtan and Osanloo (2009)	Clay and sand	42–49	0.4–0.8
	Clay and sand	25	0.77

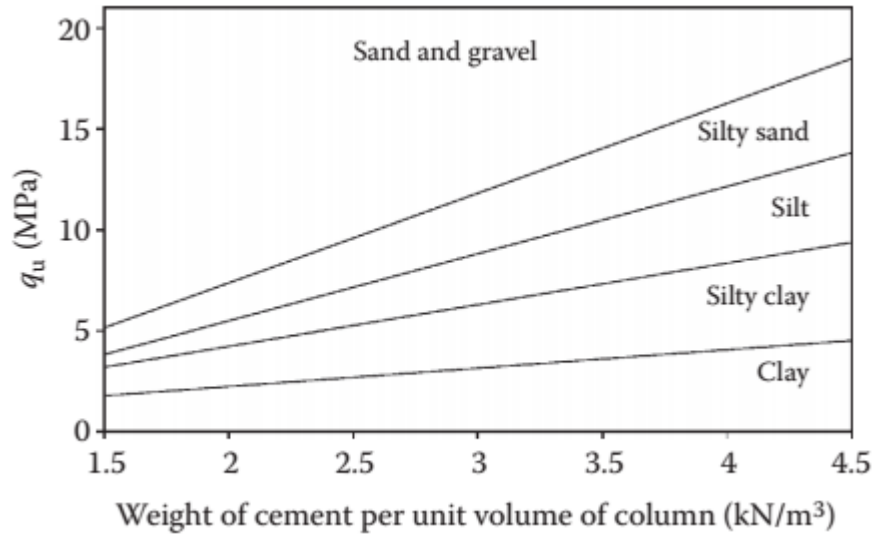


Figure 3.13. The ranges of uniaxial compressive strength for different soil types and variable injected amounts of cement. (Source: Fiorotto, 2000.).

It is assumed that, the mechanical behavior of the jet grout column is linear elastic and super plastic material. According to that, the tensile strength is negligible.

The results support the idea that it can be convenient to correlate stiffness and strength via a simple linear relation which is given in Figure 3.15:

$$E_{50\%} = \beta_E q_u \quad (3.10)$$

In practice, the strength of the jet grout column can be evaluated based on given correlations in this chapter. In addition, the strength can be estimated according to unconfined compression (UC) tests on columns.

As mentioned before, jet grout columns used for water cut off structure due to low permeability of the material. The soilcrete material is accepted impermeable. The mixture of grout and soil is creates an intense structure. Soil grains are surrounded cement grout: therefore ranges of permeability coefficient (Darcy coefficient 'k') are between  $10^{-7}$  and  $10^{-9}$  (m/s) (Croce et al. 2014 ).

### 3.5 Jet Grout Structures

Various jet grouted structures may be produced by overlapping columns and arranging application geometry. The jet grouted structures can also be reinforced with

the insertion of metal or fibreglass bars or tubes, which can provide flexural and tensile resistance if needed .

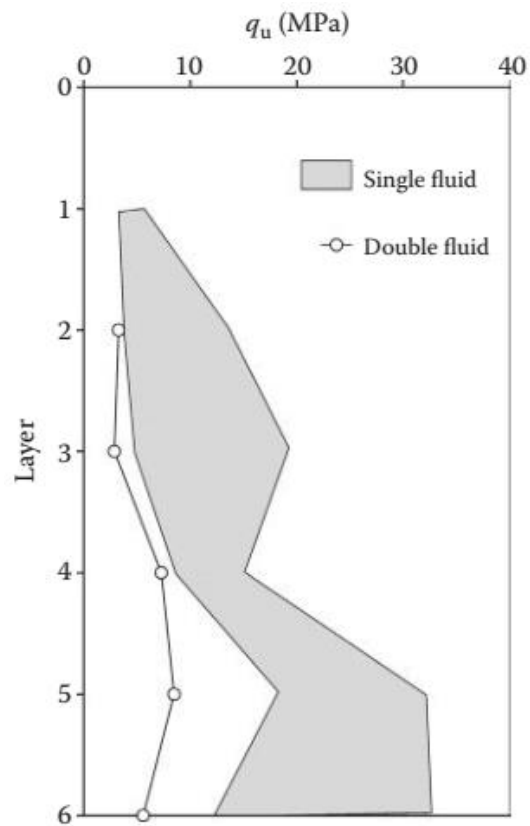


Figure 3.14. The comparison of methods in point of uniaxial compressive strength versus depth. ( Source: Van der Stoel, 2001.).

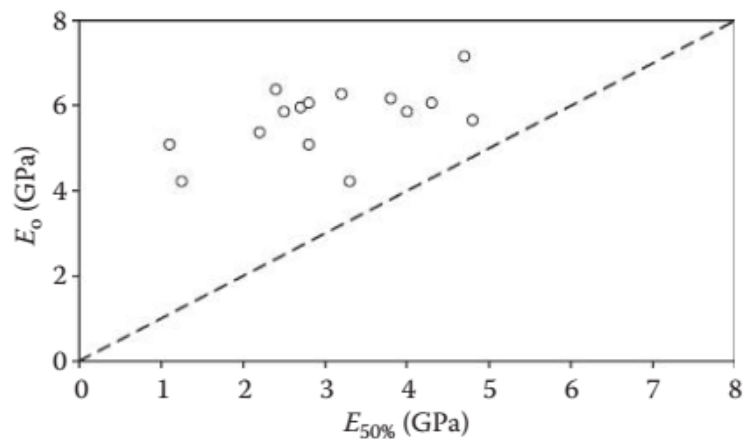


Figure 3.15. Elasticity for large strains modulus  $E_{50\%}$  values change small strain Elasticity for small strains modulus  $E_0$  of jet grout (Croce et al. 2014 ).

In any case, considering the wide variety of geometries that can be obtained by jet grouting treatments, it is possible to classify the consolidated elements based on both their shape and their function. In particular, with reference to the first aspect, it is possible to distinguish three main categories, namely, one-dimensional, two-dimensional and three-dimensional elements.

As seen in previous studies, there is several jet grout technique for remediation of liquefaction, besides it could be grouped under three methods (figure 3.16.):

- Discrete Grid Columns
- In-Ground Shear Wall Grids (Lattice – Cell Design)
- Block and Wall Type
- 

Table 3.6. The variety of values of the coefficient  $\beta_E$  depends on soil types and young modulus for different strain conditions in the literature. (Croce et al. 2014).

<i>Reference</i>	<i>Definition of E</i>	<i>Soil type</i>	$\beta_E$
Mongiovi et al. (1991)	Tangent unspecified	Gravel	280–1000
Lunardi (1992)	Secant at 40% $q_u$	Gravel and sand	500–1200
Nanni et al. (2004)	Tangent unspecified	Gravel and sand	440–1000
Croce et al. (1994)	Tangent unspecified	Sandy gravel	210–670
Croce and Flora (1998)	Secant at $\varepsilon_a = 0.01\%$	Silty sand	220–700
Nanni et al. (2004)	Tangent unspecified	Silty sand	330–830
Fang et al. (2004)	Tangent at 50% of the failure stress	Silty sand	300–750
Fang et al. (2004)	Tangent at 50% of the failure stress	Silty sand, silty clay	100–300
Lunardi (1992)	Secant at 40% $q_u$	Silt and clay	200–500

### 3.5.1 Discrete Grid Columns

The most commonly used technique in jet grouting applications, just producing discrete columns. This geometry depends on either economic requirements or design requirements. It is noted that discrete columns mean the soil among columns must be stayed untreated (figure 3.17.).

The most common one-dimensional elements consist of individual isolated columns, the length of which is much larger than the diameter. Thus, stiffness and strength of the overall jet grouted structure may be smaller than the values of a jet grout column. Consequently the balance of treatment must be carefully designed, especially composite structure properties, considering both treated and untreated soil mechanical properties.

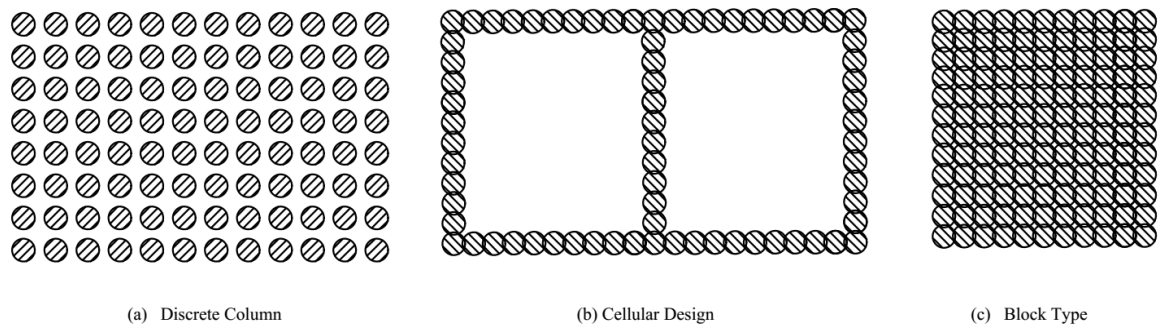


Figure 3.16. Different methods of jet grout application (a): Discrete columns, (b): Cellular (Lattice) Columns, (c): Block Type of Columns.

- Strengthening of soil as volumetric ratio in the soil because of mechanical advantages,
- Support the structures relying on according to bearing capacity is higher than the surrounding soil, even if the soil liquefies.

### 3.5.2. Block Type

Block and wall type is an array, which contains jet grout columns placed as a single big block of jet grouted structure as shown in figure 3.18. If it is necessary, reinforcement can be added in the block. According to tensile stresses on the block, steel or fiberglass bars or steel tubes are used to support of block, and that can be jointed to the foundation.

The most typical massive reinforcement consists of a block of jet grouted structure to reduce settlements and provide adequate resistance to vertical and horizontal loads. The working principle of this jet-grouted structure is the transfer of loads to more competent underlying strata or an enlargement of the foundation base

to enhance the spreading of loads to the surrounding soil. Such massive reinforcements are sometimes associated with piled foundations to provide additional resistance and enhance the performance of these systems (Miyasaka et al. 1992).



Figure 3.17. Discrete jetgrout columns.

Jet grouted structures can be used to produce retaining structures. These structures can be temporary or sometimes permanent according to demands. Hence, the location of jet grout columns is arranged to produce the three-dimensional geometry of retaining structure. The columns intersect each other provided that integrity of the structure.

In deep excavations, jet grouted block method is used to cut off the water in the bottom. The configuration of the column is adjust to produce a shell structure as shown in figure 3.19. On the other hand, for deep excavations the columns are arranged on the sides along one or more parallel lines to form long vertical diaphragms.



### 3.5.3 In-Ground Shear Wall Grids (Cell Design)

The design concept is based on overlapping jet grout columns to form a cellular structure (figure 3.20), reducing the overall deformability of the ground and limiting the development of major shear strains. The cell of jet grout columns reduce the pore pressure, by reducing the shear strains in the soil, inside the treated block.

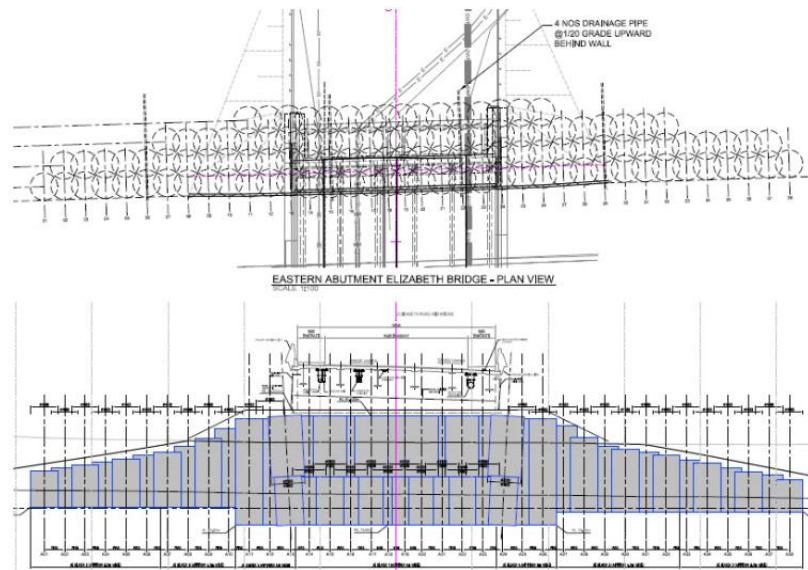


Figure 3.18. Jet grouted mass gravity wall: (a) plan view and (b) elevation (Vincent et al. 2014)



Figure 3.19. An example of jet grout block (Source: zakladani.cz)

A grid of in-ground walls improves a liquefiable site by:

- Reducing earthquake-induced shear strains in the treatment zone, thereby limiting pore pressure generation.

- Containing the enclosed soil should it liquefy, and thus contributing to the composite strength.
- Acting as a barrier to the migration of excess pore pressures from the adjacent untreated zones into the treatment area.

Can be used in a wide variety of soils, including sensitive clays, silts, and sandy silts.

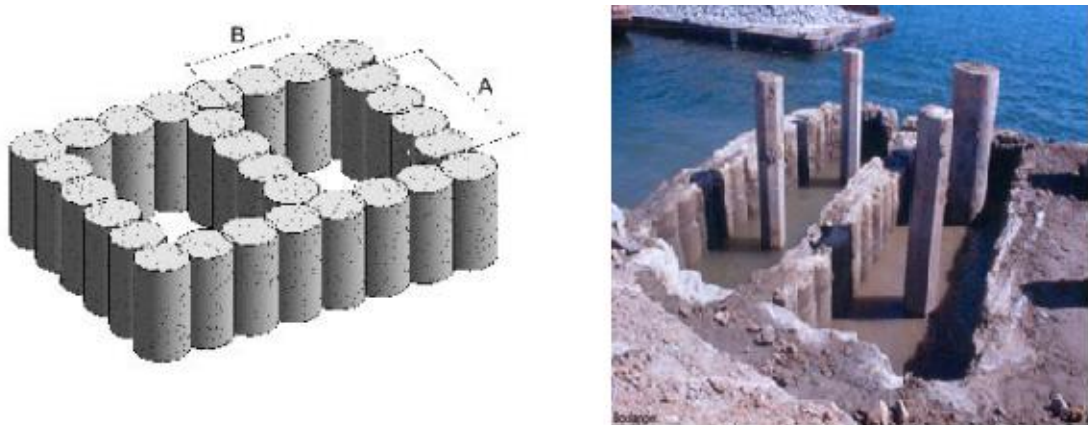


Figure 3.20. Cellular design of jet grout columns (a): plan dimension of cell, (b): an example application near the sea(Source Bolunger., 2012).

### 3.6 Application Control and Monitoring

Although working about soils and with soils almost invariably involves a degree of unpredictability, jet grouting can be counted as one of the most controllable among grouting techniques due to the grouted outcome being dependent to a large degree on various operating parameters. Quality control of the various aspect of jet grouting is thus very important in ensuring effective execution. In general, monitoring and control focus on areas such as parameter control during grouting, verification of results, and effects of grouting on the immediate environment.

If the issues should be summarized, the control and inspection procedures in ground improvement projects with jet injection are essential due to the following uncertainties:

- Whether the dimension (diameter) and column mechanical properties (undrained shear strength and deformation module) are provided in the manufactured components, provided in the design,
- Whether the column-ground interaction is appropriate for the intended behavior in the design,
- Whether manufacturing has a negative impact on environmental structures.

To avoid problems; not just the operators control the process of production, should be monitored and controlled by the engineers in real time, who responsible for the application.

In case of an interruption of the process is even temporarily, treatment of soil effects. Especially where the integrity is essential such as impermeable cutoffs and bottom plugs, tunnel canopies or cellular in ground walls, monitoring of the process is primary importance. The starting locations of drills is determined the following process, but it is just not enough alone. In addition, even integrity and not a cause of particular concern, the lack of controls on perforation and grouting may cause serious problems. Mostly because defects usually appear after the completion of the work. When it becomes, fixing them is very expensive and technically difficult.

Control of the operating parameters (such as jetting pressures, grout flow, lift and rotation rates, etc.) during jet grouting is crucial to the quality of the final result. A proper set of operating parameters will ensure that the grouted columns attain specified dimensions and that the grout distributed evenly within the soil. The actual column dimensions and properties achieved are highly situational.

After the application, integrity and quality of the column could not be observed without excavating the surrounding area of the column or application of any geophysical test. The integrity and quality of cementation must be carefully controlled because they are of primary importance for the success of treatment. In some cases, especially buildings which demand of treatment is high (such as the dam, bridge, and governmental buildings), test columns is built (figure 3.21.). Thus sonic echo tests, coring test and investigation excavation (figure 3.22.) could be done. Various dynamic tests can also be used to determine the homogeneity of cementation in jet-grouted bodies. Sonic echo test (sonic logging) is one of the dynamic tests (figure 3.23. and 3.24.).



Figure 3.21. Test columns (Source: Kellerindia.)

Their basic principle consists of determining the propagation velocity of primary and secondary waves travelling through a definite space. The propagation velocity of waves is determined, knowing the distance between the source and the receiver, by measuring with an oscilloscope the time to cover this distance. Assuming the material equivalent to an elastic medium, the speed of wave propagation can be correlated to the stiffness of the material in the examined portion. Particular care is recommended when this technique is applied using compressive wave velocity in fully saturated materials because water may affect the results.

To evaluate acceptable values according to treatment coring samples should be occurred along the column. The results of coring show quality change of grouting with depth. A practical method to evaluate some mechanical parameters are consulted to Rock quality designation (RQD), or the Core Recovery (CR) index. Thus the effectiveness of cementation is quantified (Yoshitake et al. 2003). Nevertheless, in circumstance which the bearing ratio is important, horizontal or vertical loading tests could be used according to the case. As seen in figure 3.25, the vertical loading test setup contains reaction columns, hydraulic jack, and sensors (load cell, strain gauge, lvdt).



Figure 3.22. Investigation excavation and diameter control of jet grout column (Source: Gökalp and Düzceer 2000).



Figure 3.23. Sonic integrity test over the jet grout column (Gökalp and Düzceer 2000).

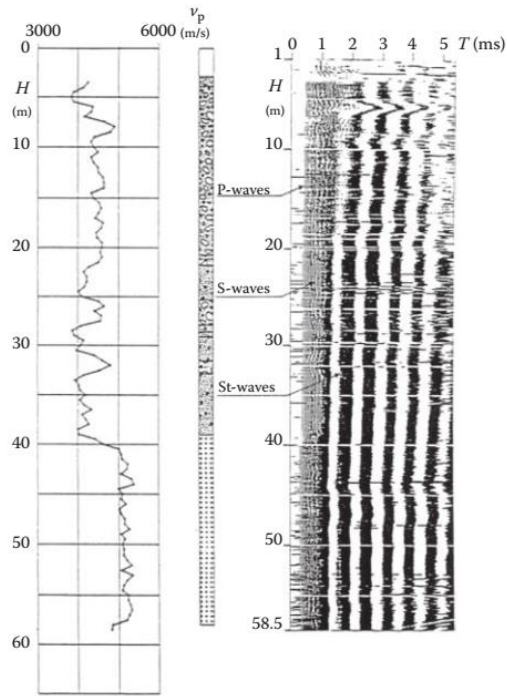


Figure 3.24. Measurement of the quality of jet grouting with sonic logging (Croce et al. 2014).

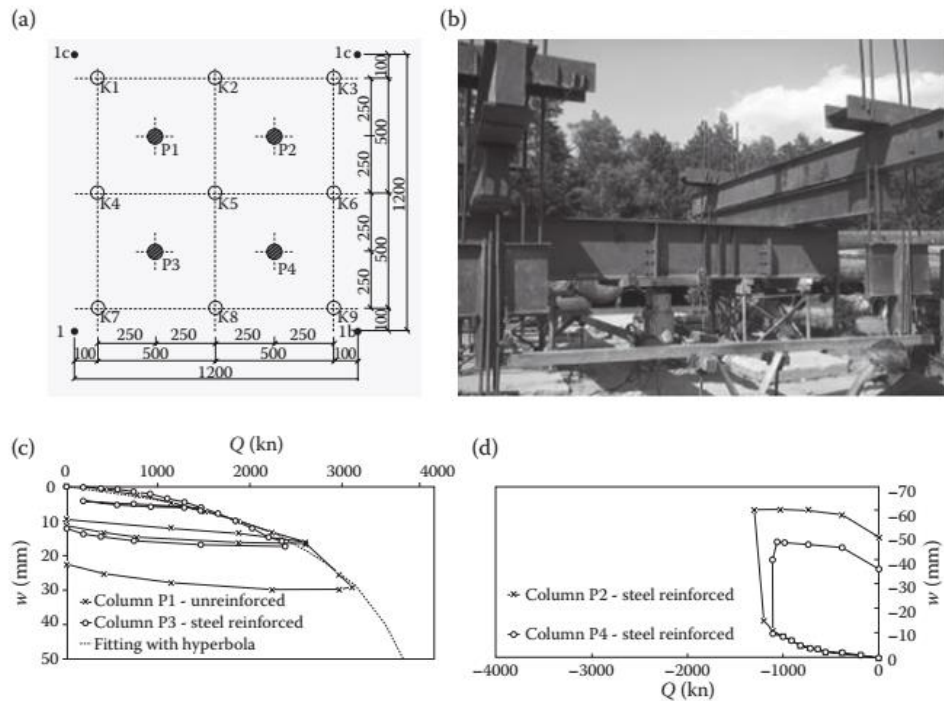


Figure 3.25 Axial loading tests on jet grouting columns (a) experimental setup; (b) picture taken during a compression loading test; (c) results of compression test; (d) results of pullout test. (Source: Bzówka, 2009.).

### 3.7 Use of Jet Grout Against Liquefaction

Liquefaction is one of the major problems in liquefiable soils during earthquakes as mentioned in Chapter 2. Because of these destructive effects of liquefaction, its mitigation became very essential. Recent researches are focused on developing treatment methods for liquefaction. To avoid the liquefaction, treatment provides fundamentally densification and increase of shear stress capacity of the soil. As a result of this in the treated soil is reduced the generation of excess pore water pressure when the ground motion such as earthquake affected.

It should be noted that the liquefaction phenomena occur typically in loose sandy soils, which are particularly suitable for jet grouting treatment. Jet-grout columns are widely used to reduce liquefaction induced hazards in geotechnical engineering practice. The jet-grout columns resist bigger than the soil shear stress depends on earthquake according to the case histories and experiments. Thus soil with the high modulus columns decreases liquefaction potential and its effect. The jet-grout columns resist bigger shear stresses than the soil according to the case histories and experiments. Thus soil with the high modulus columns decreases liquefaction potential and its effect (Rayamajhi et al. 2012, Mitchell and Wentz 1991, Adalier et al. 2003, Martin et al. 2004).

Cooke studied the using jet grouting method under an embankment slope at existing highway bridges to reduce the risk of liquefaction damage due to the earthquake in 2000. The jet grouted soil structure support the embankment against softening due to liquefaction during the earthquake motion. The deformations are restrained depends on jet grouted soil stiffness. The stiffness of untreated soil is very low compared to jet grouted soil. In the study presented; the shear capacity of jet grouted soil relies on the strength of its material.

A jet grout application was investigated in a study, which is performed by Yilmaz et al. on the soil improvement in the Beydag dam against liquefaction in 2008. Properties of the earthquake anticipate that PGA is equal 0.32g and magnitude is 7 at the site. The soil type of site is alluvial and which can be determined as two different layers. That layers are diatomaceous silt and one layer of volcanic ash. In that study, liquefaction potential was calculated depends on the simplified method. Also, the factor of safety for

the liquefaction potential was obtained. To avoid the liquefaction jet-grout technique was used depends on the replacement ratio. Thus the replacement ratio required to reach the intended factor of safety was obtained.



## CHAPTER 4

# DESIGN OF JET GROUTING CELLS TO MITIGATE SOIL LIQUEFACTION UNDER A HISTORICAL BUILDING

### 4.1. Introduction

Fundamentally, the jet grouting applications provide reinforcing for liquifiable soils to reduce the results of the problem as the displacements or to reduce the reasons of the problem as the shear stresses depends on the earthquakes.

It seems logical that the design of jet-grouted structures, like for any other structure, should be developed following a number of logical steps, going from site characterization to cost assessment and passing through the verification of serviceability and ultimate limit states. However, with respect to conventional geotechnical structures, it is commonly recognized that the technological aspects of jet grouting play a more important role. It follows that, in common practice, the designer provides only simple indications on the jet grouting project, which is then specified only at the construction stage, by following some trial-and-error procedure on site (Croce et al. 2014 ).

In this case, an existing building is studied liquefaction potential and its remediation under earthquake effect, which is located in Konak/İzmir. The first design step reported in the flowchart consists of performing geotechnical investigations aimed at the characterization of the subsoil. Particular attention must be paid to the determination of the properties that play a relevant role in the jet grouting process and to the examination of the stratigraphic conditions to identify the variations, even local, of the soil characteristics able to affect the properties of jet-grouted elements. These experimental data which are given in appendix (A), should be carefully examined on the basis of previous experiences to determine whether a given soil is suitable for jet-grouted treatment. Heavily overconsolidated clays, cemented soils and rocks are typical examples in which the usefulness of jet grouting is questionable (Croce et al. 2014).

After the soil properties are obtained, liquefaction potential is calculated by using the simplified procedure depending on the CSR and CRR values. Moreover, the factor of safety tables are prepared due to evaluated liquefaction potential. According to calculations, liquefiable layers are observed.

Finally, design of the jet grout structure is determined. The replacement ratio required to reach the intended factor of safety was obtained. For this study, the existing historical building is the main issue. Thus most effective geometry and minimum column diameter are the goals for mitigation of liquefiable soil layers. The jet grout cells are decided between the different arrangement of columns in various possible ways to create one-, two- or three-dimensional elements.

## **4.2. Site Investigation and Sub Soil Condition**

The building is in Konak borough and the distance from the Aegean sea is 173m. The building was reconstructed in 1980 by governorship and registered by the ministry of culture and tourism. Figure 4.1 shows the front facade of the building. In 2017 restoration construction was started in the building. The building has reinforced concrete frame and aerated concrete masonry. The architectural limitations, lack of suitable structural materials and past construction approaches have active role in the structural performance. The geometry of frame and masonry is not suitable for earthquake resistant structural behavior. Based on performance analysis the building is under restoration and seismic retrofitting construction. According to restoration project the walls should change from aerated concrete masonry blocks to coursed rubble wall. As a result, dead load is increased, due to that earthquake load is increased. When the foundation of the building is investigated, 5 different investigation excavations were made in two blocks (H-block and I-block) which is shown in figure 4.2. According to the investigation excavations, the foundations of blocks were observed, which is spread raft foundation with beams. The foundation elevation drawings are prepared as seen in figure 4.3. That conditions were considered in foundation performance and settlement analysis.

The depths of the foundation are -5.0m for H block and -2.5m for I block. Also the mean length of the short edge of the raft is accepted 20m. According to that, the significant depth is accepted 30m.



Figure 4.1. The front view of the building.

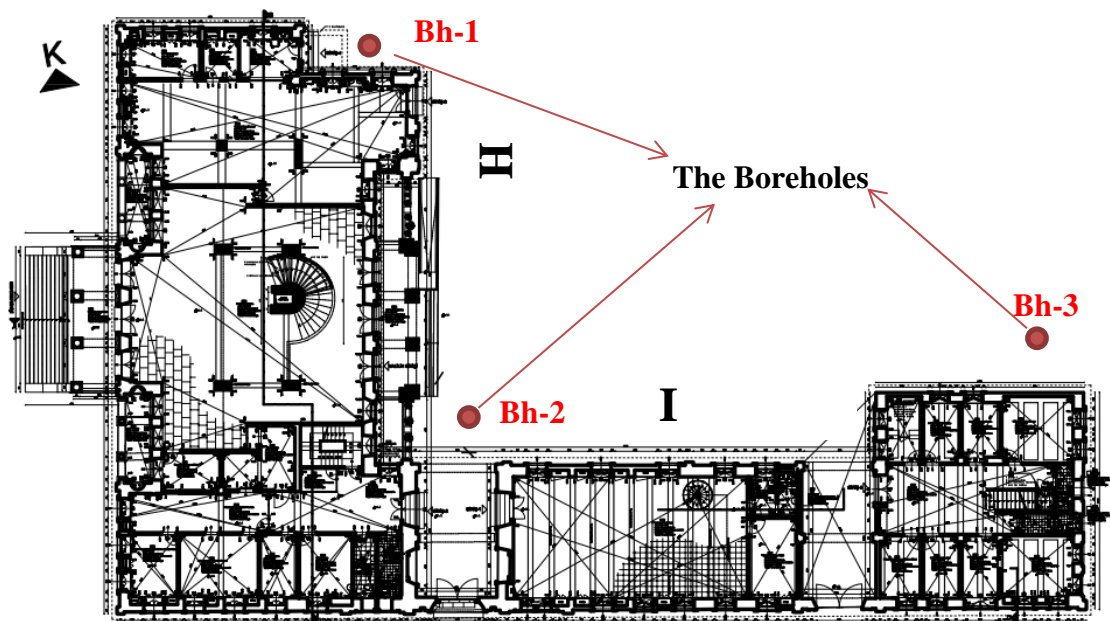


Figure 4.2. Plan of the blocks and the locations of the three boreholes.

In terms of structural health, soil conditions are important as structure performance. In dynamic or static load conditions if a failure occurs in the subsoil, the

structure is directly affected. Considering these circumstance, soil conditions were investigated. Three boreholes were drilled for investigation. Locations of boreholes are chosen for especially determining soil parameters under the building as presented in figure 4.3. As seen in figure 4.4. a hydraulic rotary drill machine was used for the boreholes. Groundwater level was also measured, and it is observed in -2.10m depth. In this study, standard penetration tests (SPT) (figure 4.5.) and multichannel analysis of surface waves (MASW) method were conducted in order to determine the soil mechanical properties and observe the soil profile. Besides, several undisturbed and disturbed soil samples were obtained from boreholes. The details of the test, boreholes and investigation results are given in Appendix A.

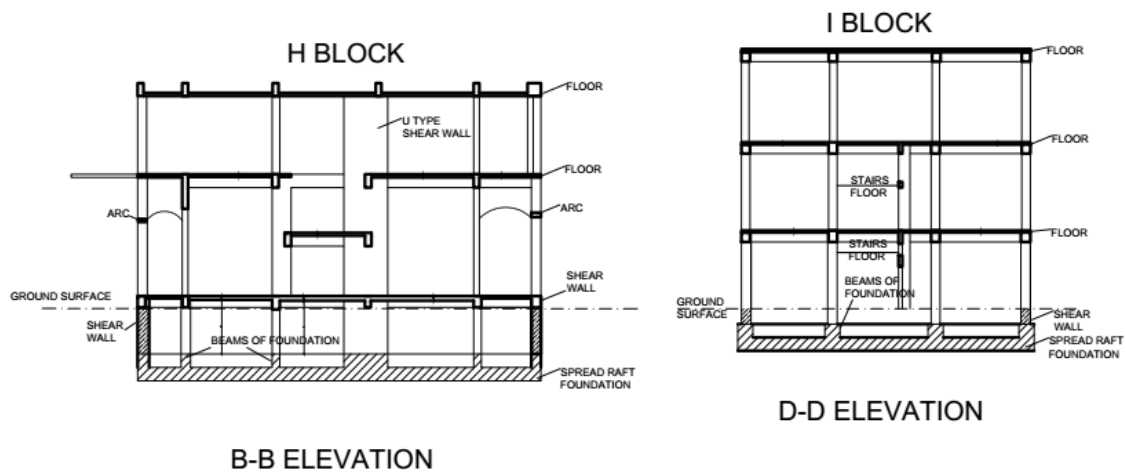


Figure 4.3. B-B elevation and D-D elevation drawings.

Soil profile and engineering parameters were obtained as a result of the site investigation. The susceptible soils are located in the profile until 24.5m depth. The silty soils are mostly (except some layers you can find in appendix) non-plastic.

### 4.3. Calculation of Liquefaction Potential

For this study, for the all boreholes and SPT tests are considered to evaluate liquefaction potential by the method of cyclic stress approach (Chapter 2). The cyclic resistance ratio and the cyclic stress ratio are obtained and determined the factor of safety.

All normalized standard penetration resistance was calculated and recorded, using the equation and factors given above. The effective overburden pressure correction is calculated for all specific depths by using equation (2.4). The correction factors are given above (that were mentioned in chapter 2) is put in the place in equation (2.3), to obtain SPT  $(N_1)_{60}$ .

Once the  $(N_1)_{60}$  results are obtained, according to sieve analysis fines content correction is applied by using the equation (2.5). That sieve analyzes were made on the collected disturbed samples from the site, and the results are given in the appendix.

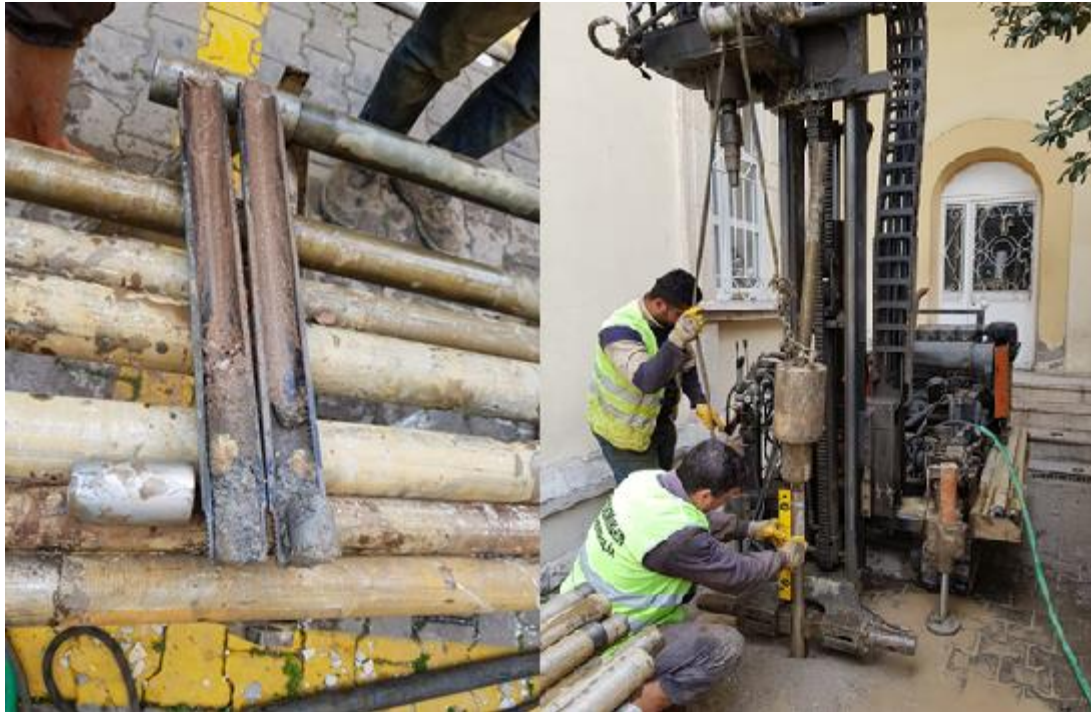
Then,  $CRR_{M=7.5}$  is calculated by using the equation (2.6.) As it was seen CRR value was derived for the influence of specific earthquake. In this study, the magnitude of the design earthquake is given as  $M=6.5$  in site investigation report (Özdemirler Sondaj ve zemin etüdü, 2018). Consequently, earthquake magnitude correction is used from table 2.4.



Figure 4.4. Drilling machine.

Considering equations (2.11) and (2.12), stress reduction factors are calculated, and spatial design short period spectral acceleration coefficient is obtained from maps

of official earthquake risk assessment. For this case  $S_{DS}$  value is 1.09. With these coefficients CSR values are calculated.



(a)

(b)

Figure 4.5. SPT sampler (a) and testing (b).

. In this study factor of safety ((FS), equation (2.1) ) is calculated for each three borehole and all depths of susceptible soil layers. Moreover, liquefaction data tables were generated for all boreholes. These tables were given in the appendix. The summary of liquefaction potential is given in table 4.1, in which the factor of safety values change by depth could be investigated.

When the factor of safety values are considered, it is seen that liquefaction potential is high under a possible design earthquake motion. According to Table 4.2, the investigated soil could liquify.

#### **4.4. Mitigation of Liquefaction Under An Existing Building**

The studies above are made to determine the liquefaction problem. In this section, a suitable procedure is tried to choose for the mitigation of liquefaction under registered building. For open ground as it is known very well, there are several remediation methods such as:

1. Dynamic compaction,
2. Vibro compaction,
3. Stone columns,
4. Deep mixing,
5. Grout injection (compaction injection, permeation injection),
6. Driven Piles (Compaction Piles),
7. Earthquake drains,
8. Jet-grout (In ground shear wall cells).

For our case, there is an existing building. That means, the soil improvements should be made under the raft foundation and at the same time the surrounding buildings have to keep services still. Under these circumstances; dynamic compaction, driven piles, earthquake drains, vibro compaction methods could not be applied. Other methods are assessed in terms of application conditions.

These conditions are:

1. Suitable for inside conditions or under foundation applications,
2. Improvement effectiveness,
3. Application control and monitoring,
4. Potential effects on the building (tilting, settlement... etc.),
5. Duration of application,
6. Cost control.

In terms of conditions above, the jet grout method is chosen. Inside working, application monitoring, making example columns, consumption control, mobility are the advantages of jet grout application methodology.

Table 4.1. Soil profile of the site from boreholes.

Depth	Borehole 1	Borehole 2	Borehole 3
(m)	-	-	-
1.7	GM	GM	GM
3.2	GM	GM	GM
4.7	GM	SM	GM
6.2	GM-GP	SM	GM-GP
7.7	GM-GP	GM	ML
9.2	ML	GM	ML
10.7	ML	GM	ML
12.2	ML	GM	ML
13.7	ML	GM	ML
15.2	CL	CL	CG
16.7	CL	CL	CG
18.2	CL	CL	CG
19.7	CL	CL	CG
21.2		SC-GC	CG
22.7			CG
24.2			CL
25.8			CL
28.0			CI

Table 4.2. Factor of safety values according to depth for all boreholes.

Borehole-1		Borehole-2		Borehole-3	
Depth	FS	Depth	FS	Depth	FS
(m)	-	(m)	-	(m)	-
1.7	0.28	1.7	0.29	1.7	0.3
3.2	0.21	3.2	0.35	3.2	0.3
4.7	0.28	4.7	0.4	4.7	0.3
6.2	0.50	6.2	0.43	6.2	0.77
7.7	0.30	7.7	0.45	7.7	0.57
9.2	0.32	9.2	0.46	9.2	0.27
10.7	0.35	10.7	0.45	10.7	0.28
12.2	0.38	12.2	0.44	12.2	0.27
13.7	0.34	13.7	0.42	13.7	0.29
15.2	0.33	15.2	0.41	15.2	0.36



In ground shear wall cells design is planned for under foundation soil:

- Additional shear strain due to ground motion is restricted in the mitigation area, therefore excess pore pressure could not also be increased.
- Surrounding the soil provides strengthening depends on the composite mechanical properties.
- Surrounding the soil provides impermeability for the boundaries of cells. The excess pore water pressure could not transmitted from untreated areas into the treatment area due to the impermeable boundaries.

Cells should also resist the inertial force of the unimproved soil mass surrounded by the improved soil grids and the dynamic earth pressure exerted from the original soil located on the outside of the improved zone. A schematic of external forces acting on the improved soil grids during an earthquake is shown below in figure 4.6.

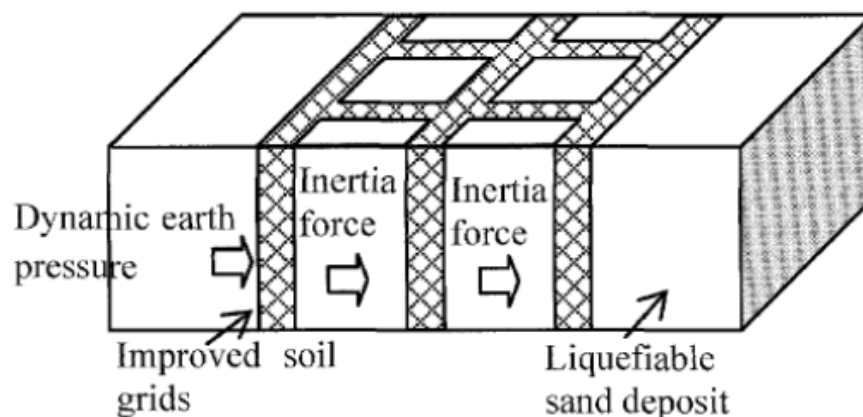


Figure 4.6. External forces applied to jet grout cells during an earthquake.(Source: Jeremic, 2010).

H block has  $860\text{m}^2$ , and I block has  $440\text{m}^2$  foundation area. The soil improvement is planned through 15m depth for I block and through 10m depth for H block because of the basement.

Soil conditions are suitable to improve by jet grouting. The single fluid method is chosen, because of the simplicity of parameters and easy to application control such as diameter, and fluid pressure. The control and simplicity depends on the single erosive, which is the grout. These factors should be considered, when the project and planning processes are continuous.

Table 4.3. Recommended application parameters intervals (according to Croce et al. 2014) for single fluid system and values to be used in this study.

Parameters	Symbol	Unit	Typical values of improvement	Values to be applied
Lifting step range	$\Delta S$	mm	40-50	45
Ave.lifting speed	$V_r$	mm/s	4.0-10	6.25
Rotational velocity	$\omega$	rpm	5.0-40	20
Nozzle diameter	$d$	mm	2.0-8.0	2
Number of nozzles	$M$	-	1-2	2
Grout pressure	$P_g$	MN/m <sup>2</sup>	30-55	40
Air flow rate	$P_a$	bar	-	-
Water flow rate	$P_w$	bar	-	-
Grout flow rate	$Q_g$	L/s	2.0-10	2
W-C ratio by weight	w/c	-	0.60-1.25	1

As mention in Chapter 3, the diameter of the jet grout column is designed according to necessities of problems. The engineering parameters of jet grout column is obtained according to chapter 3. The diameter of columns is an essential parameter about jet-soil interaction, and soil-jet area ratios ( $a_r$ ) is affected directly. The cell design improvement aspect is to create confined soil grids. This cell grids provide increasing shear stress capacity of subsoil. For all cells  $a_r$  and shear modulus of improved soil are calculated in the design process. Moreover, the parameters of the jet grout application is determined according to calculations.

The jet grouting dimaeters are given for borehole-1 in Table 4.4. The jet grout column mechanical properties are given for borehole-1 in Table 4.7.

After jet grout parameters were determined, than composite soil parameters, were calculated using equations given below (Barksdale and Bachus 1983):

$$\gamma_{comp} = \gamma(1 - a_r) + \gamma_{jg}a_r \quad (5.1)$$

$$c_{comp} = c_s(1 - a_r) + c_{jg}a_r \quad (5.2)$$

$$\phi_{comp} = \tan^{-1}(a_r \tan(\phi_{cj}) + ((1 - a_r)(\tan(\phi_{cj}))) \quad (5.3)$$

$$E_{comp} = E_s(1 - a_r) + E_{jg}a_r \quad (5.4)$$

In table 4.13 jet grout – soil composite parameters are given, where  $\gamma_{comp}$  is the unit weight of the composite material,  $c_{comp}$  is the cohesion of the composite material,  $E_{comp}$  is the modulus of elasticity of the composite material. Those calculations are essential for numerical analysis because treated soil was considered as composite material due to limitations of the two dimensional (2D) modeling.

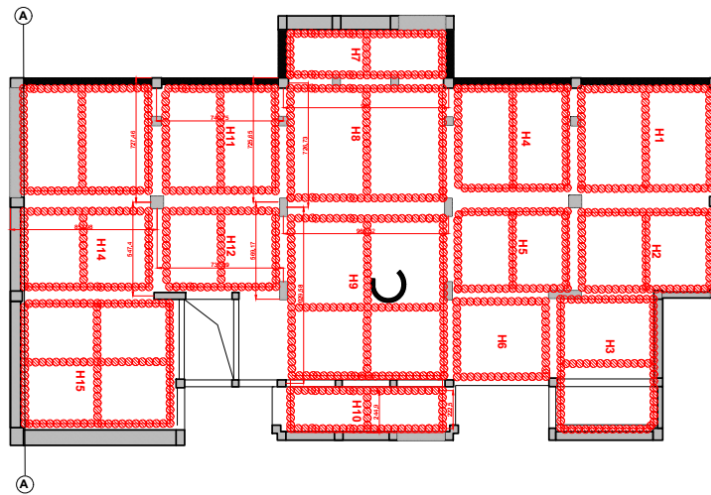


Figure 4.7. Application plan drawings of jet grout cells the plan of H block



Figure 4.8. Application plan drawings of jet grout cells of I block.

The effect of columns were expressed by Baez in 1995 against liquefaction in earthquake shear stresses as the ratio of earthquake shear stresses reduced after recovery to shear stresses on the original ground as shown in equation 5.5.

$$K_G = \frac{\tau_s}{\tau_d} = \frac{CSR_i}{CSR} \quad (5.5)$$

In equation 5.5,  $K_G$  is cyclic reduction factor,  $\tau_s$  is shear stress in the soil,  $\tau_d$  is shear stress generated by the earthquake and  $CSR_i$  is cyclic stress ratio after the improvement. The cyclic reduction factor was improved by researchers. Besides, the cyclic reduction factor is modified by Boulanger for cell design due to the numerical analysis in 2012.

$$K_G = \frac{1}{\gamma_r G_r C_G a_r + (1 - a_r)} \quad (5.6)$$

In the equation 5.6,  $\gamma_r$ : unit deformation factor is accepted equal to one for cell design,  $C_G$ : shape factor is accepted equal to 0.5 for cell design. An example calculation of jet grouting parameters are given in Appendix A.

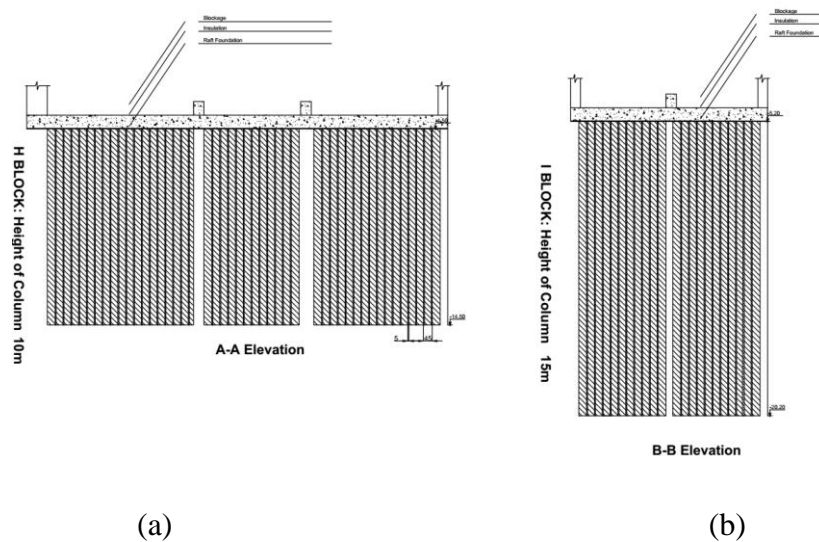


Figure 4.9. Elevation drawings of jet grout cells (a): the section of H block, (b): the section of I block.

Table 4.4. Calculated jet grout column diameter parameters for the borehole-1.

Borehole 1	Depth	Mean Dia.	$\gamma_s$	SPT N	$D_{mean}$	$D_{design}$
	(m)	(m)	kN/m <sup>3</sup>	-	m	m
	1,5-1,95	1.7	19.9	4	0.85	0.68
	3.00 - 3.45	3.2	19.9	4	0.85	0.68
	4.50 - 4.95	4.7	19.9	10	0.67	0.54
	6.00 - 6.45	6.2	17.7	24	0.54	0.43
	7.50 - 7.95	7.7	17.7	15	0.61	0.49
	9.00 - 9.45	9.2	19.7	8	0.71	0.57
	10.00 - 10.45	10.7	19.7	10	0.67	0.54
	12.00 - 12.45	12.2	19.7	12	0.64	0.51
	13.50 - 13.95	13.7	19.7	9	0.69	0.55
	15.00 - 15.45	15.2	19.7	8	0.71	0.57

Table 4.5. Calculated jet grout column diameter parameters for the borehole-2.

Borehole 2	Depth	Mean Dia.	$\gamma_s$	SPT N	$D_{mean}$	$D_{design}$
	(m)	(m)	kN/m <sup>3</sup>	-	m	m
	1,5-1,95	1.7	19.91	4	0.85	0.68
	3.00 - 3.45	3.2	19.91	4	0.85	0.68
	4.50 - 4.95	4.7	19.91	6	0.76	0.61
	6.00 - 6.45	6.2	17.66	34	0.50	0.40
	7.50 - 7.95	7.7	17.66	30	0.51	0.41
	9.00 - 9.45	9.2	19.72	5	0.80	0.64
	10.00 - 10.45	10.7	19.72	6	0.76	0.61
	12.00 - 12.45	12.2	19.72	5	0.80	0.64
	13.50 - 13.95	13.7	19.72	6	0.76	0.61
	15.00 - 15.45	15.2	19.72	11	0.66	0.53

Table 4.6. Calculated jet grout column diameter parameters for the borehole-3.

	Depth	Mean Dia.	$\gamma_s$	SPT N	$D_{mean}$	$D_{design}$
	(m)	(m)	kN/m <sup>3</sup>	-	m	m
Borehole 3	1,5-1,95	1.7	19.91	4	0.85	0.68
	3.00 - 3.45	3.2	19.91	4	0.85	0.68
	4.50 - 4.95	4.7	19.91	6	0.76	0.61
	6.00 - 6.45	6.2	17.66	34	0.50	0.40
	7.50 - 7.95	7.7	17.66	30	0.51	0.41
	9.00 - 9.45	9.2	19.72	5	0.80	0.64
	10.00 - 10.45	10.7	19.72	6	0.76	0.61
	12.00 - 12.45	12.2	19.72	5	0.80	0.64
	13.50 - 13.95	13.7	19.72	6	0.76	0.61
	15.00 - 15.45	15.2	19.72	11	0.66	0.53

Table 4.7. Calculated jet grout column mechanical parameters for the borehole-1.

	Depth	$q_u$	$(q_u)_{design}$	$\beta_E$	$E_{50}$	$G_s$	$G_c$	$G_r$	$a_r$	$K_G$
	(m)	MN/m <sup>2</sup>	MN/m <sup>2</sup>	-	KN/m <sup>2</sup>	kN/m <sup>2</sup>	kN/m <sup>2</sup>	-	-	-
Borehole 1	1,5-1,95	6.00	3.75	350	1312500	4006.875	468750	117.0	0.24	0.068
	3.00 - 3.45	6.00	3.75	350	1312500	3824.851	468750	122.6	0.24	0.065
	4.50 - 4.95	6.00	3.75	350	1312500	4049.846	468750	115.7	0.24	0.068
	6.00 - 6.45	6.00	3.75	350	1312500	7962.132	468750	58.9	0.24	0.128
	7.50 - 7.95	6.00	3.75	350	1312500	7108.253	468750	65.9	0.24	0.115
	9.00 - 9.45	6.00	3.75	350	1312500	3740.632	468750	125.3	0.24	0.063
	10.00 - 10.45	6.00	3.75	350	1312500	3816.893	468750	122.8	0.24	0.065
	12.00 - 12.45	6.00	3.75	350	1312500	3669.122	468750	127.8	0.24	0.062
	13.50 - 13.95	6.00	3.75	350	1312500	3744.914	468750	125.2	0.24	0.063
	15.00 - 15.45	6.00	3.75	350	1312500	4040.926	468750	116.0	0.24	0.068

Table 4.8. Calculated jet grout column mechanical parameters for the borehole-2.

Borehole2	Depth	$q_u$	$(q_u)_{design}$	$\beta_E$	$E_{50}$	$G_s$	$G_c$	$G_r$	$a_r$	$K_G$
	(m)	MN/m <sup>2</sup>	MN/m <sup>2</sup>	-	KN/m <sup>2</sup>	kN/m <sup>2</sup>	kN/m <sup>2</sup>	-	-	-
	1,5-1,95	6.00	3.75	350	1312500	4006.875	468750	117.0	0.24	0.068
	3.00 - 3.45	6.00	3.75	350	1312500	3824.851	468750	122.6	0.24	0.065
	4.50 - 4.95	6.00	3.75	350	1312500	4049.846	468750	115.7	0.24	0.068
	6.00 - 6.45	6.00	3.75	350	1312500	7962.132	468750	58.9	0.24	0.128
	7.50 - 7.95	6.00	3.75	350	1312500	7108.253	468750	65.9	0.24	0.115
	9.00 - 9.45	6.00	3.75	350	1312500	3740.632	468750	125.3	0.24	0.063
	10.00 - 10.45	6.00	3.75	350	1312500	3816.893	468750	122.8	0.24	0.065
	12.00 - 12.45	6.00	3.75	350	1312500	3669.122	468750	127.8	0.24	0.062
13.50 - 13.95	6.00	3.75	350	1312500	3744.914	468750	125.2	0.24	0.063	
15.00 - 15.45	6.00	3.75	350	1312500	4040.926	468750	116.0	0.24	0.068	

Table 4.9. Calculated jet grout column mechanical parameters for the borehole-3.

Borehole 3	Depth	$q_u$	$(q_u)_{design}$	$\beta_E$	$E_{50}$	$G_s$	$G_c$	$G_r$	$a_r$	$K_G$
	(m)	MN/m <sup>2</sup>	MN/m <sup>2</sup>	-	KN/m <sup>2</sup>	kN/m <sup>2</sup>	kN/m <sup>2</sup>	-	-	-
	1,5-1,95	6.00	3.75	350	1312500	4006.875	468750	117.0	0.24	0.068
	3.00 - 3.45	6.00	3.75	350	1312500	3824.851	468750	122.6	0.24	0.065
	4.50 - 4.95	6.00	3.75	350	1312500	4049.846	468750	115.7	0.24	0.068
	6.00 - 6.45	6.00	3.75	350	1312500	7962.132	468750	58.9	0.24	0.128
	7.50 - 7.95	6.00	3.75	350	1312500	7108.253	468750	65.9	0.24	0.115
	9.00 - 9.45	6.00	3.75	350	1312500	3740.632	468750	125.3	0.24	0.063
	10.00 - 10.45	6.00	3.75	350	1312500	3816.893	468750	122.8	0.24	0.065
	12.00 - 12.45	6.00	3.75	350	1312500	3669.122	468750	127.8	0.24	0.062
13.50 - 13.95	6.00	3.75	350	1312500	3744.914	468750	125.2	0.24	0.063	
15.00 - 15.45	6.00	3.75	350	1312500	4040.926	468750	116.0	0.24	0.068	

Table 4.10. Calculated jet grout column liquefaction potential parameters for the borehole-1.

Borehole 1	Depth (m)	(CSR) Before	(CSR) Improved	(CRR) M=6.5	FS
	1,5-1,95	0.28	0.02	0.1	5.2
	3.00 - 3.45	0.34	0.02	0.09	4.1
	4.50 - 4.95	0.38	0.03	0.1	3.9
	6.00 - 6.45	0.41	0.05	0.33	6.2
	7.50 - 7.95	0.43	0.05	0.26	5.1
	9.00 - 9.45	0.44	0.03	0.12	4.4
	10.00 - 10.45	0.43	0.03	0.13	4.5
	12.00 - 12.45	0.42	0.03	0.12	4.5
	13.50 - 13.95	0.4	0.03	0.12	4.7
	15.00 - 15.45	0.39	0.03	0.14	5.4

Table 4.11. Calculated jet Grout column liquefaction potential parameters for the borehole-2.

Borehole 2	Depth	CSR Before	CSR Improved	CRR M=6.5	FS
	1,5-1,95	0.29	0.02	0.10	5.1
	3.00 - 3.45	0.35	0.02	0.09	4.0
	4.50 - 4.95	0.40	0.03	0.10	3.7
	6.00 - 6.45	0.43	0.05	0.33	5.9
	7.50 - 7.95	0.45	0.05	0.26	4.9
	9.00 - 9.45	0.46	0.03	0.12	4.2
	10.00 - 10.45	0.45	0.03	0.13	4.3
	12.00 - 12.45	0.44	0.03	0.12	4.3
	13.50 - 13.95	0.42	0.03	0.12	4.5
	15.00 - 15.45	0.41	0.03	0.14	4.76



Table 4.12. Calculated jet Grout column liquefaction potential parameters for the borehole-3.

Borehole 3	Depth	CSR Before	CSR Improved	CRR M=6.5	FS
	1,5-1,95	0.28	0.02	0.10	5.2
	3.00 - 3.45	0.34	0.02	0.09	4.1
	4.50 - 4.95	0.38	0.03	0.10	3.9
	6.00 - 6.45	0.41	0.05	0.33	6.2
	7.50 - 7.95	0.43	0.05	0.26	5.1
	9.00 - 9.45	0.44	0.03	0.12	4.4
	10.00 - 10.45	0.43	0.03	0.13	4.5
	12.00 - 12.45	0.42	0.03	0.12	4.5
	13.50 - 13.95	0.40	0.03	0.12	4.7
	15.00 - 15.45	0.39	0.03	0.14	5.41

Table 4.13. Calculated jet grout - soil composite parameters.

Depth	$\gamma$	$a_r$	$\gamma_{jg}$	$\gamma_{comp}$	$c_s$	$c_{jg}$	$c_{comp}$	$\phi_s$	$\phi_{comp}$	Es	Ejg	$E_{comp}$
(m)	kN/m <sup>3</sup>	-	kN/m <sup>3</sup>	kN/m <sup>3</sup>	kN/m <sup>2</sup>	kN/m <sup>2</sup>	kN/m <sup>2</sup>	degree	degree	kPa	kPa	kN/m <sup>2</sup>
1.7	19.9	0.24	22	20.41	8	6000	1446.1	29.20	56.39	9616.5	5793043	1397639
3.2	19.9	0.24	22	20.41	8	6000	1446.1	28.20	56.09	9179.6	5793043	1397307
4.7	19.9	0.24	22	20.41	10	6000	1447.6	29.42	56.46	9719.6	5793043	1397717
6.2	17.7	0.24	22	18.70	10	6000	1447.6	41.55	60.31	19109.1	5793043	1404853
7.7	17.7	0.24	22	18.70	10	6000	1447.6	39.55	59.65	17059.8	5793043	1403296
9.2	19.7	0.24	22	20.27	19	6000	1454.4	27.69	55.93	8977.5	5793043	1397153
10.7	19.7	0.24	22	20.27	15	6000	1451.4	28.15	56.07	9160.5	5793043	1397292
12.2	19.7	0.24	22	20.27	15	6000	1451.4	27.23	55.79	8805.9	5793043	1397023
13.7	19.7	0.24	22	20.27	15	6000	1451.4	27.71	55.94	8987.8	5793043	1397161
15.2	19.7	0.24	22	20.27	15	6000	1451.4	30.20	56.7	10102.3	5793043	1398008

## CHAPTER 5

# NUMERICAL ANALYSIS OF LIQUEFACTION MITIGATION

### 5.1. Introduction

In this chapter, the numerical analysis for liquefaction and its remediation are discussed. There are different analysis methods, different material models and different software solutions developed for geomechanics approaches. Data and case study are given for finite difference models. Pore pressure generation for liquefaction due to ground acceleration will be examined by the finite difference method (FDM). Within the scope of this chapter, the details of these numerical simulations of the results are presented with the numerical models and their parameters are given below.

FLAC (Fast Lagrangian Analysis of Continua) is an explicit finite difference numerical program for engineering mechanics computation. It was first developed in 1986 specifically to perform analyses on microcomputers operating on Microsoft Windows systems. Today, the software is designed to take advantage of multi-core processing for high-speed computation of model grids containing several thousand elements. Typical engineering problems were solved in several hours using the original FLAC. With the current FLAC, the solution time has reduced considerably. FLAC was originally developed for geotechnical and mining engineers, and since then, this versatile program has become an essential analysis and design tool in a variety of civil, mining, and mechanical engineering fields (ITASCA, Flac8 Basics 2015).

Both FLAC's Finite Difference Method (FDM) and the Finite Elements Method (FEM) turn a group of differential equations into matrix equations for each element, relating forces at nodes to displacements at nodes. There is not much difference between FEM and FDM for elastic materials. Moreover, FLAC has some differences:

1. Flac is more reliable than implicate FEM for plastic collapse loads and plastic flow, because of the mixed discretization diagram is accurate (Marti and Cundall 1982) .
2. When a static problem is solved the software uses dynamic equations of motion. It provided that calculations to be stable.
3. The explicit method gives better results for nonlinear conditions even large strain problems. However, the duration of solving these problems is shorter than implicit method.
4. FLAC can use constitutive without any regulation operation.
5. FLAC makes identification operations of elements according to row and column array.
- 6.

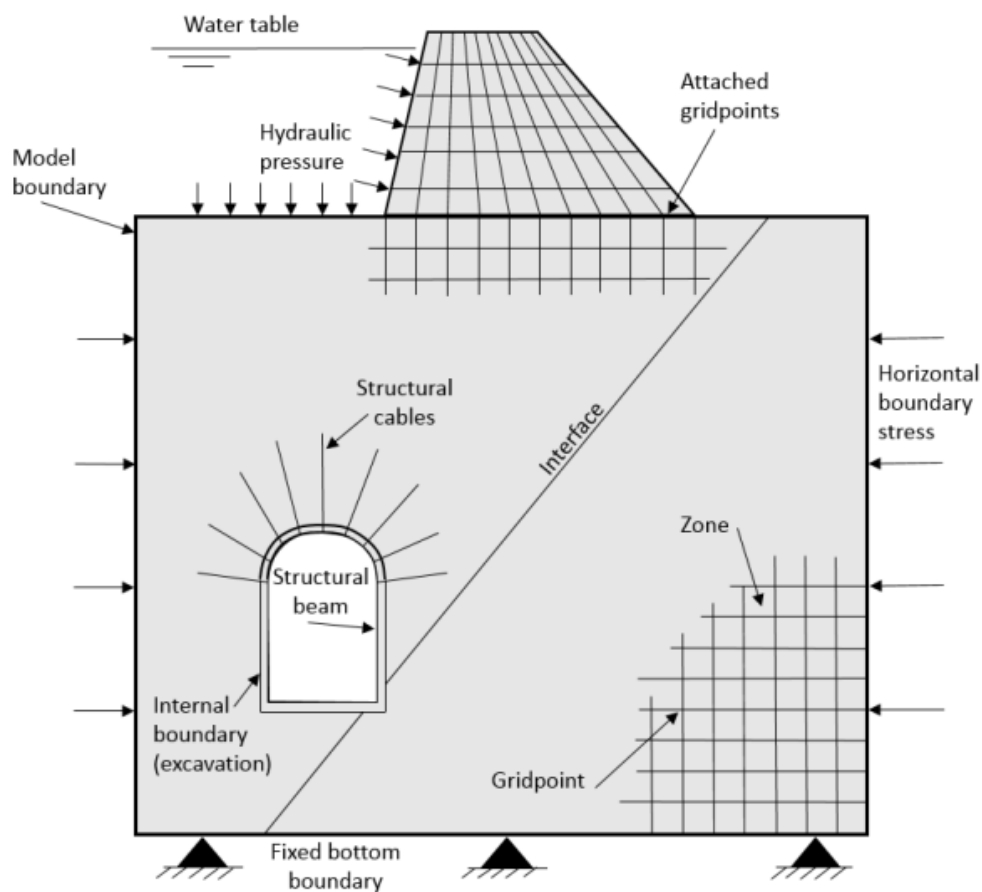


Figure 5.1. Elements of a FLAC model(Source: Flac, 2008).

In this study, numerical analysis were repeated to improve the results. The numerical analysis stages are given below:

1. Initial Conditions,
2. Static Loading Stage,
3. Dynamic Loading stage.

The first stage is to ensure initial conditions, which is contained geometric generations, soil materials, groundwater, gravity, boundary conditions, initial soil pressures. The second stage is to generate a foundation as a beam element and to apply structural loads. The third stage is to apply dynamic conditions and acceleration.

These stages were repeated before and after soil treatment. Treated soil conditions were modeling as composite soil. This composition is included soil and jet grout columns both.

## **5.2. Background of Method**

One of the numerical methods is the finite difference method for solving complicated problems (Desai and Christian 1977). The differential equations are solved by using initial and boundary conditions. In the method, physical variables are determined in terms of algebraic derivatives.

The finite difference method is used set of algebraic equations to solve. The theme of the finite difference method is focused on approximating differentials. In contrast to this, weighted residual methods evaluate the integral of a differential equation and optimize an approximation such that the integrals of the correct and the approximated solutions match on a given domain. Therefore, these equations use integral approximations.

The most important issue is that the concept of calculations should be understood if to get to the approach of the solution. The difference is a static situation calculation included the dynamic equations. It is useful for large deformation problems because calculations are stable even under nonlinear material conditions. In physical conditions every strain cause to kinetic energy, which must be dissipated and damped.

FLAC models this process directly because inertial terms are included kinetic energy is generated and dissipated.

In figure 5.2, the logic of calculation is expressed. As seen in the loop, the method calls the equations of motion to derive new velocities and displacements by using stresses and forces. After that, strains are derived from velocities, and new stresses from strain rates. Every turn of the loop takes time, which is called the time step. The main feature is the strains, velocities and stresses updated in every turn of the loop.

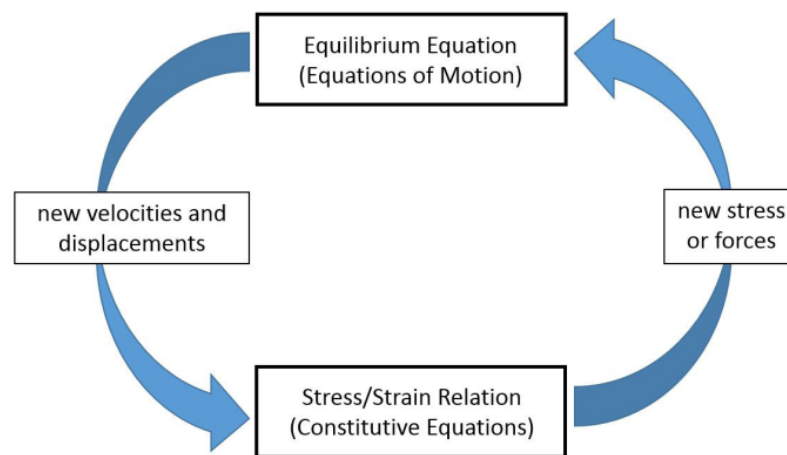


Figure 5.2. Basic explicit calculation cycle.

### 5.3. Model Geometry and Boundary Conditions

The main objective of this study is to carry out two-dimensional finite difference modelling of the foundation and sub soil conditions. Other important discuss is the jet grout improvement behavior and its effect on the liquefaction mechanism. Therefore, a general raft foundation geometry was selected for the analysis with the soil layers. The cross-section of the selected foundation along a representative of mean geometry in the latitudinal direction is shown in figure 5.3.

The foundation of the building, side walls, and the basement floor are represented as beam elements in the numerical model. The width of the foundation is 21.0 m and depth of foundation is 5.0m. The thickness of the raft is 0.7m, the thickness

of the side walls are 0.3 m accepted in the model. The total horizontal length of the model is taken to be 200.0m, which is ten times the base width of the foundation in order to minimize boundary effects. The depth of the model is accepted 30.0m according to boreholes.

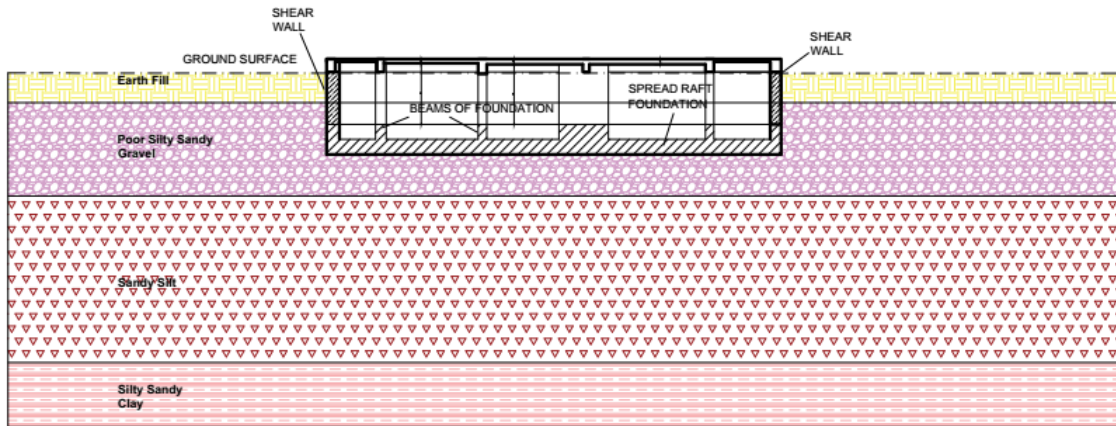


Figure 5.3. Foundation geometry and the soil profile.

In this study, the numerical analysis contains three different calculation steps:

1. Initial stage:

In this stage, initial and boundary conditions of the problem environment are determined for general static conditions.

2. Static loading stage:

In this stage, structural elements and its loads are determined due to balanced the internal stresses before the dynamic loading.

3. Dynamic Loading stage:

In this stage, dynamic loading conditions and dynamic boundary conditions are determined.

For the first and second stage of analysis have standard fix boundary conditions, which are horizontal fixed boundaries for sides, vertical and horizontal both fixed boundaries for the bottom. In dynamic load conditions boundary conditions should be different from the static boundary conditions. For sides free-field conditions and for the bottom quiet boundary conditions are applied as shown in figure 5.4.

In this study, the grid (mesh) generation is important for calculations. Calculation speed depends on grid size, as well as the accuracy of calculations depends. The modeling conditions, such as grid size, effect on the wave propagation process in dynamic analysis. Numerical distortion can occur on wave transmission.

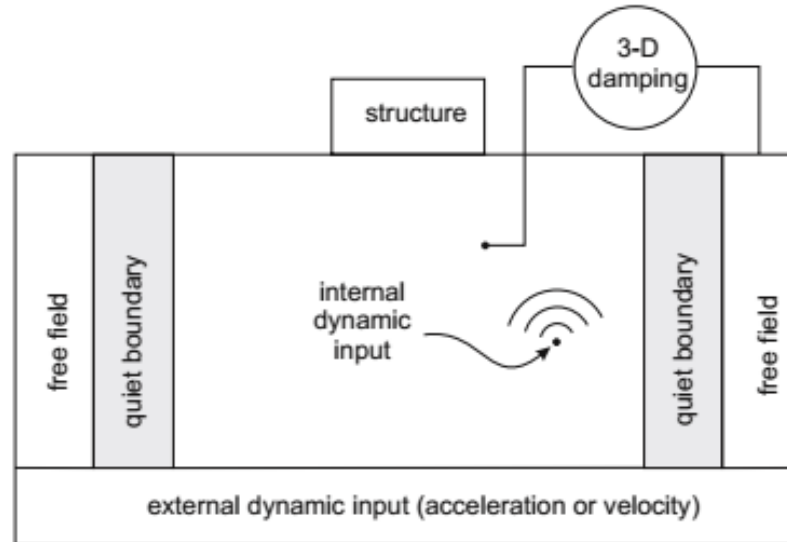


Figure 5.4. The rigid base type of dynamic loading boundary conditions available in Flac (Source: Flac, 2008).

The wave speed and frequency of a wave are predominant on wave transmission. These parameters are considered when the model is build. According to Kuhlemeyer and Lysmer (1973), mesh grids must not be bigger than one-tenth of the wavelength of input motion. It is expressed as in below;

$$\Delta l \leq \frac{\lambda}{10} \quad (5.1)$$

Where  $\lambda$  is the wavelength associated with the highest frequency component that contains considerable energy.

Before the major analysis mesh optimization should be done. In this study, ten different minor analyses are run for mesh convergence. In these analyses, the same

initial, boundary and material conditions are provided. The main issue of minor analyses is to control time step and accuracy. Vertical displacements are controlled for the accuracy in all models where it is under the middle grid point of the raft. The mesh convergence results are given in table 5.1.

Table 5.1. Mesh convergence parameters.

Model No.	Number of Grids Points	Mesh Count	Mesh Size	Time Step	y-Disp(max)	Aspect Ratio
	X-dir. x Y-dir.	-	m2	s	cm	-
1	201x31	6000	0.833	4.10E-06	2.45	1.00
2	100x31	3000	1.667	5.70E-06	3.3	2.00
3	32x21	640	7.813	1.18E-05	4	4.17
4	21x21	400	12.500	7.89E-06	2	6.67
5	33x11	320	15.625	4.12E-05	4	2.08
6	17x21	320	15.625	1.36E-05	6.5	8.33
7	21x11	200	25.000	7.53E-05	3.5	3.33
8	17x11	160	31.250	4.87E-05	4.5	4.17
9	21x6	100	50.000	1.56E-04	4	1.67
10	41x21	800	6.250	1.20E-05	-	3.33

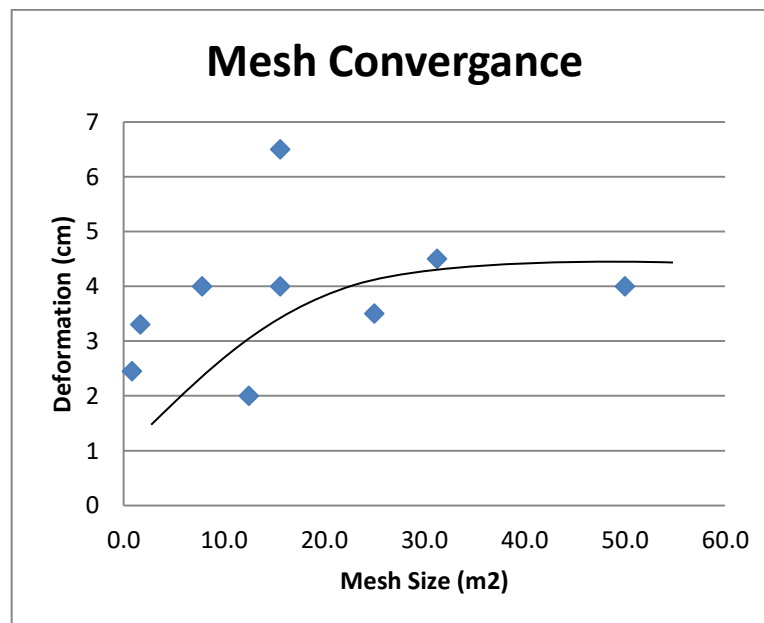


Figure 5.5. Mesh convergence results according to the relation between mesh size and deformation.



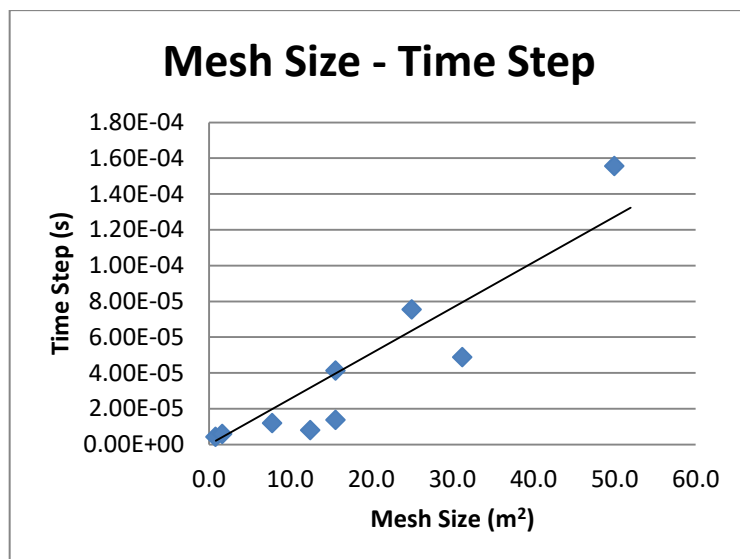


Figure 5.6. Mesh convergence results according to the relation between mesh size and time step.

As seen in figure 5.5, the vertical deformations were dependent on mesh size in a narrow rate. Aspect ratios of meshes were investigated, and some of them were not suitable. The aspect ratio should be lower than the 3.5 value. In figure 5.5, line represents relation between mesh and deformation. The deformation are increasing with the mesh size until the mesh size reaches 30 m<sup>2</sup>, after that the deformations stay still. For the opposite, the mesh size is decreasing with the deformations. The reason is that fine mesh provides accurate calculations. However, when the mesh size is decreasing, the time step is increasing (in Figure 5.6). Moreover, mesh counts have an influence on the duration of calculations as the time step has. For this case, the deformations are close each other. Therefore choosing a relatively coarse mesh is also beneficial.

Besides proper displacement results have to be considered. The grids are decided as 21x11, according to the mesh convergence results.

#### 5.4. Materials Used in Model

FLAC is, an explicit finite-difference program for engineering mechanics computations as explained before; it simulates the behavior of the continuum, which

could be structures, soil, rock or other materials that undergo plastic flow when their yield limits are reached. The physical behaviour of materials is turned into mathematical and logical material models for calculations. One of the critical things is decide on the material model. The material models used for numerical modeling are shown in table 5.2.

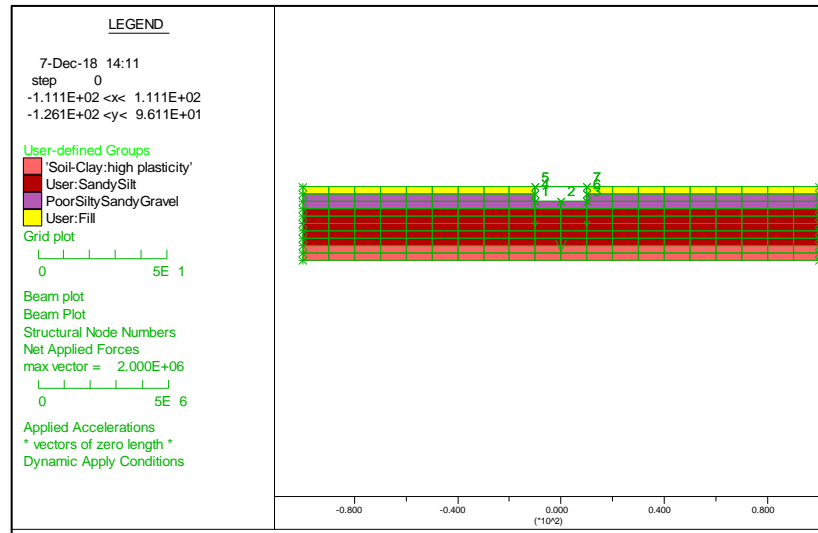


Figure 5.7. General model geometry: boundaries, materials, vertical loads, and structure.

Table 5.2. Material Models and their short description.

Material	Material Model	Description
Earht Fill	Mohr- Coulomb	Elastic Perfectly plastic
Poor Silty Sandy Gravel	UBS Sand	Effective stress plasticity model
Sandy Silt	UBS Sand	Effective stress plasticity model
Sandy Silty Clay	Mohr- Coulomb	Elastic Perfectly plastic

### 5.4.1 Mohr-Coulomb Model

The Mohr-Coulomb model is often used in the analyses of rock and soil mechanics problems. The model defines the shear failure, which depends on the

cohesion and friction parameters of the material. Some laboratory experiments showed that, Mohr-Coulomb failure criterion could be used for soils and like concrete material (Vermeer and deBorst, 1984).

In this study, the Mohr-Coulomb criterion is used for two materials. These materials have a significant similar attribute, such as under non-liquefiable conditions. The properties of materials are given below in table 5.3.

Table 5.3. Mohr-Coulomb material properties.

Material	Bulk Modulus	Shear Modulus	Density	C	$\phi$	Dilation	Tension
Unit	Pa	Pa	kg/m <sup>3</sup>	Pa	°	-	-
Earth Fill	5.00E+06	3.75E+06	2030	7845	30	10	0
Sandy Silty Clay	8.00E+06	4.80E+06	1900	37265	15	0	0

#### 5.4.2 UBC Sand Constitutive Model

In this study, UBCSAND Constitutive Model version 904aR is used. UBCSAND is an effective stress plasticity model for use in advanced stress-deformation analyses of geotechnical structures. This model is used to observe the liquefaction behavior of granular soils in dynamic loading conditions. The model calculates the stresses for each loading cycle depends on the mobilized stress ratio. Using the mobilized stress ratio provides dropping the location of the yield surface. Correspondingly change of the yield surface, plastic volumetric strains are generated by using flow rule. Moreover, the pore water pressures are calculated in synchronized with others (Byrne and Beaty 2011).

Reloading behavior of soil skeleton is anticipated to respond elastically. However, the plastic strains generated in every cycle due to reach previous maximum stress ratio. This behaviour of reloading cycles is given in figure 5.7.

Model input parameters are seen in table 5.4. As seen in the table the parameters are not related to just material behavior, besides analysis condition and initial conditions are related. Liquefiable material properties are given in table 5.5 for using in the UBCSAND model.

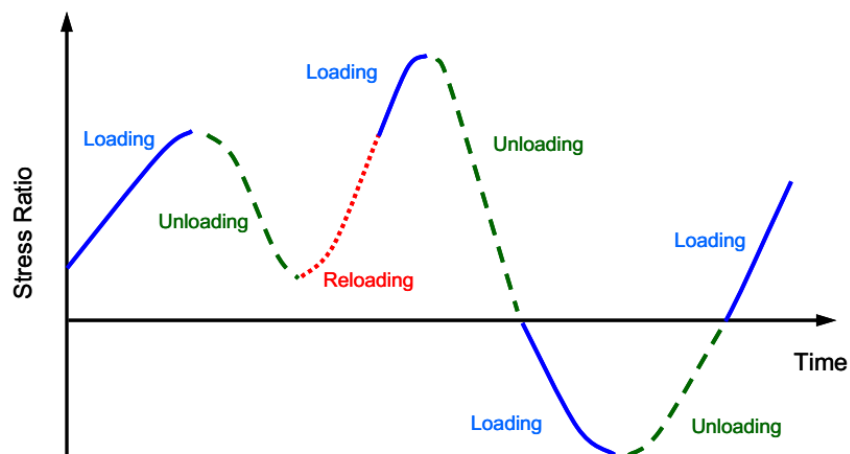


Figure 5.8. Stress ratio history showing loading, unloading, and reloading (Source: Byrne and Beaty 2011).

### 5.4.3 Structural Elements

Structural elements are divided into two groups according to the dimension of element for two-dimensional softwares.

Generally, linear (1-D) elements used to represent the interaction of structures (such as tunnel liners, rock bolts, cable bolts or support props) with soil or rock mass. Non-linear effects are possible with cable elements, rock bolts, or support elements. In this case beam elements are used to simulate foundation, side walls, and floor.

Beam elements are used to determine two-dimensional structural elements. Moreover its each node have three degrees of freedom (x-translation, y-translation, and

rotation). Beam elements are used to determine two-dimensional structural elements. Moreover its each node have three degrees of freedom (x-translation, y-translation, and rotation).

Table 5.4. Main input parameters of UBCSAND Constitutive Model version 904aR.

Parameter	Description
<i>General:</i>	
m_n160	Relative density index defined as characteristic value of $(N_1)_{60cs}$
m_pa	Atmospheric pressure in model units
<i>Elastic stiffness:</i>	
m_kge	Value of $G_{max}/m\_pa$ at mean effective pressure $(\sigma'_m)= 1$ atm.
m_ne	Stress dependence of $G_{max}$ defined by $(\sigma'_m/m\_pa)^{m\_ne}$
m_kb	Value of $B/m\_pa$ at $\sigma'_m= 1$ atm where B = bulk modulus of soil skeleton.
m_me	Stress dependence of B defined by $(\sigma'_m/m\_pa)^{m\_me}$
<i>Plastic shear stiffness and flow rule:</i>	
m_kgp	Plastic shear modulus number. Defines initial slope of hyperbolic relationship.
m_np	Stress dependence of plastic shear modulus defined by $(\sigma'_m/m\_pa)^{m\_np}$
m_rf	Hyperbolic fitting coefficient (see
m_hfac1	User-controlled factor applied to plastic stiffness. Typically used to modify $K_\sigma$ behavior.
m_phicv	Constant volume friction angle to define boundary between dilative and contractive stress states
<i>Strength:</i>	
m_phif	Maximum friction angle that can be mobilized.
<i>Model control variables:</i>	
m_sat	Average saturation of element (usually set by FISH function)
m_static	Set = 1 for static analysis or initial setup. Set = 0 for earthquake analysis
m_ratmax	Set = 0 to reinitialize stress history. Typically use at start of earthquake.

Table 5.5. Liquefiable material properties.

Material	N1,60	Atm Press.	Density	Porosity	$\phi$	Condition Sta/Dyn	Saturation
Unit	-	Pa	Kg/m3	-	°	-	-
Poor Silty Sandy Gravel	12	100000	1800	0.3	40	1	1
Sandy Silt	7	100000	1990	0.2	28	1	1
After Soil Improvement							
Poor Silty Sandy Gravel	51	100000	1800	0.3	52	1	1
Sandy Silt	35	100000	1990	0.2	46	1	1

Beam elements can be joined together with one another and/or the grid. Beam elements can carry bending moments. Strength parameters are assigned for compressive and tensile yield stress. In this study, beam elements mechanical properties are given in table 5.6.

Table 5.6. Beam elements properties in the model.

Beam ID	Dens	Height	Width	Young's Modulus	Compressive Yield Strength	Tensile Yield Strength
-	kg/m <sup>3</sup>	m	m	Pa	Pa	Pa
1001	2.40E+03	0.7	1	1.40E+07	1.00E+07	8.69E+05
1002	2.40E+03	1	1	1.40E+07	1.00E+07	8.69E+05

## 5.5. Dynamic Analysis

The dynamic analysis is repeated before and after the soil improvement. The liquefaction triggering conditions are compared before and after improvement according to dynamic analysis.

For this analysis the acceleration is applied on the bottom boundary (edge) of the model. An artificial sinusoidal motion is applied in a horizontal direction. The equation of motion is given below:

$$a = A \times \sin(\omega t) \quad (5.2)$$

Where  $a$  is acceleration,  $A$  is amplitude,  $\omega$  is angular frequency, and  $t$  is dynamic time. For our study maximum amplitude ( $a_{\max}$ ) is 0.45, this value is chosen according to peak ground acceleration of the site. Frequency ( $f$ ) is 2.0 Hz. The graphic of motion is shown in figure 5.8. The Applied forces and motion are shown in figure 5.9.

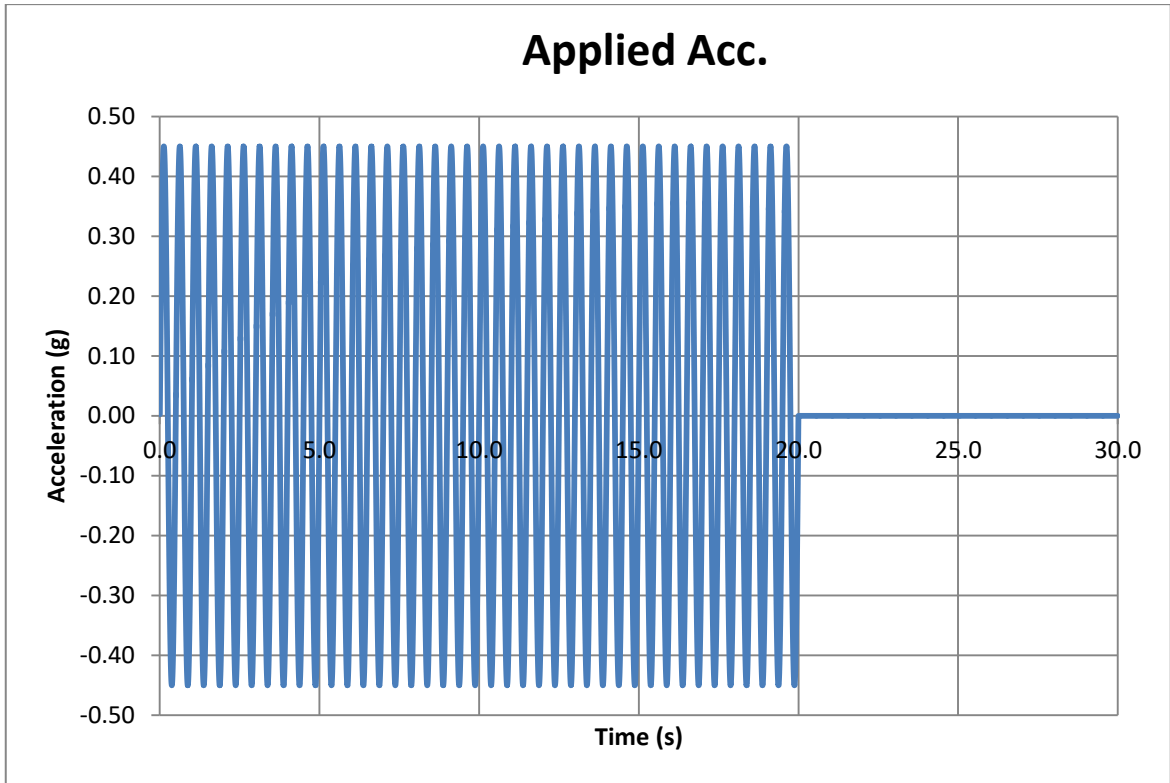


Figure 5.9. The acceleration – time relationship applied in solution.

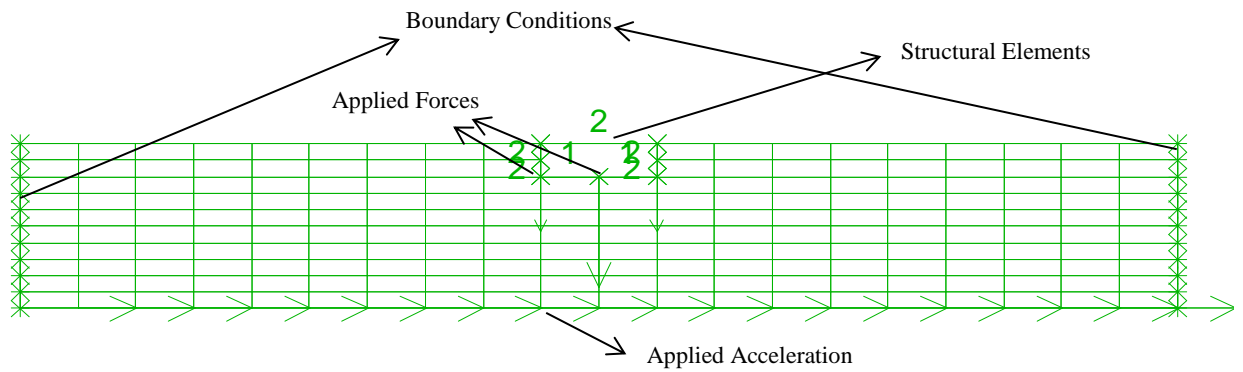


Figure 5.10. Model conditions, applied forces and the direction of applied acceleration.

The acceleration given in the bottom is transmitted and performed along the depth of the model. As a result of this model grid points deformed, and UBCSand model run to simulate liquefaction behavior.

## 5.6. Analysis Results

Once the dynamic and static analysis were completed, the results were studied. For static conditions, neither deformation nor bearing capacity problems were obtained. Before the dynamic analysis, static analysis were performed to prepare the model conditions for dynamic analysis. If static conditions were not controlled and prepared, dynamic analysis results are not accurate, and physical conditions could not conveniently modelled. In the static analysis stage to ensure that, the unbalanced force graphic was plotted and checked. Dropping of the unbalanced force is indicated that calculations performed well according to initial, boundary and loading conditions by every iteration. As shown in Figure 5.10, the unbalanced force is converged to zero; which means our model is stable, and there is no geometric error in the model according to the initial loading conditions.

The dynamic stage analysis was performed after the static stage was completed. The total and effective stress against time graphic is given in figure 5.6. Where the green line is represents average total stress, the cyan line shows effective stress, the red line shows the pore pressure at the middle of foundation. As it can be seen in the figure, effective stress is decreasing, while total stress is increasing. That can be understood from the figure; the effective stress is decreased due to the pore pressure increasing. Moreover, effective stress is became zero for the several time intervals.

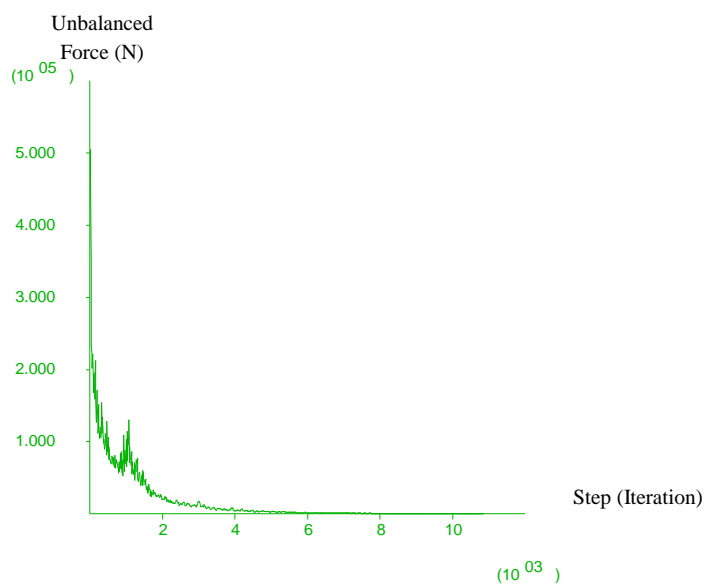


Figure 5.6. The unbalanced force of static stage.



To control the triggering of liquefaction, the ratio of excess pore pressure to initial effective stress ( $r_u = \Delta u / \sigma_{v0}'$ ) is obtained. When excess pore pressure value is equal to effective stress ( $r_u = 1$ ), liquefaction is triggered. According to figure 5.12(a), liquefaction is triggered in 0.45 seconds. However, according to figure 5.12(b) we observed high instantaneous excess pore pressure ratio values after 5.0 seconds. The main reason for this values is after 5.0 seconds effective stress equal to zero as it seen in Figure 5.11 after that, for several time intervals the values were pass over to zero line; moreover, the values are relatively very small in comparison with excess pore pressure values. If the displacements under the foundation against time charts are considered, the remarkable increase could be observed in 0.5 seconds.

The resultant deformations were checked in the dynamic analysis to be understand the deformation behavior of soil under the foundation. As can be seen in Figure 5.13, the soil was deformed significantly in the horizontal direction. The maximum deformation vector was 106.2 cm. As a result, the deformation under the foundation was obtained 70 cm sliding in the horizontal direction and 10 cm uprising in the vertical direction.

After the soil improvement, soil conditions are changed. Therefore, numerical analysis were repeated and liquefaction triggering conditions were controlled. The effective stress, excess pore pressure, and displacements were obtained under the foundation. As seen in Figure 5.15, the effective stress was not became to zero depends on the improvement.

The pore pressure generation was not enough to equal to effective stress. Figure 5.16 shows that excess pore pressure ratio was obtained under the one point in improved soil conditions. The resultant deformations were checked again after the soil improvement in the dynamic analysis to be understood the deformation behavior of soil under the foundation. As can be seen in Figure 5.17, the deformations of soil were significantly decreasing in the horizontal and vertical direction. As a result, the deformation under the foundation was obtained 0.48 meters sliding in the horizontal direction and 0.007 meters down in the vertical direction. The general deformation of model was 0.45 meters, According to this relatively deformation is 0.03 meters under the foundation.

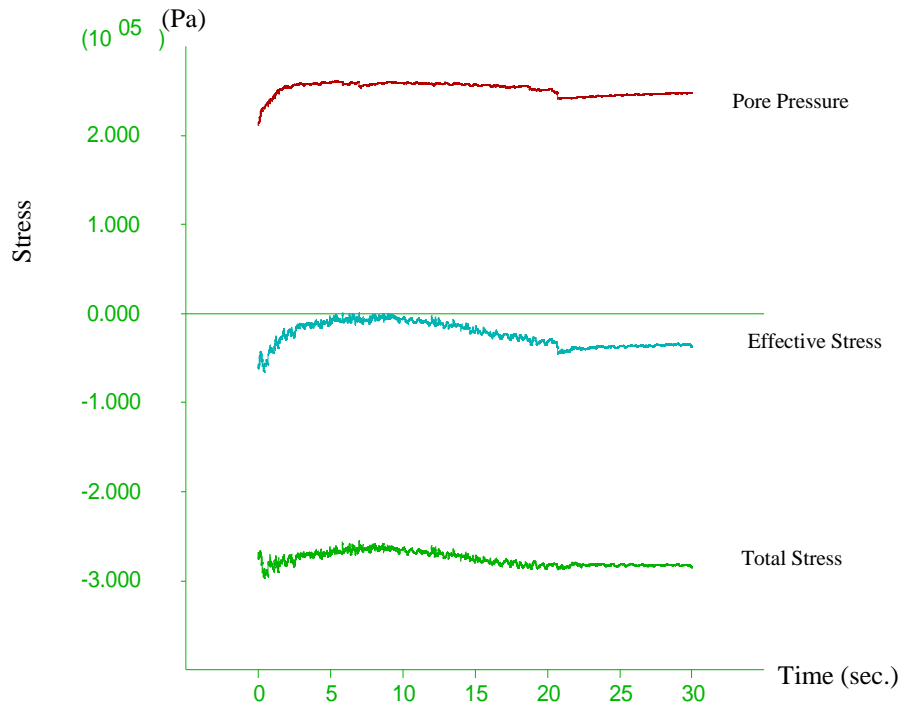


Figure 5.7. Total, effective stress and pore pressure versus time; before the foundation soil improvement.

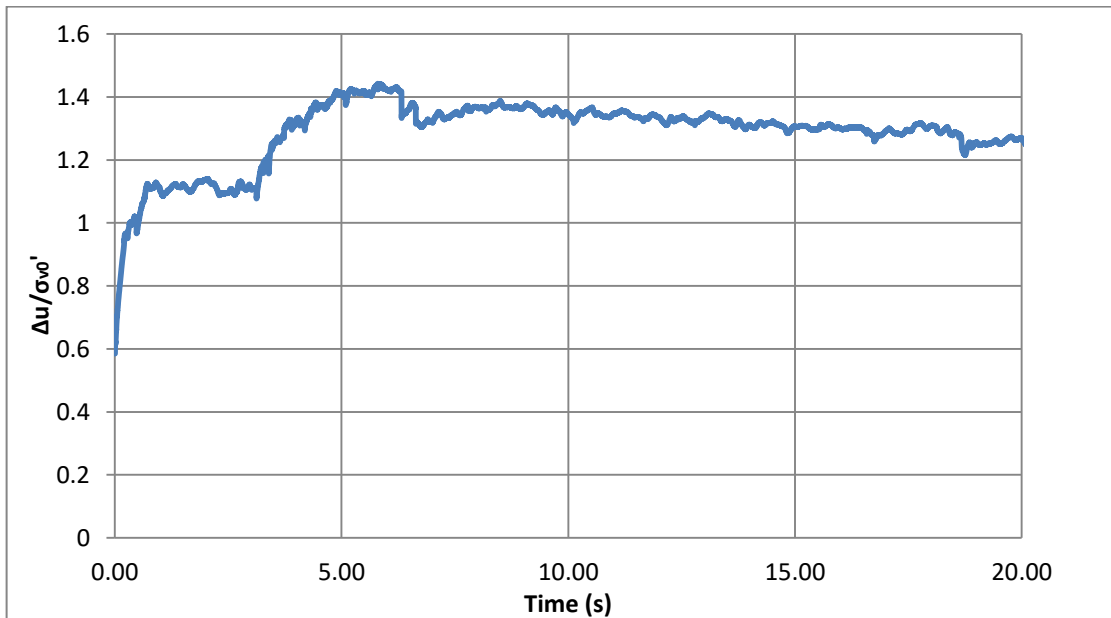


Figure 0.8. Excess pore pressure ratio ( $r_u$ ) before the foundation soil improvement.

The results of excess pore pressure ratio and deformations could be compared in table 5.7. The table shows us the differences between before and after improvement of subsoil.

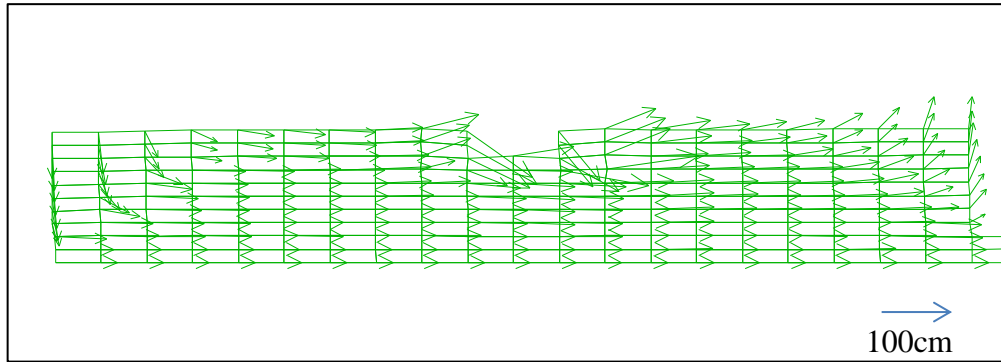


Figure 5.9. Horizontal displacement vectors before the foundation soil improvement and maximum horizontal displacement is 106.2 cm.

Before the improvement, the liquefaction was occurred and, deformations were high. The maximum values occurred in the 20th seconds depends on the earthquake effect. Then, deformations were started to decrease. After the improvement, pore pressure generation was limited therefore the liquefaction did not occurred. Moreover, the deformations were in the limits. The maximum values occurred in the 30th seconds, and those deformations were started to decrease 20 seconds depend on the normal damping of the earthquake motion.

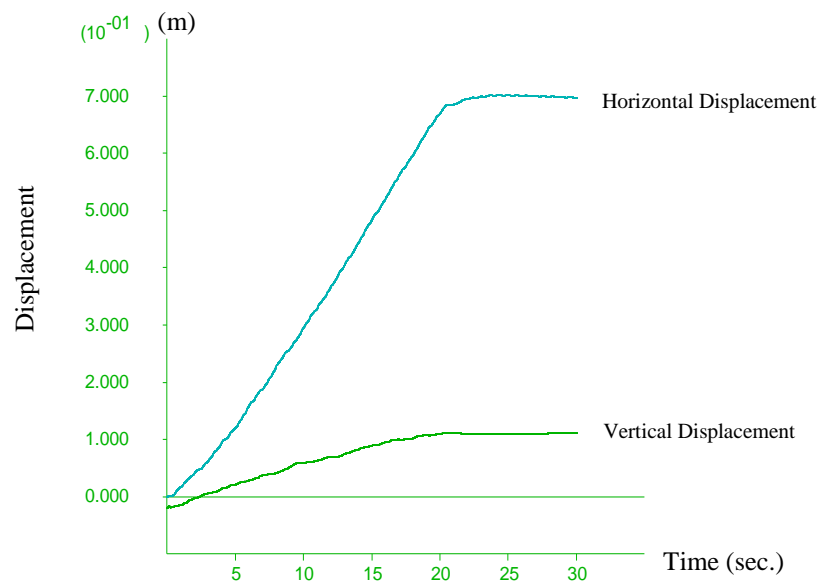


Figure 5.10. Horizontal and vertical displacement under the foundation, before the foundation soil improvement.

Table 5.7. The excess pore pressure ratio and deformation, and their times under the foundation before and after improvement.

	<b>ru</b>	<b>Relative Displacement in 20s</b>	<b>Displacement in 30s</b>
	-	(m)	(m)
BeforeThe Improvement	1<ru (Liquefaction triggering time=0.5s	0.25 (X-direction)	0.03 (X-direction)
After The Improvement	1>ru (No liquefaction)	0.1 (Y-direction)	0.007 (Y-direction)

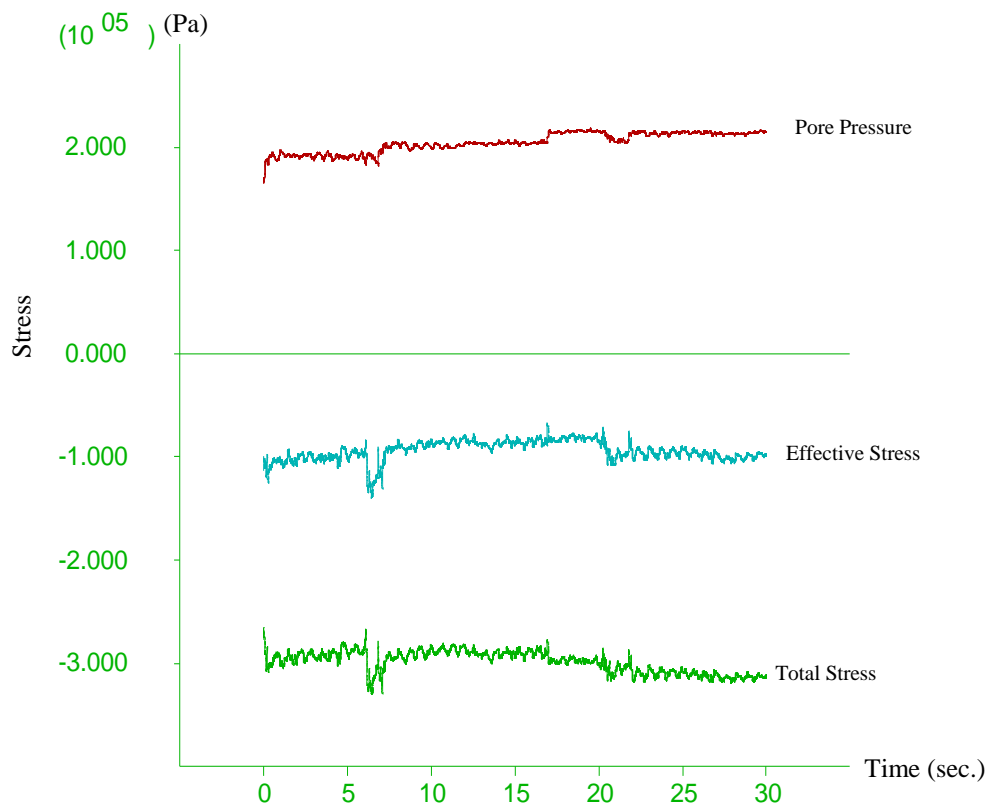


Figure 5.11. Total, effective stress and pore pressure versus time; after the foundation soil improvement.

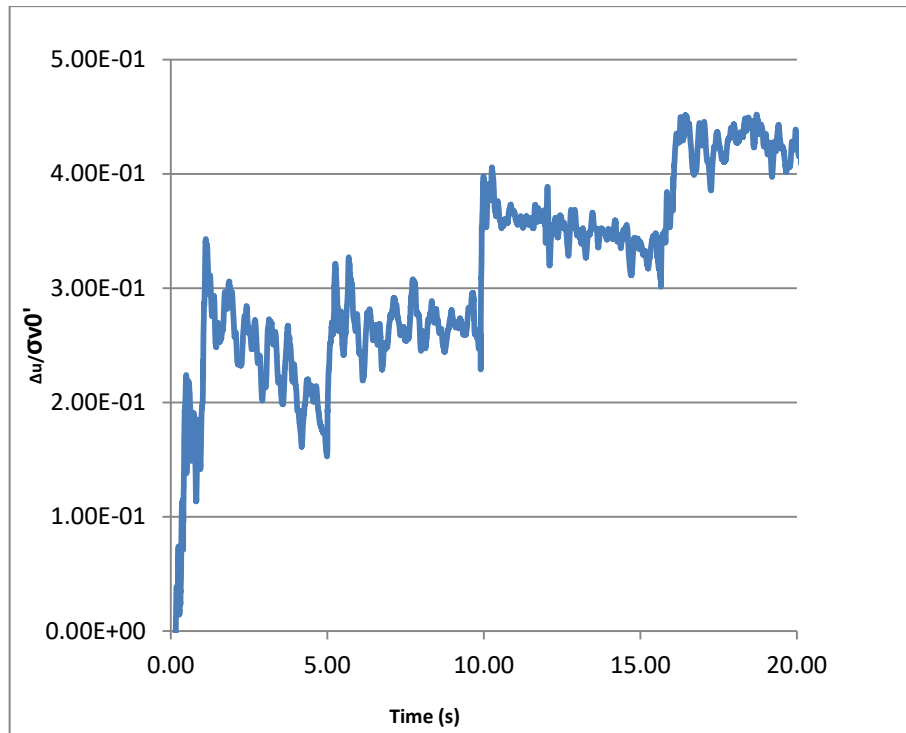


Figure 5.12. Pore pressure ratio ( $r_u$ ) versus time, after the foundation soil improvement.

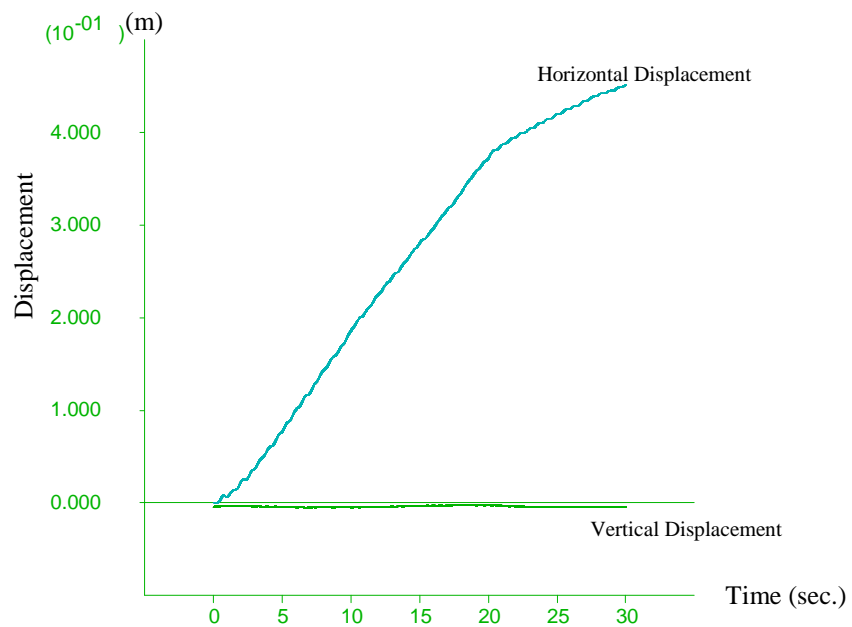


Figure 5.13. Horizontal and vertical displacement under the foundation, after the foundation soil improvement.

## CHAPTER 6

### CONCLUSION

#### 6.1. Summary of Findings

In this study, initially, SPT, MASW tests were carried on the site. Besides, disturbed samples which were used to determine gradation, fine content, consistency limits and shear strength parameters; were collected. The data from all these experiments used to analyze and investigate the subsurface conditions of a structure which is prone to liquefaction.

According to the results of studies, the liquefaction triggering phenomena and a method for mitigation of liquefaction were examined based on numerical analysis, it is established that;

- The liquefaction evaluation results based on the SPT tests show that, the liquefaction may occur under earthquake loading.
- The liquefaction is triggered in case there is no improvement in the soil.
- Subsoil was not observed a bearing capacity problem in the static stage of analysis.
- Under the improved soil conditions, it is observed that; liquefaction was not triggered. The excess pore pressure level did not exceed the effective stress.
- Deformations were limited below acceptable values.

The main issue is the liquefaction potential of the subsoil, as mentioned before bearing capacity of the subsoil is enough to transferr loads from the superstructure. The static loading stage of the numerical analysis showed that displacements are within acceptable limits. The jet grouting cells increased the subsoil resistance against the liquefaction. The subsoil shear capacity is increased with jet grouted cells because of

composite material behavior. The soil mechanics properties are improve with confinement effect, as it is known.

In this study, the jet grouted cells were designed to provide better confinement in the subsoil, and more shear capacity depends on jet grouted material properties. The volumetric contributions of jet grout columns were considered as the treatment approach in the designing stage. After the improvement, jet grout columns and soil were considered to behave a composite material. Thus, the mechanical parameters were calculated according to jet grout - soil composite material. As it can be seen in the results of numerical analysis were shown that jet grout-soil composite could resist against earthquake-induced additional shear stresses. Moreover, pore pressure generation was limited comparing to effective stress due to improvement.

The diameter of the columns was chosen as 45cm, which allows lower pore water pressure in the application of treatment. Thus, the building is less compromised. High pressures could be caused by differential displacement and tilting under the building during the jetting application. The volumetric treatment ratio is suitable for the ordinary jet grout application. The area of the cells was determined considering the volumetric treatment ratio. Any change is in the question due to application on the site, design can be change the cells to the grids.

## **6.2. Suggestions for Future Research**

There are several suggestions for the future resea

1. The analysis can also be repeated by 3-dimensional softwares also (such as Flac-3D). In these analyses, improved soil properties should be instucted more realistically, as the soil is surrounded with intersecting jet grout columns.
2. A parametric study can be done by changing the column diameter and cell area.
3. After improving the soil, strength of cells can be evaluated by performing cone penetration test (CPT).
4. The dynamic analysis could be repeated changing the sinusodial motion to a suitable earthquake. After the analysis, the effect of earthquake motion can be analysed and compared.

5. Deformations and cracking mechanism of jet grouted columns should be investigated to determine the inground shear wall behaviour because the stiffness of jet grout is the main feature against the shear stresses. If somehow cracks are occurred and developed on the jet grout column, it causes reducing stiffness and generating pore water pressure.



## REFERENCES

- AFAD, 2018. Bina Deprem Yönetmeliği, Türkiye.
- Andrews, D.C.A., Martin, G.R. 2000. Criteria For Liquefaction Of Silty Soils. 12th World Conference of earthquake Engineering, New Zealand.
- ASTM D6032-08 2009. "Standard test method for Marsh funnel viscosity of clay construction slurries" West Conshohocken, PA.: American Society for Testing and Materials.
- Baez, J. I. 1995. A Design Model For The Reduction Of Soil Liquefaction By Using Vibro-Stone Columns. Ph.D. thesis, Univ. of Southern California, Los Angeles.
- Beatty, M. H., and P. Byrne., 2011. UBCSAND constitutive model version 904ar. Documentation Report, UBCSAND Constitutive Model on Itasca UDM Web Site.
- Bergschneider B., 2002. Zur Reichweite beim Düsenstrahlverfahren im Sand, PhD thesis, Bergische Universität Wuppertal Fachbereich Bauingenieurwesen.
- Boulanger R., W. 2012. "Shear reinforcement effects of liquefaction mitigation" PEER Annual Meeting Berkeley, CA, October 26-27.
- Beatty M.H., Byrne. P.M., 2011. Ubcсанд constitutive model version 904ar.Itasca UDM Web Site, page 69.
- Bzówka, J., 2009. Współpraca kolumn wykonywanych techniką iniekcji strumieniowej z podłożem gruntowym (Interaction of jet grouting columns with subsoil).

Monograph, Gliwice, Poland: Silesian University of Technology Publishers [in Polish]: 244 p.

Cooke H.G. 2000. Ground Improvement for Liquefaction Mitigation at Existing Highway Bridges. PhD thesis, Department of Civil and Environmental Engineering Virginia Polytechnic Institute.

Croce P., Flora A. and Modoni G., 2014 “Jet grouting technology, Design and Control” CRS Press: Taylor and Francis Group.

Cetin K.O., et al. 2004. SPT Based probabilistic and deterministic assessment of seismic soil liquefaction potential. ASCE J Geotech Geoenviron Eng;130(12):1314–40.

Duzceer, R., Gökalp, A., 2003, Construction and Quality Control of Jet Grouting Applications in Turkey, Proceedings Third I.C. Grouting & Ground Treatment”, GSP No 120, 10-12 Febr, 2003, pp. 281-293, New Orleans

Desai, C.S., Christian J.T., 1977. Numerical methods in geotechnical engineering. McGraw-Hill Book Company, No. of Pages: 783.

Ecemis N., 2013. Simulation of seismic liquefaction: 1-g model testing system and shaking table tests. European Journal of Environmental and Civil Eng. 17(10): 899-919.

Erginağ U. C., 2015. A Parametric Investigation Study By Numerical Analysis On The Contribution Of Jet Grout Columns For Liquefaction Mitigation, Master Thesis, Dokuz Eylül Üniversitesi

Erol A. O., Bayram Z., “Jet enjeksiyon yöntemi” Yüksel Proje, Ankara 2018.

Eurocode 8, 1994. Earthquake Resistant Design of Structures, ENV 1998-2, Brussels.

Fiorotto, R., 2000. Improvement of the Mechanical Characteristics of Soils by Jet Grouting, personal communication,

“FLAC Manual”, 2011. Itasca.Consulting Group Inc.

Hara A., Tokiharu O., Masanori N., Shumpei T., Tadashi B., (1974) “Shear Modulus and shear strength of cohesive soils” *Soils and Foundations*, Vol.14, Issue 3, Page:1-12.

Idriss, I. M. 1999. An update to the Seed-Idriss simplified procedure for evaluating liquefaction potential. Proc., TRB Workshop on New Approaches to Liquefaction, Pub. No. FHWA-RD-99-165, FHA

Idriss I.M., Boulanger R.W., 2006. Semi-empirical procedures for evaluating liquefaction potential during earthquakes. *Soil Dynamics and Earthquake Engineering*, 26, 115–130.

Idriss, I.M., Boulanger, R.W. 2008. Soil liquefaction during earthquakes. *Earthquake Engineering Research Institute*, MNO-12.

Ishihara, K. 1985. Stability of Natural Deposits During Earthquakes. *Proceedings of the 11th International Conference on soil Mechanics San Frasisco*, Vol.1. 321-376.

Ishihara, K. 1996. *Soil Behaviour in Earthquake Geotechnics*. Oxford University Press.

Japan Jet Grouting Association, 1986. JSG method, technical information. Tokyo, Japan.

JEREMÍĆ B. 2010. *Theoretical Geomechanics*. ECI 284 Winter.

- Kramer, S.L., 1996. Geotechnical earthquake engineering. Prentice-Hall Civil Engineering and Engineering Mechanics Series, Upper Saddle River, NJ: Prentice Hall, | c1996, 1.
- Kovacs, M., Rush, A. T., Beck, A. T., & Hollon, S. D. 1981. Depressed Outpatients Treated With Cognitive Therapy Or Pharmacotherapy: A One Year Follow-Up. Archives of General Psychiatry, 38, 33-39doi:10.1001/archpsyc.1981.01780260035003.
- Kuhlmeyer, R.L., Lysmer, J. 1973. Finite element method accuracy for wave propagation problems. Journal of the soil mechanics and foundation division, 99,421-427.
- Liao, S.S.C., Whitman, R.V. 1986. Catalouge of Liquefaction and Non-Liquefaction Occurrences during Earthquakes. Report, Department of Civil Engineering, MIT, Cambridge.
- Liao, S. S. C., Veneziano, D., Whitman, R. V. 1988. Regression Models for Evaluating LiquefactionProbability, Journal of Geotechnical Engineering, Vol. 114, No 4, April, pp.389-410.
- Lunardi, P., 1997. Ground improvement by means of jet grouting. In Proceedings of the International Conference on Engineering, 1(2), 65-85
- Marti, J., Cundall, P.A., 1982. Mixed discretization procedure for accurate solution ofplasticity problems. Int. J. Num. Methods Anal. Methods Geomech. 6, 129–139
- Martin, J. R. II, Olgun, C. G., Mitchell, J. K., and Durgunoglu, H. T. 2004. High-modulus columns for liquefaction mitigation. Journal of Geotechnical and Geoenvironmental Engineering, 130(6): 561-571.
- Mayne P.W., 2007. Cone Penetration Testing State-of-Practice. NCHRP Project 20-05 Topic 37-14.

- Modoni, G., Croce, P., Mongiovi, L. (2006). Theoretical modelling of jet grouting. *Géotechnique*, 56(5), 335-347
- Moseley, M. P. and Kirsch, K. 2004. *Ground Improvement* (2nd edition). Spon Press in an imprint of Taylor & Francis group, U. K., ISBN 0 415 27455 9. pp: 119-160.
- Olgun, C.G., ve Martin, J.R. (2010). Seismic performance of soil-mix panel reinforced ground. 5th Int. Conf. on Recent Advances in Geotechnical Earthquake Engineering and Soil Dynamics, San Diego, California.
- Özdemirler Sondaj ve Zemin Etüdü (2018). İzmir Province, Konak Borough, Ahmet Ağa District, 39 Map section, 208 Block, 28 Parcel Site Investigation Report of Building. Project Name: İzmir hükümet konağı binası performans analizi projesi, March 2018.
- Robertson, P.K., Wride C.E., 1998. Evaluating cyclic liquefaction potential using the cone penetration test. *Canadian Geotechnical Journal*, Vol. 35(3), 442-459.
- Seed, H.B., Idriss, I.M, and Arango, I. (1983) “Evaluation of liquefaction potential using field performance data”, *J. Geotech. Eng., ASCE*, 109(3): 458-482.
- Seed, R. B., et al., 2003. Recent advances in soil liquefaction engineering: a unified and consistent framework. 26th Annual ASCE Los Angeles Geotechnical Spring Seminar
- Shibazaki, M., Yoshida, H., Matsumoto, Y. 1996. Development of a soil improvement method utilizing cross jet. In *Grouting and deep mixing* (eds R. Yonekura and M. Shibazaki), pp. 707–710. Rotterdam, the Netherlands: Balkema.
- Shibazaki, M. 2003. State of practice of jet grouting. *Grouting and ground treatment*, ASCE, Reston, VA, 198–217.

- Stark, T.D., Olson, S.M. 1995. Liquefaction Resistance Using Cpt And Field Case Histories. *Journal of Geotechnical and Geoenvironmental Engineering*, Vol 121, No 12.
- Stoel, A., 2001. *Grouting for Pile Foundation Improvement*, DUP Science, Delft.
- Suzuki, Y., Koyamada, K., Tokimatsu, K., Taya, Y., and Kubota, Y. 1995. Empirical correlation of soil liquefaction based on cone penetration test. *Proc., 1st Int. Conf. Geotechnical Earthquake Engineering*, K. Ishihara, ed., A. A. Balkema, Rotterdam, The Netherlands, 369–374.
- Terzaghi, K., & Peck, R. B., 1948. *Soil mechanics in engineering practice* (2nd Edition). John Wiley and Sons, Inc.
- Terzaghi, K., Peck, R., & Mesri, G., 1996. *Soil mechanics in engineering practice* (3rd Edition). New York: Wiley.
- Tornaghi R., 1989. “Trattamento Colonnare dei Terreni Mediante Gettiniezione (Jet grouting)” *Proceedings of the 17th National Conference of Geotechnical Engineering*, Taormina, Italy, April 26-28, Pages:193-203
- Van der Stoel A. E. C., 2001. *Grouting for Pile Foundation Improvement: PhD thesis*, Delft University Press, 217 pp.
- Vermeer, P.A., de Borst, R., 1984. Non associated plasticity for soils, concrete and rock. *Heron*; 29(3):3–64.
- Vincent, P., Nguyen, V., Hubaut, A., 2014. Case Study: Jet Grouted Mass Gravity Wall To Stabilise Bridge Abutment Upgrade. *Earth Structures & Retention Conference*, Australia.

- Xanthakos, P., Abramson, L. W., Bruce, D. A., 1994. Ground Control and Improvement: New York: John Wiley & Sons, Inc.: 670 p.
- Yahiro T., Yoshida H., 1973. Induction grouting method utilizing high speed water jet. In Proceedings 8th International Conference on Soil Mechanics and Foundation Engineering
- Yılmaz, D., et al. 2008. Liquefaction analysis and soil improvement in Beydag dam. *Geotech Geol Eng* 26: 211. <https://doi.org/10.1007/s10706-007-9158-z>
- Youd, T. L., et al. 2001. Liquefaction resistance of soils: Summary report from the 1996 NCEER and 1998 NCEER/NSF workshops on evaluation of liquefaction resistance of soils. *Journal of Geotechnical and Geoenvironmental Engineering*, Vol. 127(10), 817–833.
- Youd, T. L., & Noble, S. K., 1998. Liquefaction criteria based on probabilistic analyses. In NCEER Workshop on Evaluation of Liquefaction Resistance of Soils, National Center for Earthquake Engineering Research Technical Report NCEER-97-0022, 201–216.

## **APPENDIX A**

### **SITE INVESTIGATION DATA EXAMPLE And CALCULATION OF A JET GROUT**



# A-1 Site Investigation Data

www.ozdemirlerzeminetudu.com

## TEMEL SONDAJ LOGU

SONDAJ (Borehole) No:		SK-1																																
Sayfa (Page) No:		1																																
<b>ÖZDEMİRLER SONDAJ VE ZEMİN ETÜDÜ İNŞ. SAN. TİC. LTD. ŞTİ.</b> Kızılay Mahallesi 511/1 Sk. No:5 D:1 Bornova / İZMİR Tel-Fax: +90(232) 343 79 16 e-mail: ozdemirler1@gmail.com		SONDAJ YERİ: İzmir / Konak / Ahmetoğlu Mah. 39 Parça, 208 Ada, 28 Parsel PROJE İSMİ: İZMİR HÜKÜMET KONAĞI BİNASI PERFORMANS ANALİZİ PROJESİ																																
SONDAJ DER. / Boring Depth	20.45m	MUH.BOR.DER. / casing Depth	(NQ-20.45 m.)																															
DELİK ÇAPI / Hole Diameter	(B89-89 mm.)	YASSI ve Ölçüm Tarihi/GW. & Derf.	2.10 METRE																															
SONDAJ MAK. & YÖNT. / D.Rig & Met	D-750 / Rotary	KOORDİNAT / Coordinate (N-S) X	4252268.52																															
BAŞ.BİT.TAR. / Start Finish Date	09.03.2018 / 09.03.2018	KOORDİNAT / Coordinate (E-W) Y	511366.45																															
SONDÖR. / Driller	Emre ÇİFLİK	SONDAJ KOTU / Elevation (m)																																
Sondaj Derinliği	STANDART PENETRASYON										Jeoteknik Tanımlama	Zemin Profili	Kum Yüzdeleri %	ROD%	Ayrışma Derecesi	Çatlak Sıklığı																		
	No	Derinliği	Darbe				N30 Grafiği																											
			0-15	15-30	30-45	N30	10	20	30	40							50																	
1																																		
2	SPT1	1.50-1.96	2	1	3	4																												
3	SPT2	3.00-3.45	1	2	2	4																												
4																																		
5																																		
6	SPT3	6.00-6.45	11	11	13	24																												
7																																		
8	SPT4	7.50-7.95	6	8	7	15																												
9	SPT5	9.00-9.45	3	5	3	8																												
10																																		
11	SPT6	10.50-10.95	5	4	6	10																												
12	SPT7	12.00-12.45	4	5	7	12																												
13																																		
14	SPT8	13.50-13.95	8	4	5	9																												
15	SPT9	15.00-15.45	5	4	4	8																												
16																																		
17	SPT10	16.00-16.95	5	6	10	16																												
18	SPT11	18.00-18.45	7	5	12	17																												
19																																		
20	SPT12	20.00-20.45	6	8	8	16																												
21																																		
22																																		
23																																		
24																																		
KUYU SONU: 20.45 METRE																																		
İmza-Kase																																		
Projeyi Hazırlayan : Jeoloji Müh: Murat Turanoğlu																																		
ZEMİN DEĞERLENDİRMESİ		AYRIŞMA DEREJESİ (W)		KAYA NİTELİĞİ RQD(%)		ÇATLAK SIKLIĞI		DAYANIMLILIK		Kinklar-100cm		İnce Tanerli Oran		İri Tanerli Oran																				
N 0-2 Ç. Yumuşak	N 0-4 Ç. Gevrek	W1 Taze (Ayrışmamış)	W2 Az Ayrışmış	W3 Orta Derecede Ayrışmış	W4 Ayrışmış	W5 Tamamen Ayrışmış	0-25 Çok Zayıf	25-50 Zayıf	50-75 Orta	75-90 İyi	90-100 Çok İyi	<1 Maaflı	1-3 Az Gatalık Kırımlı	3-10 Kırımlı	10-50 Çok Çatalıklı Kırımlı	>50 Parçalanmış	I-Dayanımsız	II-Orta Dayanımsız	III-Orta Zayıf	IV-Zayıf	1 Beyrek	1-2 Orta	2-10 Siki	10-20 Çok Siki	%5 Pek Az	%5-15 Az	%15-35 Çok	%35-50	%5 Pek Az	%5-20 Az	%20-50 Çok	%50-100		
N 3-4 Yumuşak	N 5-10 Gevrek																																	
N 5-6 Orta Kat.	N 11-30 Orta																																	
N 6-13 Orta	N 31-60 Sıkı																																	
N 13-30 Sert	N 60 Çok Sıkı																																	

Figure A.1. Borehole log-1 (Özdemirler 2018).

## TEMEL SONDAJ LOGU

SONDAJ (Borehole) No:		SK-2																																	
Sayfa/Page No:		1																																	
<b>ÖZDEMİRLER SONDAJ VE ZEMİN ETÜDÜ İNŞ. SAN. TİC. LTD. ŞTİ.</b> Kızılay Mahallesi 511/1 Sk. No:5 D:1 Bornova / İZMİR Tel-Fax:+90(232) 343 79 16 e-mail:ozdemirler1@gmail.com																																			
SONDAJ YERİ: İzmir / Konak / Ahmetpaşa Mah. 39 Pafta, 206 Ada, 28 Parsel PROJE İSİMİ: İZMİR HÜKÜMET KONAĞI BİNASI PERFORMANS ANALİZİ PROJESİ																																			
SONDAJ DER. / Boring Depth	20.50m	MUH.BOR.DER. / Casing Depth	(NG-20.50 m.)																																
DELİK ÇAPLI / Hole Diameter	(B89-89 mm.)	YASSI ve Ölçüm Tarihi/GWL & Date	2.10 METRE																																
SONDAJ MAK. & YÖNT. / D.Rig & Met.	D-750 / Rotary	KOORDİNAT / Coordinate (N-S) X	4252254.41																																
BAŞ.BİT.TAR. / Start Finish Date	09.03.2018 / 09.03.2018	KOORDİNAT / Coordinate (E-W) Y	511383.55																																
SONDÖR / Driller	Emre ÇİFLİK	SONDAJ KOTU / Elevation (m)																																	
SondaJ Derinliđi	STANDART PENETRASYON										Jeoteknik Tanımlama	Zemin Profili	Karet Yüzdesi %	RQD%	Ayrışma Derecesi	Çatlak Sıklığı																			
	No	Derinliđi	Darbe				N30 Grafiđi																												
			0-15	15-30	30-45	N30	10	20	30	40							50																		
1																																			
2	SPT1	1.50-1.95	2	2	3	5																													
3	SPT2	3.00-3.45	5	6	5	11																													
4	SPT3	4.50-4.95	7	8	14	22																													
5	SPT4	6.00-6.45	9	10	13	23																													
6	SPT5	7.50-7.95	20	21	25	46																													
7	SPT6	9.00-9.45	7	9	16	25																													
8	SPT7	10.50-10.95	8	10	14	24																													
9	SPT8	12.00-12.45	5	6	11	17																													
10	SPT9	13.50-13.95	6	8	7	16																													
11	SPT10	15.00-15.45	7	6	9	16																													
12	SPT11	16.50-16.95	5	6	8	14																													
13	SPT12	18.00-18.45	8	11	11	22																													
14	SPT13	19.50-19.95	7	10	14	24																													
15	Karot	20.00-20.50																																	
16																																			
17																																			
18																																			
19																																			
20																																			
21																																			
22																																			
23																																			
24																																			
KUYU SONU: 20.50 METRE																																			
İmza-Kase																																			
ProjeYi Hazırlayan : Jeoloji Müh: Murat Turanođlu																																			
ZEMİN DEĞERLENDİRMESİ		AYRIŞMA DERECESİ (W)		KAYA NİTELİĞİ RQD(%)		ÇATLAK SIKLIĞI		DAYANIMLILIK		Kerirler-100cm		İnce Tanefl Oran		İri Tanefl Oran																					
Ince Tanefl	İri Tanefl	W1	W2	W3	W4	W5	W6	W7	W8	W9	W10	W11	W12	W13	W14																				
N:0-2 Ç. Yumuşak	N:0-4 Ç. Gevşek	W1 Taze (Ayrılmamış)	W2 Az Ayrılmış	W3 Orta Derecede Ayrılmış	W4 Ayrılmış	W5 Tamamen Ayrılmış	0-25 Çok Zayıf	25-50 Zayıf	50-75 Orta	75-90 İyi	90-100 Çok İyi	41 Masif	1-3 Az Çatlaklı-Kirikli	3-10 Kirikli	10-50 Çok Çatlaklı Kirikli	>50 Parçalanmış	I-Dayanimsiz	II-Orta Dayanimsiz	III-Orta Zayıf	IV-Zayıf	V-Çok Zayıf	1 Seyrek	1-2 Orta	2-10 Sıkı	10-20 Çok Sıkı	%5 Pek Az	%5-15 Az	%15-35 Çok	%35-50 Çok	%5 Pek Az	%5-20 Az	%20-50 Çok			
N:3-4 Yumuşak	N:5-10 Gevşek																																		
N:5-6 Orta Kat.	N:11-30 Orta																																		
N:9-13 Kati	N:31-60 Sıkı																																		
N:30 Sert	N:60 Çok Sıkı																																		

Figure A.2. Borehole log-2 (Özdemirler 2018).

## TEMEL SONDAJ LOGU


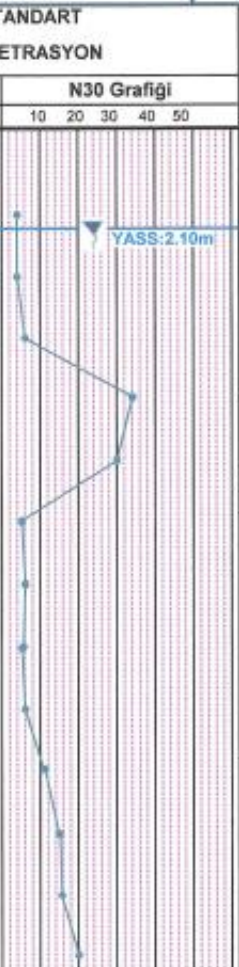
SONDAJ (Borehole) No:		SK-1																	
Sayfa(Page) No:		1																	
 <b>ÖZDEMİRLER SONDAJ VE ZEMİN ETÜDÜ İNŞ. SAN. TİC. LTD. ŞTİ.</b>		SONDAJ YERİ: İzmir / Konak / Alimetağa Mah.																	
Kızılay Mahallesi 511/1 Sk. No:5 D:1		39 Pafta, 208 Ada, 39 Parsel																	
Bornova / İZMİR Tel-Fax: +90(232) 343 79 16		PROJE İSMİ: İZMİR HÜKÜMET KONAĞI BİNASI PERFORMANS ANALİZİ PROJESİ																	
e-mail: ozdemirler1@gmail.com																			
SONDAJ DER. / Boring Depth	30.00m	MUH.BOR.DER. / Casing Depth	(NQ-30.00 m.)																
DELİK ÇAPLI / Hole Diameter	(889-89 mm.)	YASS ve Ölçüm Tarihi/GW. & Date	2.10 METRE																
SONDAJ MAK. & YÖNT / G.Rig & Met.	D-750 / Rotary	KOORDINAT / Coordinate (N-S) X	4252265.88																
BAŞ.BİT.TAR. / Start Finish Date	09.03.2018 / 09.03.2018	KOORDINAT / Coordinate (E-W) Y	511342.83																
SONDÖR / Driller	Emre ÇİFLİK	SONDAJ KOTU / Elevation (m)																	
Sondaç Derinliği	STANDART PENETRASYON										Jeoteknik Tanımlama	Zemin Profili	Kurut Yüzdesi %	RGD%	Ayrışma Derecesi	Çetlek Sıklığı			
	No	Derinliği	Darbe				N30 Grafiği												
			0-15	15-30	30-45	N30	10	20	30	40							50		
1																			
2	SPT1	1.50-1.95	2	2	2	4													
3	SPT2	3.00-3.45	1	1	3	4													
4																			
5	SPT3	4.50-4.95	3	2	4	6													
6	SPT4	6.00-6.45	25	18	16	34													
7																			
8	SPT5	7.50-7.95	11	13	17	30													
9	SPT6	9.00-9.45	4	2	3	5													
10																			
11	SPT7	10.50-10.95	2	2	4	6													
12	SPT8	12.00-12.45	3	2	3	5													
13																			
14	SPT9	13.50-13.95	4	3	3	6													
15	SPT10	15.00-15.45	4	5	6	11													
16																			
17	SPT11	16.50-16.95	5	8	6	15													
18	SPT12	18.00-18.45	4	7	9	16													
19																			
20	SPT13	19.50-19.95	6	9	11	20													
																			
<b>Imza-Kese</b>																			
Projeyi Hazırlayan : Jeoloji Müh: Murat Turanoğlu																			
ZEMİN DEĞERLENDİRMESİ		AYRIŞMA DERESESİ (W)		KAYA NİTELİĞİ RGD(%)		ÇATLAK SIKLIĞI		DAYANIMLILIK		Kinklar-100cm		İnce Tanerli Oran		İri Tanerli Oran					
Ince Tanerli	İri Tanerli	W1	Taze (Ayrılmaz)	0-25	Çok Zayıf	<1	Mesif	I-Dayanımlı	1	Seyrek	%0	Pek Az	%5	Pek Az					
N0-2 Ç. Yumuşak	N0-4 Ç. Gevrek	W2	Az Ayrılmış	25-50	Zayıf	1-3	Az çatlaklı-Kırıntılı	II-Orta Dayanımlı	1-2	Orta	%5-15	Az	%5-20	Az					
N3-4 Yumuşak	N5-10 Gevrek	W3	Orta Derecede Ayrılmış	50-75	Orta	3-10	Kırıntılı	III-Orta Zayıf	2-10	Sıklık	%15-35	Çok	%20-50	Çok					
N5-8 Orta Katı	N11-30 Orta	W4	Ayrılmış	75-90	İyi	10-50	Çok Çatlaklı Kırıntılı	IV-Zayıf	10-20	Çok Sık	%35	W							
N9-13 Kırıntılı	N31-80 Sıkı	W5	Tamamen Ayrılmış	90-100	Çok İyi	>50	Parçalanmış												
N30 Sıkı	N50 Çok Sıkı																		

Figure A.3. Borehole log-3 Depth: 0-20m (Özdemirler 2018).

## TEMEL SONDAJ LOGU

SondaJ Derinliđi		STANDART PENETRASYON										Jeoteknik Tanımlama	Zemin Profili	Karot Yüzdesi %	ROD%	Ayrışma Derecesi	Çatlak Sıklığı
No	Derinliđi	Darbe			N30 Grafiđi												
		0-15	15-30	30-45	N30	10	20	30	40	50							
21	SPT14	21.00-21.45	5	9	18	27											
22																	
23	SPT15	22.50-22.95	7	11	13	24											
24	SPT16	24.00-24.45	9	9	11	20											
25																	
26	Karot	25.50-27.00															
27	Karot	27.00-28.50															
28																	
29	Karot	28.50-30.00															
30	KUYU SONU:30.00 METRE																
31																	
32																	
33																	
34																	
35																	
36																	
37																	
38																	
39																	
40																	
İmza-Kese																	
ProjeYi Hazırlayan : Jeoloji Müh: Murat Turanođlu																	
ZEMİN DEĞERLENDİRMESİ		AYRIŞMA DERECEĐİ (W)			KAYA NİTELİĐİ RQD(%)	ÇATLAK SIKLIĐI	DAYANIMLILIK	Kirikler-100cm	İnce Tanerli Oran	İri Tanerli Oran							
İnce Tanerli	İri Tanerli	W1-4	Ç. Gevrek	W1 Taze (Ayrılmaması)	0-25 Çok Zayıf	01 Masif	I-Dayanımlı	1 Seyrek	%0 Çok Az	%5 Çok Az							
İİ-3-4 Yumuşak	İİ-5-10 Gevrek	W2	Az Ayrışma	W2 Az Ayrışma	25-50 Zayıf	1-3 Az Çatlaklı-Kirikli	II-Orta Dayanımlı	1-2 Orta	%5-15 Az	%5-20 Az							
İİİ-5-8 Orta Kat	İİİ-11-30 Orta	W3	Orta Derecede Ayrışma	W3 Orta Derecede Ayrışma	50-75 Orta	3-10 Kirikli	III-Orta Zayıf	2-10 Sıkı	%15-35 Çok	%20-30 Çok							
İV-10 Kırı	İV-31-80 Sıkı	W4	Ayrılmaması	W4 Ayrılmaması	75-90 İyi	10-50 Çok Çatlaklı Kirikli	IV-Zayıf	10-20 Çok Sıkı	%35 Ya	%35 Ya							
İV-10 Sert	İV-50 Çok Sıkı	W5	Tanımlanmayan Ayrışma	W5 Tanımlanmayan Ayrışma	90-100 Çok İyi	>90 Parçalanmış	V-Dayanımlı	>20 Çok Sıkı	%50 Çok	%50 Çok							

Figure A.4. Borehole log-3 depth: 20-30m (Özdemirler 2018).

Proje Adı / Project Name	EYMİR HÜKÜMET KONAĞI Binası		Laboratuvar No/Lab. No	2018-230		
İşveren / Owner	ÖZDEMİRLER MÜHENDİSLİK LTD.ŞTİ.		Deney Tarihi / Date of Test	14.03.2018		
Parsel/Ada/Parsel	39/208/28		Bak. Rapor No			
<b>LOKASYON BİLGİLERİ</b>						
Sondaj No:	SK-2		Deney Başlangıç Tarihi:	14.03.2018		
Numune No:	SPT		Deney Bitiş Tarihi:	15.03.2018		
Derinlik (m):	13.50-13.95		Kuru Num. Ağ.(g):	70.90		
<b>ELEK ANALİZİ DENEYİ</b>						
Elek No	Elek Göz Açıklığı (mm)	Her Elekte Kalan Ağrılık (g)	Kümülatif Elekte Kalan Ağrılık (g)	Her Elekte Kalan (%)	Kümülatif Elekte Kalan (%)	Toplam Elekten Geçen (%)
No:1 1/2"	37.5	0.00	0.00	0.00	0.00	100.00
No:3/4"	19	0.00	0.00	0.00	0.00	100.00
No:3/8"	9.5	0.00	0.00	0.00	0.00	100.00
No:4	4.75	0.00	0.00	0.00	0.00	100.00
No:10	2.00	0.00	0.00	0.00	0.00	100.00
No:16	1.18	0.00	0.00	0.00	0.00	100.00
No:30	0.60	2.01	2.01	2.83	2.83	97.17
No:40	0.43	1.12	3.13	1.58	4.41	96.59
No:100	0.150	1.01	4.14	1.42	5.84	94.16
No:200	0.075	1.25	5.39	1.76	7.60	92.40
Elek Altı		65.51	70.90	92.40	100.00	0.00
<b>ELEK ANALİZİ DENEYİ GRAFİĞİ</b>						
<b>SONUÇLAR</b>						
<b>ELEK ANALİZİ</b>						
D <sub>10</sub> =						
D <sub>30</sub> =						
D <sub>60</sub> =						
C <sub>u</sub> =						
C <sub>c</sub> =						
ÇAKIL YÜZDESİ (%) = 0.00						
KUM YÜZDESİ (%) = 7.60						
SILT VE KİL YÜZDESİ (%) = 92.40						
w <sub>n</sub> (%) = SU MUHTEVASI						
USCS = ZEMİN SINIFI						
CI						

"Bu deney TS 19000-1/Mart 2006 Madde 5.1.6.1 Deney 6 (A) ve Madde 5.1.6.2 Deney 6 (B) standartlarına göre yapılmıştır.  
\*Laboratuvarımız 4708 sayılı kanun gereği T.C.Çevre ve Şehircilik Bakanlığı Yapı İşleri Genel Müdürlüğü tarafından verilen 02/07/2014 tarih ve 0481 No'lu laboratuvar izin belgesine sahiptir.  
\*Tüm hakları ZEM-Son Mühendislik Jeolojik Araştırma İnş. San. ve Tic. Ltd. Şti.'ye aittir.  
\*Bu deney formu izinsiz hiçbir şekilde çoğaltılıp kopya edilemez.  
R FR 04 / Yay. Tar. 15.12.2013 / Rev. No ve Tarihi :00

DENEY YAPAN  
**ERGİNACAR**  
Jeolojik Mühendislik  
Orda Sici No: 18130

DENEY LOMAYLAYAN  
**HADİP KACMAZ**  
Jeolojik Mühendislik  
Orda Sici No: 18130

Figure A.5. Test results of the soil samples (Özdemirler 2018).

## A-2 Calculation Of A Jet Grout

In this part, calculation of the jet grouting parameters are given an example for a certain depth of a borehole.

For Borehole-2:

Spt  $N_{1,60}=11$  at -15m depth, design parameters:  $D_s=0.45$  m,  $p_g=40$  MN/m<sup>2</sup>,  $v=4$  mm/s,  $w=15$  rpm,  $d=3$  mm,  $Q_g=5$  lt/s,  $w/c=1$ .

$$E'_p = \frac{40 \times 5}{4} = 50 \rightarrow E'_n = 0.9 \times 50 = 45$$

$\Lambda^*$ ,  $\beta$ ,  $\delta$ ,  $\alpha_e$ ,  $D_{ref}$  are chosen in the figures which are given in the chapter 3.

$$D_{mean} = 45 \times \left[ \frac{1 \times 7.5 \times 45}{75} \right]^{0.2} \times \left[ \frac{11}{1.5} \right]^{-0.25} = 0.66m$$

$$D_{design} = 0.8 \times 0.66 = 0.53m$$

$q_u=6$  MN/m<sup>2</sup> is decided first according to soil type and experience. Also,  $q_u$  could be decided according to empirical equations.

$$q_{u(design)} = \frac{6}{1.6} = 3.75 \text{ MN/m}^2$$

$$E_{50} = 350 \times 3.75 = 1312500 \text{ kN/m}^2$$

G modulus of the jet grout could be obtained from  $E_{50}$  value and using Poisson ratio ( $\nu$ ).

$$G_r = \frac{G_g}{G_s} \rightarrow G_r = \frac{468750}{4040.93} = 116.0$$

$a_r$  value could be decided according to requirements of project. In this case,  $a_r=0.24$ .

$$K_G = \frac{1}{(1 \times 0.5 \times 116 \times 0.24) + (1 - 0.24)} = 0.068$$

CSR and CRR is calculated before in Chapter 4  $CSR_i = 0.0686 \times 0.41 = 0.03$

Factor of safety against to liquefaction:

$$FS = \frac{0.14}{0.03} = 4.67$$

## **APPENDIX B**

### **JET-GROUT PLANS and ELEVATIONS**

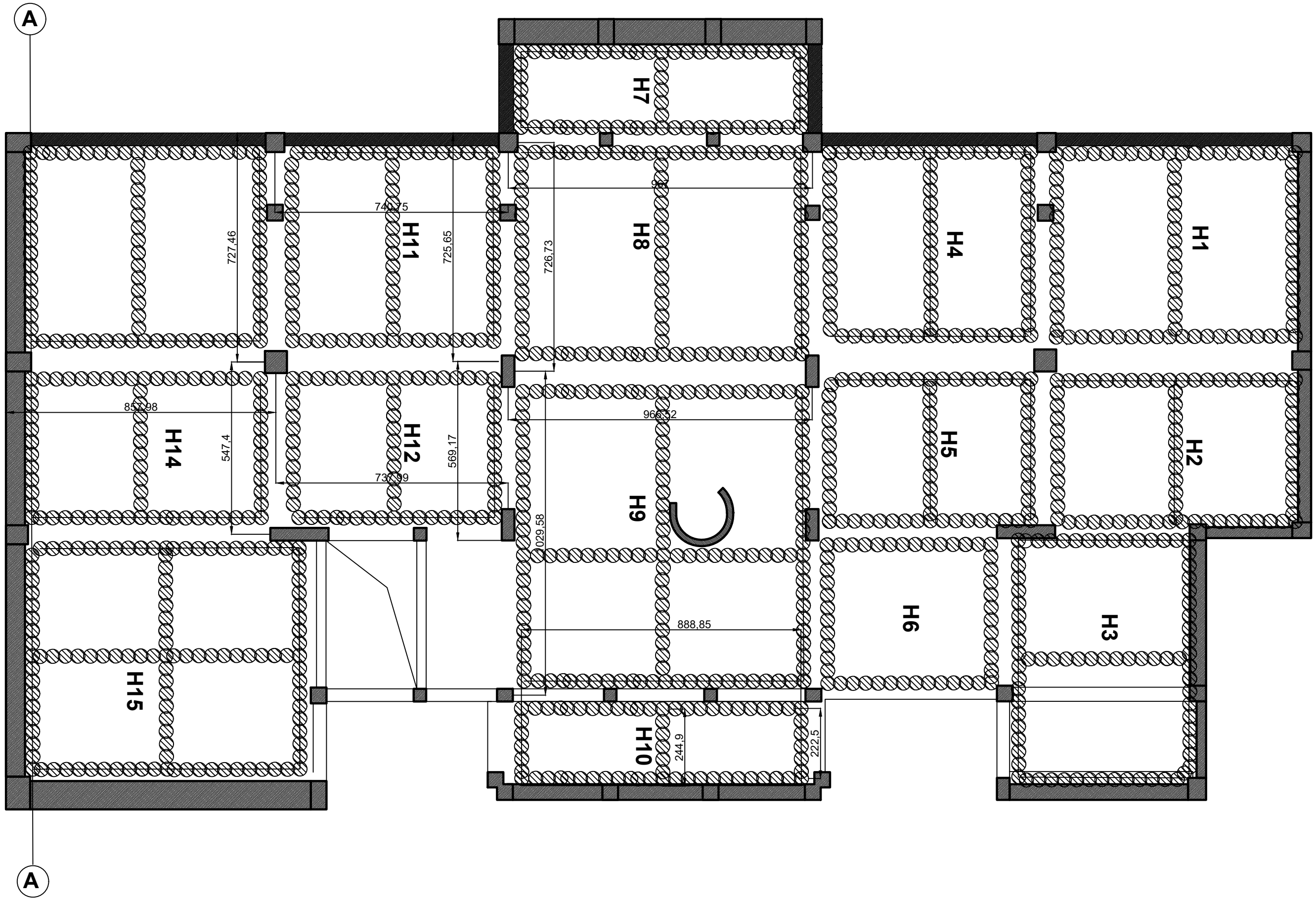
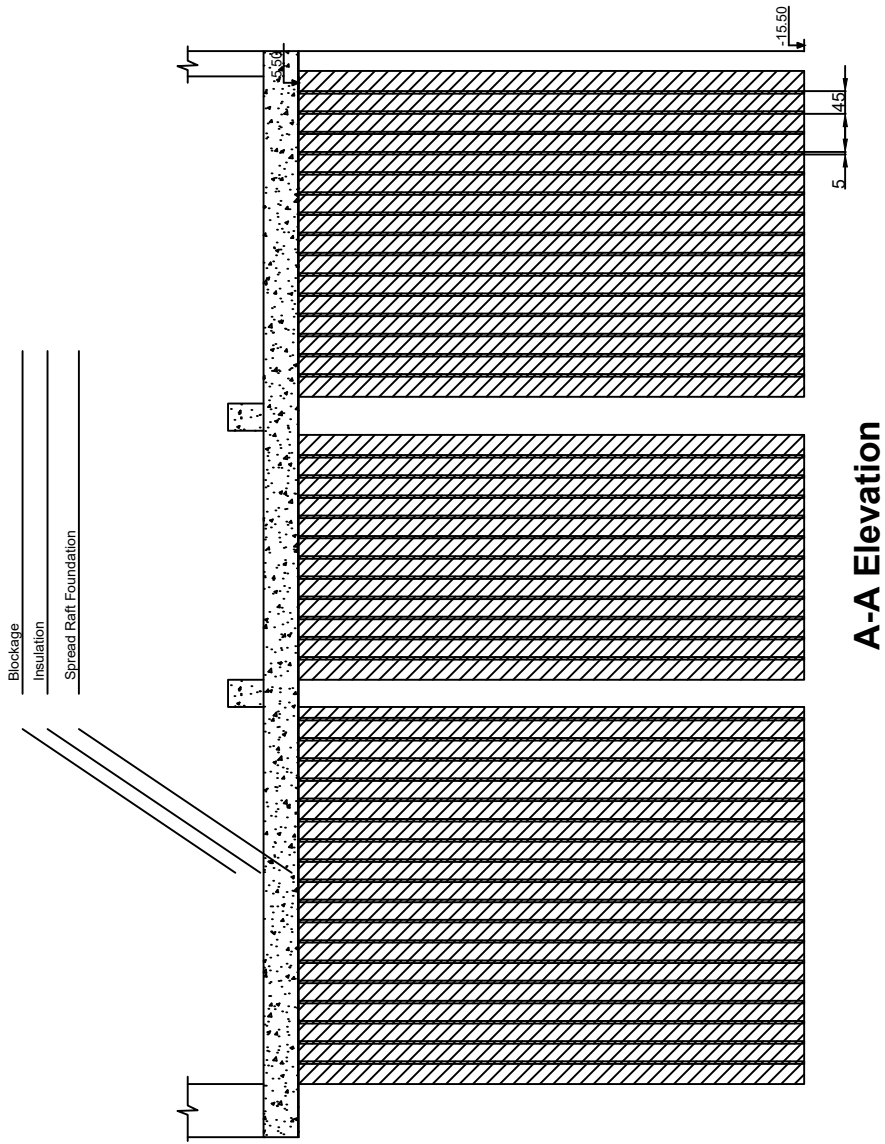


Figure B.1 Application plan of H Block





**H BLOCK: COLUMN HEIGHT 10m**

Figure B.1 Elevation drawing of H Block

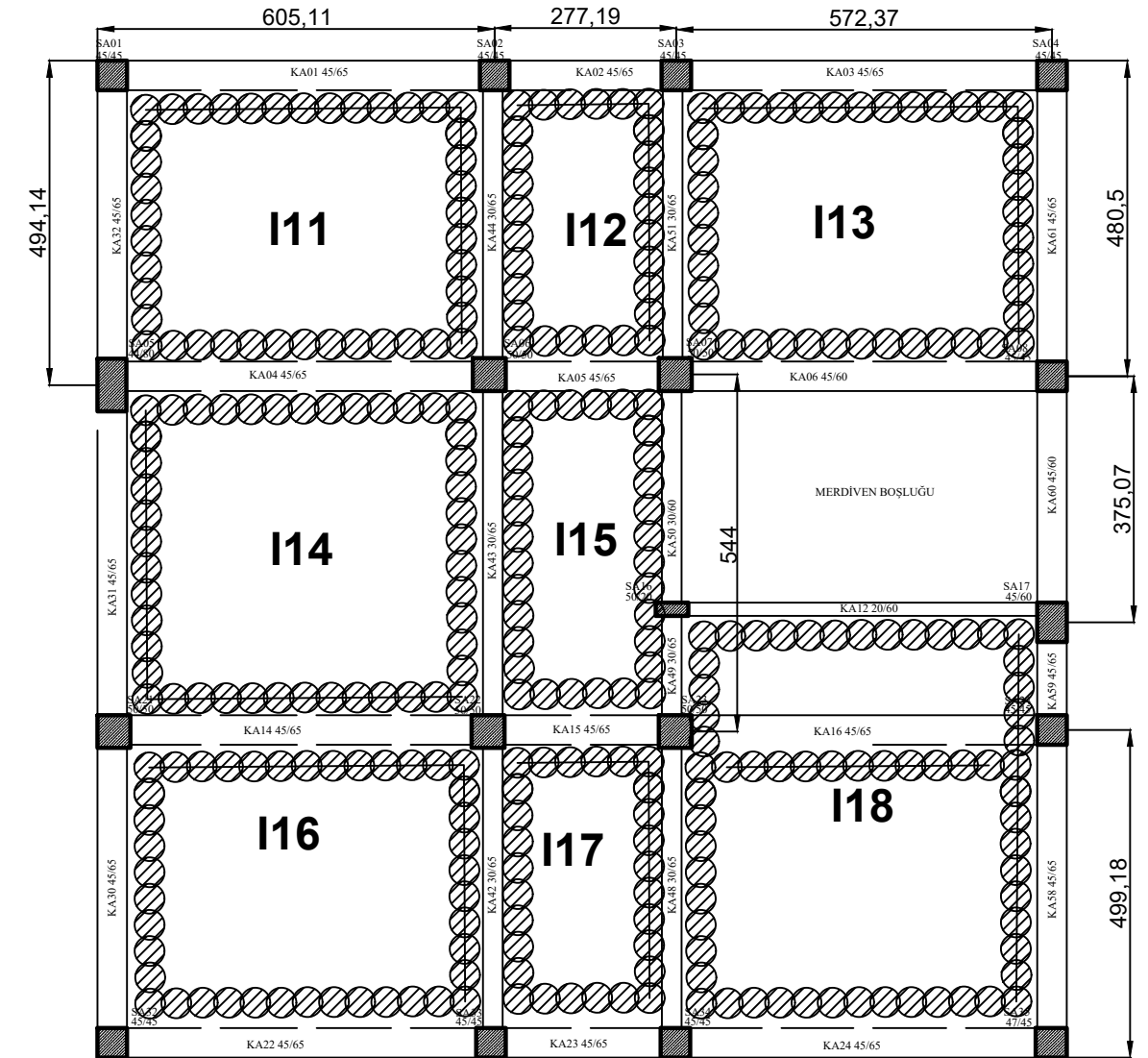
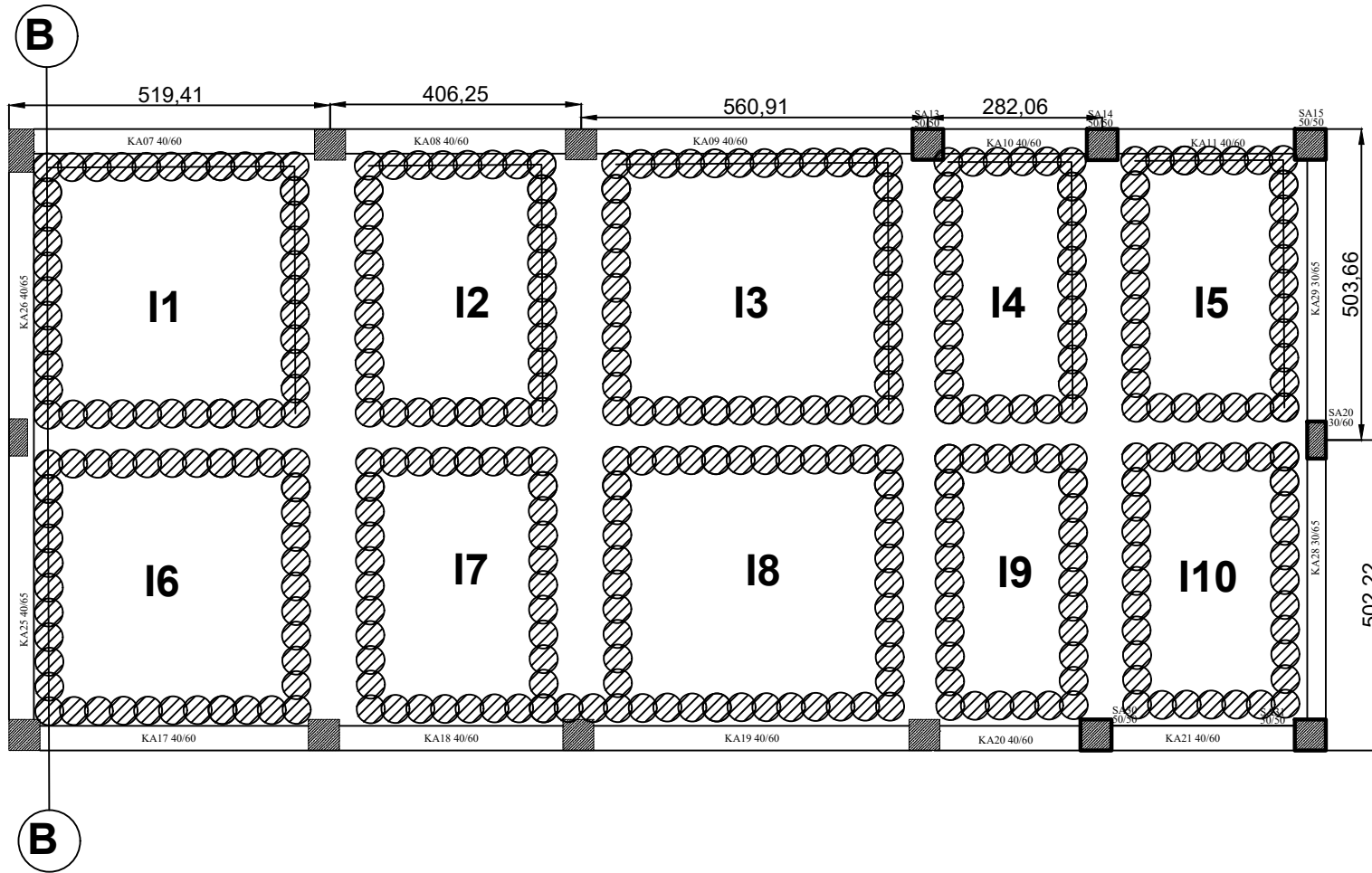
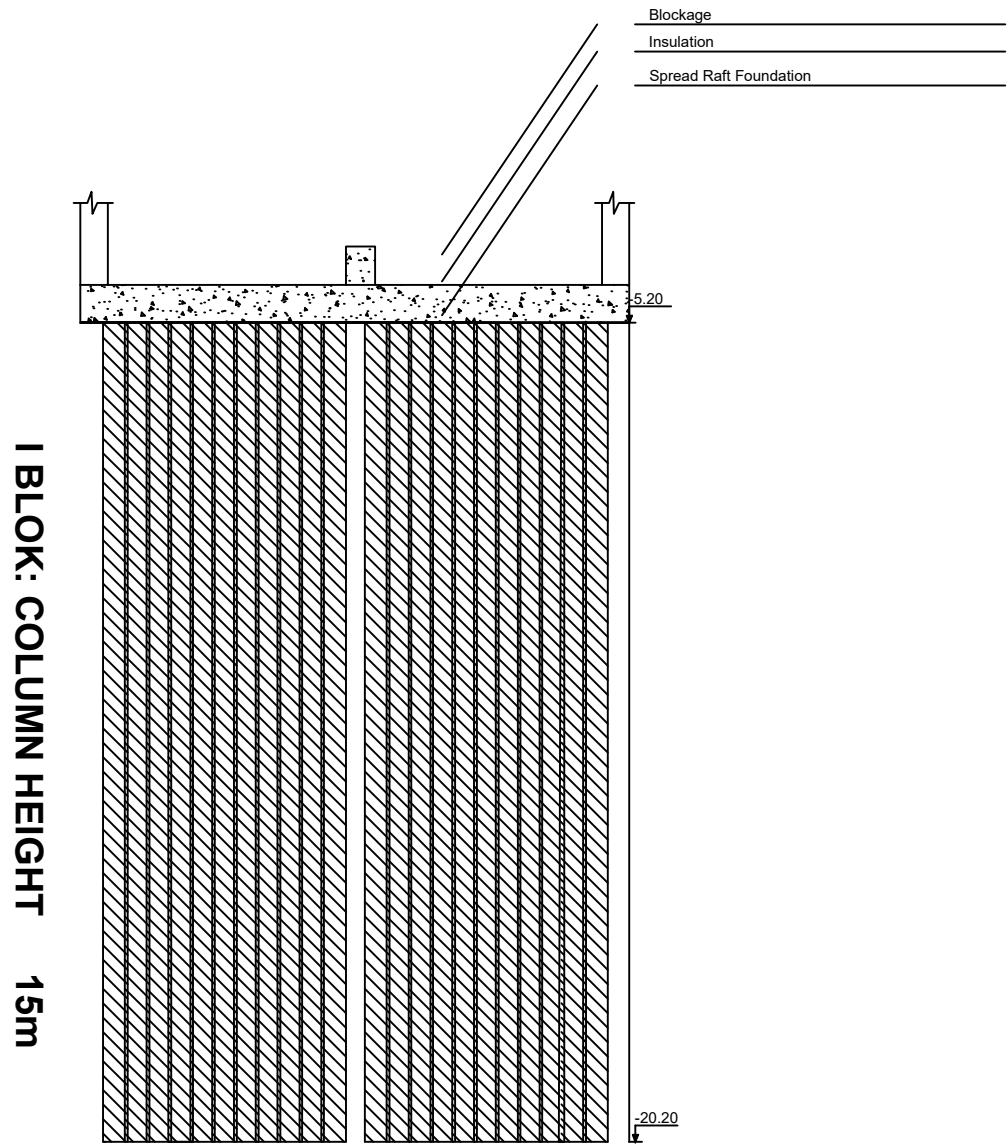


Figure B.2 Application plan of I Block



**B-B Elevation**

Figure B.2 Elevation drawing of I Block